Theses and Dissertations

Summer 2011

Hydrologic and biogeochemical signatures in intensively managed catchments: data synthesis and development of a passive surfacewater quality sampler

Samuel James Boland
University of Iowa

Recommended Citation

Boland, Samuel James. "Hydrologic and biogeochemical signatures in intensively managed catchments: data synthesis and development of a passive surfacewater quality sampler." MS (Master of Science) thesis, University of Iowa, 2011.
https://doi.org/10.17077/etd.2y90xzi0.

HYDROLOGIC AND BIOGEOCHEMICAL SIGNATURES IN INTENSIVELY

MANAGED CATCHMENTS: DATA SYNTHESIS AND DEVELOPMENT OF A

PASSIVE SURFACEWATER QUALITY SAMPLER

by

Samuel James Boland

A thesis submitted in partial fulfillment
of the requirements for the Master of
Science degree in Civil and Environmental Engineering
in the Graduate College of
The University of Iowa

July 2011

Thesis Supervisor: Assistant Professor Nandita Basu

CERTIFICATE OF APPROVAL

_____

MASTER'S THESIS

_____

This is to certify that the Master's thesis of

Samuel James Boland

has been approved by the Examining Committee
for the thesis requirement for the Master of Science
degree in Civil and Environmental Engineering at the July 2011 graduation.

Thesis Committee: _____
                  Nandita Basu, Thesis Supervisor

                  _____
                  Craig Just

                  _____
                  Douglas Schnoebelen

                  _____
                  Larry Weber

To Emily

ACKNOWLEDGMENTS

ABSTRACT

This study presents a conjunctive data synthesis and technology development approach to aid in enhancing understanding of the scaling behavior of water flow and nutrient transport in intensively managed agricultural catchments. Anthropogenic modifications to the landscape, with agricultural activities being a primary driver, have resulted in significant alterations to hydrologic and biogeochemical cycles. Significant research has been directed towards understanding and predicting the changes in these cycles in an effort to mitigate the associated adverse effects. Typical modeling efforts suffer from scaling issues associated with heterogeneities that arise at the catchment scale. New parsimonious approaches that rely on emergent patterns in data have been proposed to aid current modeling efforts. This study adopts a data synthesis approach to identify emergent patterns in hydrologic and nitrogen solute behavior in the context of agricultural activities at the catchment scale. The results of the synthesis indicate a strong anthropogenic signature in agricultural landscapes through (a) decrease in variability in the streamflow distribution with increase in the proportion of the catchment that is artificially drained and (b) relatively low variability in nitrogen concentration relative to discharge. Due to the dependence of such data synthesis methods on reliable data, a new method of data collection, through the use of an innovative passive sampling device, is developed to aid in future data synthesis and subsequent modeling efforts. Initial laboratory studies towards the development of the device achieved in this thesis indicate its ability to capture flow-averaged solute concentration over a specified deployment period. Future work involves testing the device under various field deployment conditions. The relatively low cost of the device would enable the estimation of spatially distributed flow-averaged concentrations that would complement existing costlier measurement methods, and significantly aid future modeling efforts and management decisions.

TABLE OF CONTENTS

LIST OF TABLES

LIST OF FIGURES

ix

LIST OF SYMBOLS

t; T	Time
$C_s(t)$; M/L^{-3}	Concentration of the analyte in the sampler at time (t)
C_w; M/L^3	Concentration of the analyte in the solution or stream concentration of analyte/solute
k_1; L^3/MT	Uptake rate coefficient for passive sampler
k_2; T^{-1}	Offload rate coefficient for passive sampler
K_d; L^3/M	Phase-water partitioning coefficient
$M_s(t)$; M	Mass of constituent accumulated after time (t)
R_s; L^3/T	Sampling rate of passive sampler
L_a; M/T	Total load of solute across a stream cross-section
$Q_s(t)$; L^3/T	Stream Discharge
C_t; M/L^3	Temporal mean of the concentration time series
L_{et} ; M/T	Solute Load estimated based on C_t
$\forall_d$; L^3	Cumulative volume of water that has flowed through passive sampler
M_d; M	Cumulative solute mass sorbed on the device
Q_d; L^3/T	Discharge through passive sampling device
C_f; M/L^3	Flow averaged concentration
L_{ef}; M/T	Load estimate based on C_f
θ; L^3/L^3	Porosity
ρ_b; M/L^3	Bulk density
R; -	Retardation factor
$m_{t,r}$; M/M	Mass fraction of tracer remaining after deployment
Tq_{mean}; -	Flashiness Index, fraction of time the daily mean discharge exceeds the mean annual discharge
$P(X \geq x)$	Probability P that a random variable X is greater than x
$p(x)$	Probability distribution
Q_t; L^3/T	Stream discharge at time t
Q_0; L^3/T	Initial discharge value
k; T^{-1}	Recession Constant
a; -	Scaling parameter of power law function
b; -	Shape parameter of power law function
R^2; -	Coefficient of determination
$C_{f,a}$; M/L^3	Annual flow-averaged concentration
$C_{f,e}$; M/L^3	Event flow-averaged concentration
$C_{f,m}$; M/L^3	Monthly flow-averaged concentration
CV; -	Coefficient of variation
CV_C; -	Coefficient of variation of solute concentration
CV_Q; -	Coefficient of variation of discharge
K; L/T	Hydraulic Conductivity
a_R; L^2	Cross-sectional area of reservoir
dh/dt; L/T	Change in height of the reservoir over time
H_t; L	Height above datum of the reservoir water after time t
H_0; L	Initial height above datum

A; L^2 Cross-sectional area of the sampler

M_{out}; M   Mass of nitrate extracted

M_{in}; M   Mass adsorbed to the resin

CHAPTER 1: INTRODUCTION

1.1 Motivation

Anthropogenic modifications to the landscape have become globally ubiquitous. With nearly one third of the terrestrial biosphere converted into anthropogenic biomes, geologic time is considered to be entering a new epoch known as the Anthropocene [*Crutzen*, 2002; *Ellis*, 2011; *Steffen et al.*, 2007; *Zalasiewicz et al.*, 2011]. Global land cover has under-gone significant changes due to agriculture and the current intensification in agricultural activity is expected to continue into the future [*Matson*, 1997; *Ramankutty and Foley*, 1999; *Tilman*, 2001; *Vitousek*, 1997]. Agricultural activities have affected all facets of the hydrologic and biogeochemical cycles, with environmental and societal impacts at local and global scales [*Tilman*, 1999]. These include eutrophication and hypoxia of receiving water bodies [*Diaz and Rosenberg*, 2008; *Kemp et al.*, 2009; *Osterman et al.*, 2009; *Rabalais et al.*, 2002; *Rabalais et al.*, 1996; *Smith et al.*, 1999], toxicity associated with pesticide, hormonal and pharmaceutical contamination [*Durhan et al.*, 2006; *Fuortes et al.*, 1997; *Soto et al.*, 2004; *Winchester et al.*, 2009]; elevated flood risks [*Mutel*, 2010; *Prestegaard et al.*, 1994]; erosion [*Stone and Krishnappan*, 1997]; and altered flow regimes [*K E Schilling and Helmers*, 2008; *K E Schilling et al.*, 2008] which impair aquatic ecology [*Carlisle et al.*, 2010].

Of these issues, hypoxia is a critical one that is linked directly with large-scale die-offs in coastal aquatic ecosystems and reductions in marine biodiversity [*Rabalais et al.*, 2010]. The hypoxic zones emerging globally are linked directly with nutrient inputs such as nitrogen and phosphorus associated with anthropogenic activities [*Rabalais et al.*, 2010]. Agroecosystems receive 75% of reactive nitrogen produced through human activities (which has increased roughly ten-fold since the 1800's), of which most is transferred to the environment through the production and consumption of food

[*Galloway et al.*, 2003; *Galloway et al.*, 2004]. One of the primary pathways of transfer is through riverine export, which accounts for roughly 25 percent of total reactive nitrogen inputs to terrestrial areas [*Galloway et al.*, 2004]. Significant increases in riverine fluxes of carbon and phosphorus have also been linked to intensive agricultural activities [*Alexander et al.*, 2008; *Raymond et al.*, 2008]. Increased bio-fuel or food production will exacerbate the problem, with intensification of crop/soil management and expansion of croplands to meet the increasing demand (e.g., [*Donner and Kucharik*, 2008]). While the influence of anthropogenic activities on these bulk exports are apparent, understanding of the processes governing these biogeochemical cycles at the spatial scales relevant to decision-makers is still lacking [*Cooter*, 2004; *Friedrichs et al.*, 2000]. In managing these anthropogenic landscapes to minimize water-quality and associated ecological impacts, computationally efficient and reliable tools are needed for decision-making at multiple spatial scales.

This presents a quandary at regional scales, where catchment level processes are obscured by landscape heterogeneities and the complexity of intertwined small-scale physical interactions [*McDonnell et al.*, 2007; *Schaefli et al.*, 2011]. As research to address these heterogeneities progresses, so does the perceived complexity of the processes under scrutiny, to the point where current modeling efforts have become cumbersome and unwieldy [*Beven*, 1989; *Perrin et al.*, 2001]. There is no dearth of distributed models available, many of which are extensively used for such management decisions e.g., MIKE-SHE [*Abbott et al.*, 1986; *Refsgaard and Storm*, 1995]. One common feature of the distributed-parameter models used to predict catchment responses has been model calibration using "training" datasets gathered over a restricted timeline, cross-validation using other datasets, and then generating model forecasts for much longer periods. While numerous, creative ways of calibration and optimization have been developed [*Arabi et al.*, 2006; *Gupta et al.*, 1999; *Madsen*, 2003], this approach suffers from *equifinality or non-uniqueness* issues [*Beven*, 2001; *Bloschl*, 2001; *Dehotin and*

Braud, 2008; *Vache and McDonnell*, 2006; *T. Wagener et al.*, 2003] that limit the predictive ability of these models under dynamic land use and climate change scenarios. Additionally, while many models overcome equifinality and become successfully calibrated; they are only calibrated to a specific spatiotemporal context and cannot be applied in other locations in time or space [*Schaefli et al.*, 2011].

Current challenges require a more general solution that provides predictive ability in the face of non-stationarity and parameter uncertainty [*Beven*, 1989; *Milly et al.*, 2008; *Thorsten Wagener et al.*, 2010]. In contrast to the model calibration approach, a few studies have recognized the value in studying patterns with an attempt to classify catchments and identify the dominant drivers and filters of hydrologic responses associated with each catchment class [*Atkinson et al.*, 2003; *Merz and Blöschl*, 2009; *Thorsten Wagener et al.*, 2007; *Zhang et al.*, 2008]. The search for dominant processes results in the development of empirical theories based on emergent patterns of catchment response across scales, which are then generalized using theories regarding natural organization and self similarity of underlying catchment heterogeneity [*Savenije*, 2009; *Sivapalan*, 2003]. Comparative hydrology, or parsimonious modeling, in which a minimalist approach to parameters is adopted, has been put forth as a viable alternative that can more obtain more robust descriptions of catchment response [*N Basu et al.*, 2010; *McDonnell et al.*, 2007; *Perrin et al.*, 2001; *Schaefli et al.*, 2011]. Motivated by this new approach, this research investigates the hydrologic and nutrient responses of managed catchments in order to identify emergent patterns that span spatial and temporal scales. The results of this search are presented and discussed in Chapters 2 and 3.

1.2 Surface Water Monitoring Strategies

While these methods promise new potentials for decisions makers at the catchment scale, their success, particularly the approach of identifying emergent patterns,

depends heavily on available data. In fact, the success of any modeling approach is highly dependent on the data available for calibration and validation [*Beven*, 1989; *Perrin et al.*, 2001]. Consequently, research on innovative strategies for monitoring discharge and water quality in streams and receiving water bodies has been identified as an area of critical need.

Measurement technologies of stream stage and discharge has progressed since the 1880's, with stream gaging stations covering most high order (> 4) streams [*Wahl et al.*, 1995]. However, as noted by the Iowa Flood Center (IFC), we still lack critical information in the majority of lower order streams ($< 10^2$ km^2). New efforts are underway to address these limitations, with technologies such as low cost bridge-mounted sensors providing feasible options for data collection at fine spatial and temporal scales[1]. Progress involving research on innovative strategies for water quality sampling lags far behind the measurement of stream discharge. While stream stage is normally recorded at 15 minute intervals, measurements of nitrate, phosphorus, and pesticide concentrations are much sparser. This is oft times due to methods of collection being prohibitively expensive (Table 1.1).

---

[1] http://www.iowafloodcenter.org/projects/river-stage-sensors

Table 1.1. Typical methods for measurement of stream water parameters and relative costs.

Parameter	Technology	Typical Cost Range
Stage	Pressure Transducer	$3,000 - $5,000
Stage	Bridge-mounted acoustical sensor	$1,000 - $3,000
TN, TP or sediments	Automated ISCO sampler	$5,000 - $7,000
pH, conductivity, TSS, temperature	Hydrolab Sonde	$15,000 - $20,000
Nitrate	Nitratax Sonde	$15,000 - $20,000
TDS, salinity, ORP, dissolved oxygen	YSI electrode probes	$10,000 - $15,000

1.2.1 Commonly Used Water Quality Samplers

The traditional, and the most widely used, technique for water quality sampling involves grab sampling. This involves a field technician travelling to the site, manually extracting a sample of stream water, and bringing it back to the laboratory for analysis using standardized methods. This approach is limited by the number of field visits realistically possible within a year and the spatial coverage feasible using such labor intensive techniques. Typical sampling frequencies (10-12 times a year), in the limited number of streams selected for monitoring, often fail to capture the episodic character of contaminant concentrations, especially in lower order, flashier streams. Composite or automatic samplers (e.g. ISCO[2] or Sigma[3] samplers) in which a field-deployed device is programmed to take samples from the stream at fixed intervals of time or flow are the next tier in sampling strategies. The device contains multiple (typically 24), sample

[2] http://www.isco.com/products/products1.asp?PL=201

[3] http://www.hach.com/sd900-portable-sampler-with-compact-base/product?id=7640271650&callback=qs

bottles which are filled based on either a specified time or flow interval. Flows are measured and can be recorded using a pressure transducer located near the sampler inlet in the stream. Due to the programming possibilities of the device, each sample can be discrete, time-averaged, or flow-averaged based on the needs of the study. Important considerations when deploying include: cost (refer to Table 1.1), the availability of a power source, and field technicians experienced in maintenance and deployment of such devices.

The most sophisticated, and also most expensive method, involves field-based auto-analyzers that utilize ion-specific electrodes or spectrophotometric methods to quantify solutes in real-time. High temporal resolution data has been proposed as the future of solute sampling, providing a wealth of information that has been successfully used towards understanding the biogeochemical responses of catchments to precipitation inputs [*Kirchner et al.*, 2004]. However, the cost prohibitive nature of such technologically advanced probes restricts the number and breadth of sampling sites, thus reducing the spatial resolution of understanding catchment scale processes.

1.2.2 Active vs. Passive Sampling

The above methods can be encompassed by the term active sampling; an alternative approach that addresses limitations in active sampling is passive sampling. Active sampling involves the collection of water (or air) into the sampling device using a pump, or more generally, sampling that requires energy expenditure during collection. In contrast to this, passive sampling is dependent on the free flow of an analyte from the aqueous phase to a sorbent based on differentials of chemical potential between the two phases [*Vrana et al.*, 2005]. The low energy requirements and maintenance in passive sampling makes it an attractive alternative to more conventional active sampling techniques. The last two decades has seen substantial progress in the development of

passive samplers for water quality applications (Figure 1.1). These developments have been primarily in the domain of trace contaminants, either organic or inorganic, that are otherwise difficult to measure through traditional sampling techniques [*Greenwood et al.*, 2007; *Namieśnik et al.*, 2004; *Vrana et al.*, 2005].
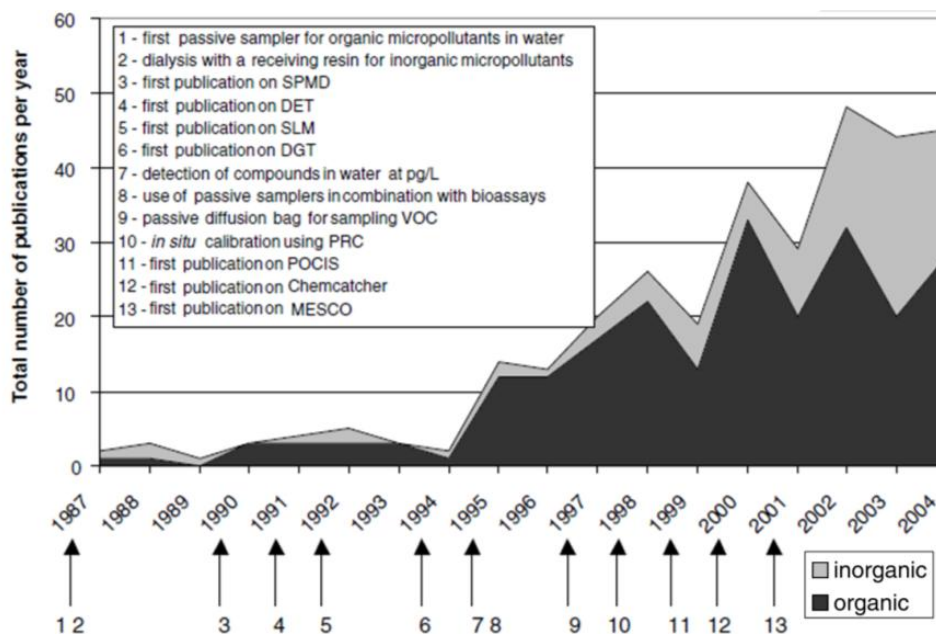
Figure 1.1. Activity in the academic community related to passive sampling advancements during the past two decades, along with major milestones in new device development, adapted from [*Vrana et al.*, 2005].

1.2.3. Discrete vs. Integrated Sampling

In addition to the advantages of minimal energy and maintenance requirements, passive sampling techniques allow for collection of integrative samples. This is advantageous due to the avoided uncertainties involved with piecing discrete samples together to formulate an accurate description of over-all water quality conditions. Linear

interpolation, autoregressive models, and multiple regression are a few examples of the techniques necessary to connect the snapshots that synoptic sampling provides [*Alewell et al.*, 2004]. In order to minimize dependence on these techniques, it is necessary to know the frequency of variations in concentration or the autocorrelation time scales and develop a synoptic sampling strategy that is at least twice this frequency. This may not be a feasible endeavor, especially when concentrations vary over relatively short timescales as illustrated in Figure 1.2, which presents discrete, flux-averaged, and continuous concentrations of nitrate, adapted from [*J Rozemeijer et al.*, 2010]. *Alewell et al.* (2004) addressed the question of optimal sampling frequency using daily nitrate measurements at a 4.2 km^2 watershed in northern Germany. Weekly sampling was found to be optimal in capturing the variability in concentration, while sub-weekly sampling frequencies in systems provide low information gains relative to the increases in costs and labor requirements [*Alewell et al.*, 2004]. However, the finding was a function of the solute of interest and the landscape characteristics (such as agricultural vs. forested). Although continuous sampling is the best way to address these issues, it is often cost prohibitive. Herein lays the value of integrated sampling. Integrated samples (solid black horizontal lines in Figure 1.2) obviate the need for interpolation, and are extremely useful when the focus is on estimating the total seasonal or annual loads. This is usually the case for assessment of hypoxia from nitrate.
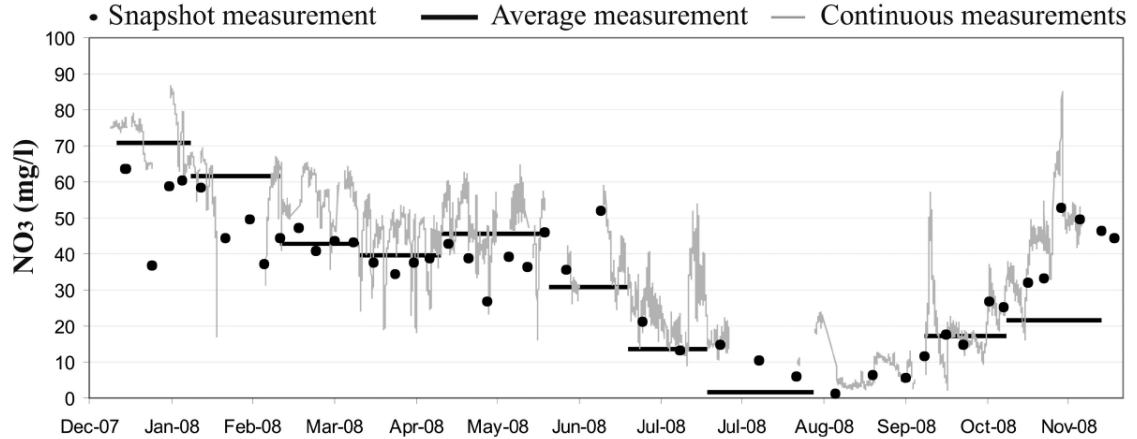
Figure 1.2. Discrete and flux-averaged values of nitrate concentration in the context of actual nitrate concentrations, adapted from [*J Rozemeijer et al.*, 2010]. The differences in values illustrate inaccuracies that result from discrete sampling.

1.3 Passive Samplers

1.3.1 Conceptual Framework

Passive samplers typically have a receiving or sorbent phase in which the chemical of interest accumulates during the course of the sampler deployment. Partitioning of the chemical between the aqueous and receiving, or sorbent, phases in passive samplers is typically described by a first-order one compartment mathematical model as shown in Equation (1.1) [*Greenwood et al.*, 2007; *Mayer et al.*, 2003; *Vrana et al.*, 2005]:

$$C_s(t) = C_w(k_1/k_2)\left(1 - e^{-k_2 t}\right) \qquad (1.1)$$

Where ($C_s(t)$; M/M) is concentration of the analyte in the sampler at time (t), (C_w; M/L^3) is the concentration of the analyte in the aqueous phase, and (k_1; L^3/MT) and (k_2; T^{-1}) are

the uptake and offload rate coefficients of the sorbent [*Vrana et al.*, 2005]. Passive samplers operate in either the equilibrium or the kinetic accumulation regimes. The equilibrium regime, as the name suggests, is based on sufficient exposure time to attain thermodynamic equilibrium between the aqueous and the reference phases. Thus, Equation 1.1 reduces to:

$$C_s(t) = C_w(k_1/k_2) = K_d C_w \qquad (1.2)$$

Where, (K_d; L^3/M) is the phase-water partitioning coefficient. The primary requirement for equilibrium based sampling is that the response time required to reach equilibrium is shorter than the fluctuations in C_w [*Mayer et al.*, 2003]. Passive diffusion bag samplers (PDBSs) are equilibrium samplers that have been used extensively for monitoring volatile organic compounds (VOCs) in water (Mayer et al. 2002). In kinetic sampling, the uptake is linearly proportional to the difference in concentration between the aqueous and receiving phases and the rate of desorption is negligible. This allows Equation (1.1) to be manipulated to create Equation (1.3):

$$M_s(t) = C_w R_s t \qquad (1.3)$$

Where (M_s) is the mass of constituent accumulated after time (t) and (R_s; L^3/T) is a sampling rate based on the product of (k_1) and "the volume of water that gives the same chemical activity as the volume of receiving phase" [*Vrana et al.*, 2005], effectively providing a volume of water that has had all of the analyte of interest removed. Kinetic samplers are highly dependent on knowledge of (R_s), which can be used to provide a time-weighted average concentration in conditions with varying concentrations [*Greenwood et al.*, 2007].

1.3.2 Time-Integrated vs. Flow-Integrated Sampling

The sampler designs that have been discussed so far are based on time-integrated sampling, or in other words the measured solute concentration in the device after an exposure time (t) is the mean of the temporally varying concentrations. The advantages of flow-integrated sampling over time-integrated sampling have been discussed in detail by *King and Harmel* (2003) in the context of active sampling devices. The progress made in passive sampling devices, however, has been primarily in the domain of time-integrated sampling.

For surface water quality assessments, a metric of significant interest is the total load (M/T) of a solute that passes through a stream cross-section over a specified exposure duration (e.g., storm event, seasonal, annual). This is used for prioritizing management decisions based on a TMDL (total maximum daily load) framework. Load, rather than concentration, is often of greater interest, especially for lower order streams since the water quality of receiving water bodies is determined by the total mass of solute that it receives. The total load (L_a; M/T) over a time interval t is given as the integral of the product of the stream discharge ($Q(t)$; L^3/T) and the stream concentration ($C_w(t)$; M/L^3) time series:

$$L_a = \int C_w(t)Q(t)dt \qquad (1.4)$$

A time-integrated passive sampler deployed in the stream-water for a duration t, measures C_t, which is the temporal mean of the concentration time series. The load L_{et} can then be estimated as the product of C_t and an independent measure of the mean streamflow distribution using a flow recorder:

$$L_{et} = C_t \int Q dt = \int C_w\, dt \int Q dt \qquad (1.5)$$

It is obvious that L_{et} and L_a are not equal, and that L_{et} is a good approximation of L_a only under very stable concentrations, i.e. very low temporal variability in $C_w(t)$.

A flow-integrated sampler is based on the principle of simultaneously measuring the cumulative volume of water that has flowed through the device ($\forall_d$; L^3), and the cumulative solute mass sorbed on the device (M_d; M). The volume of water flow over the course of sampler deployment duration (t) is obtained by integrating the discharge through the device (Q_d; L^3/T):

$$\forall_d = \int Q_d(t)\, dt \qquad\qquad (1.6)$$

Simultaneously, a cumulative mass of the contaminant will be captured based on the mass flux through the device integrated over the duration of the deployment. Mass flux through the device M_d (M/T) is defined as the water flux through the device multiplied by the concentration C_w of contaminant dissolved in the water. This is demonstrated by Equation 1.7:

$$M_d = \int Q_d(t)C_w(t)dt \qquad\qquad (1.7)$$

The flow-integrated samplers measure M_d and $\forall_d$ using methods described below, and estimate the flux-averaged concentration (C_f; M/L^3) as:

$$C_f = \frac{M_d}{\forall_d} = \frac{\int Q_d(t)C(t)dt}{\int Q_d(t)dt} \qquad\qquad (1.8)$$

The total load estimated using this technique L_{ef} can then be expressed as:

$$L_{ef} = C_f \int Q\, dt \qquad\qquad (1.9)$$

It is apparent that if a linear relationship exists between the flow through the device and the in-stream flow ($Q_d = \beta*Q$), the estimated load using this technique will be exactly equal to the actual load L_a. Further, if the relationship between discharge through the device and stream discharge can be consistently quantified as a function of the device dimensions and the external flow field, then the device can be used for simultaneous measurement of water velocity and solute loads. If this is not the case, stream discharge is more readily obtainable; either from currently available USGS gaging stations or from in-situ bridge-mounted gage sensors, or depth measuring pressure transducers.

There are currently two different groups of research that present methods for flux-averaged passive sampling. One method is based on two cartridges placed in series within a 60ml plastic syringe. This syringe is placed in the flow such that the inlet is hydraulically connected to the flow while the outlet is maintained at atmospheric pressure. The first cartridge contains an adsorbent reservoir to capture the mass load of contaminant while the second contains a salt reservoir that dissolves at a rate proportional to flow passing through the device [*de Jonge and Rothenberg*, 2005; *J Rozemeijer et al.*, 2010]. The device has been shown to be successful in low flow scenarios, however preferential flow through the device has been observed due to non-uniform salt depletion. The second group of research is presented in the following section and will provide the foundation for the new passive sampler developed in this study.

1.3.3 Passive Flux Meters (PFMs)

PFMs were originally developed for groundwater sampling [*Hatfield et al.*, 2004] and later modified for surface water sampling [*Klammler et al.*, 2007]. The design consists of a tube of sorbent material that is pre-loaded with alcohol tracers. During the duration of a deployment, water passing through the sorbent material washes the tracer away at a rate dictated by the tracer's partitioning (K_d) between the sorbed and aqueous

phases. The difference between the mass of tracer pre- and post-deployment is used for the estimation of the flow-rate through the device (Q_d). Simultaneously, the sorbent material serves to capture the mass of contaminant that is being transported by the water, which is used to estimate M_d (Equation 1.12).

$$Q_d = \frac{(1 - m_{t,r})A\theta RL}{t} \tag{1.10}$$

$$R = 1 + \frac{K_d \rho_b}{\theta} \tag{1.11}$$

$$M_d = \frac{C_s \rho_b AL}{t} \tag{1.12}$$

where (C_s; M/M) is the sorbed concentration in the device, (ρ_b; M/L^3) is the bulk density, (A; L^2) is the cross-sectional area of the sorbent material in the device, (L; L) is the length of the sorbent column, and (θ; L^3/L^3) is the porosity of the porous media. Porosity is defined as the volume of voids within a porous media divided by the total volume of the media and bulk density is defined as the mass of a porous or particulate media divided by the total volume. ($m_{t,r}$; -) is the ratios of the total mass of the tracer sorbed onto the GAC and the mass left behind post deployment, which is dictated by the retardation factor (R; -) that describes the velocity of the tracers relative to the velocity of water through the device.

In the groundwater domain, PFMs are deployed vertically in a groundwater monitoring well, such that the flow direction is normal to the orientation of the device. Since flow is steady in most groundwater scenarios, consistent relationships can be derived between flow through the device and the flow in the surrounding media. Thus PFMs in groundwater can be used for simultaneous estimation of water and solute fluxes.

The method has been successfully verified at both the laboratory and field scales and applied to investigations of contaminant plume behavior [*Annable et al.*, 2005; *Basu et al.*, 2006; *Campbell et al.*, 2006; *Cho et al.*, 2007]

The framework developed for the PFM was first adapted to applications in surface waters by *Klammler et al.* (2007) and subsequently by *Padowski et al.* (2009) during which it was re-named the passive surface water flux meter (PSFM). The primary difficulty in moving between the two domains (groundwater vs. surface water) is the orders of magnitude increase in water velocities. To address this and maintain the ability to quantify the water flux, specific sampler geometries were developed, shown in Figure 1.3. This allowed for a well-defined pressure differential to be maintained between inlet and outlet ports of a cartridge. This cartridge served in the same capacity as the PFM sorbent material; simultaneously capturing analytes while eluting a tracer proportional to the pressure differential across the cartridge. Another modification to the original PFM design was the addition of two, rather than a single, sorbent material; one to elute the tracers and one to capture the contaminant. The sorbent used to capture solutes was an anion exchange resin able to capture dissolved phosphorus.

W =11.4 cm

Cartridge

H =40 cm

32 cm

24 cm

16 cm

8 cm

Ports

2

1

Flow Direction
(profile-view)

Flow Direction
(top-view)

W =6 cm

H =64 cm

25 cm
20 cm
15 cm

Cartridge

1

2

Ports

L = 51 cm

Flow Direction
(profile-view)

Flow Direction
(top-view)
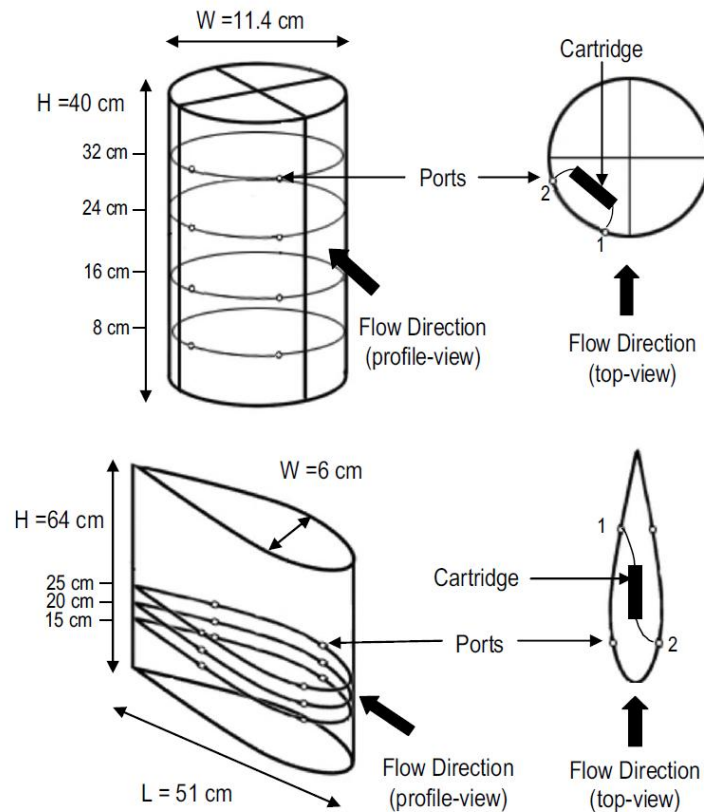
Figure 1.3. Two initial designs of the passive surface water flux meter. The water and solute fluxes measured by the device are dependent on the Joukowski flow profile around the device, which dictates the pressure differential between inlet and outlet ports of the cartridge and thus drives the flux through the cartridge. Figure adapted from *Padowski et al.* (2009).

The application of the flux meter concept to open waters was successfully verified in laboratory flume studies and in an urbanized creek receiving treated wastewater [*Padowski et al.*, 2009]. The duration of the deployments ranged from 40 to 495 minutes and the environmental settings were more or less steady-state. To develop the framework of the passive surface water flux meter further, this research will aim to modify the sampler such that it can be deployed for durations long enough to capture the dynamics

of a hydrologic event, and would be applicable under transient conditions. The laboratory experiments and results towards this end are presented in Chapter 4.

1.3 Objectives

The thesis has two distinct, but closely related objectives: (1) identify emergent patterns in the hydrologic and biogeochemical responses of intensively managed catchments using available data; (2) develop an innovative flux-integrated passive sampling device for water quality measurements that will aid future data collection efforts. The synergistic relationship between these two objectives will aid in furthering catchment scale understanding of the impacts of anthropogenic modifications to the natural environment. They are complementary in that the strength of identified patterns is dependent on the quality of data available, while effective sampling designs and strategies are in turn dependent on prescribed understanding of the processes being monitored.

A data synthesis approach will be utilized to investigate the signatures of anthropogenic modifications to the landscape. The Upper Mississippi River Basin (UMRB) is one of the most productive agricultural regions globally; with states such as Iowa contributing disproportionately to agricultural impacts such as gulf hypoxia [*Alexander et al.*, 2008]. Thus, data concerning hydrologic and nutrient fluxes across Iowan catchments will be investigated for routes to simplified understanding of catchment processes. Chapter 2 will evaluate the effect of artificial subsurface drainage on hydrologic responses in Iowan catchments. Artificial drainage is one of the most extensive manipulations of the hydrologic cycle in agricultural landscapes and thus is expected to provide a distinct signature of anthropogenic modification. Chapter 3 will explore spatial scaling regimes in the flux of a major nutrient of concern; nitrogen in the form of nitrates. This will be accomplished through the analysis of fine resolution nitrate

concentration data sampled at the outlet of three nested agricultural basins within Iowa. Spatial and temporal scale dependence of the flow averaged concentration C_f will be evaluated. Finally, in Chapter 4, laboratory studies towards the development of a passive flux-integrated sampler that directly measures C_f for nitrate are presented. Successful laboratory results indicate a new route to spatially distributed and flux integrative data collection.

CHAPTER 2: HYDROLOGIC REGIMES IN ARTIFICIALLY

DRAINED AGRICULTURAL CATCHMENTS

2.1 Introduction

The installation of artificial drainage was part of the "developmental ethos" of agriculture and has become agriculture's most extensive soil and water management activity [*Pavelis*, 1987]. Artificial subsurface drainage is performed by installing networks of pipes (tile drains or tube drains), typically 1-2 meters below the surface. The subsurface drainage system, in conjunction with surface drainage ditches, drain low lying landscapes with high water tables so that the land can be used for agriculture. It is well recognized that installation of artificial drainage has significantly altered the hydrology of these systems; however there remains controversy regarding this impact, especially at the catchment scale. Extensive reviews have been provided by [*Skaggs et al.*, 1994], [*Robinson and Rycroft*, 1999], [*Robinson*, 1989], and [*Robinson*, 1990] on the current state of knowledge and disagreement regarding the hydrologic impact of artificial drainage. However, the majority of the studies reviewed are based at the plot scale and do not necessarily translate well to the catchment scale [*Robinson*, 1990]. An additional significant feature of tile drains is that they have been found to be the primary transport route for nitrate delivery to waterways, contributing as much as 99% of total load [*Guan et al.*, 2011; *Royer et al.*, 2006].

A review of field studies (< 10 ha) indicated that soil type and climate dictated whether installation of artificial drains increased or decreased peak flows [*Robinson*, 1989]. If the water table was closer to the surface (due to high rainfall or poor permeability as in clayey soils) installation of tile drains decreased peak flows [*McLean and Schwab*, 1982; *Robinson and Beven*, 1983; *Seuna and Kauppi*, 1981] while if the water table was deeper (dry climate or permeable soils) the opposite effect was observed [*A C Armstrong*, 1983; *Robinson et al.*, 1985; *Schuch*, 1978]. [*Robinson*, 1989]

concluded that if storm discharge is fed primarily by subsurface discharge, then installation of subsurface drainage increases peak flows due to shorter flow paths and steeper gradients. In contrast, if storm discharge is fed primarily by surface discharge, drainage increases soil water storage capacity thereby reducing surface runoff and peak flows.

At the catchment scale (10 km^2 to 20 km^2), an increase in peak flows was apparent after installation of subsurface drainage in most studies reviewed [*Robinson and Rycroft*, 1999]. A 22% increase in peak flow was observed in a 20 km^2 watershed near Buckinghamshire, England, despite the fact that individual field studies within the catchment indicated reduction in peak due to installation of subsurface drains. The consistent increase in peak flow at the catchment scale was hypothesized to be a function of stream channelization which increased peak flows [*Robinson*, 1990]. At larger scales, it is often difficult to decouple the relative effects of increase in subsurface drainage versus channelization of the streams on peak flow. Field studies are "diluted" at the catchment scale and channel improvements play a larger role at these scales [*Robinson*, 1990].

Studies exploring the impact of artificial drainage at even larger scales (> 25km^2) are relatively scarce. [*Robinson and Rycroft*, 1999] cite four studies that attempted to enumerate the impact of drainage on total discharge at large scales (>1000 km^2) by quantifying impacts before and after drainage improvements within the catchments. These studies found no impact; however their results were confounded by factors including ambiguous and on-going installation dates and climate variability. Despite controversy on the effect of tile drainage on peak flows, almost all studies were consistent in their conclusion that tile drainage increased baseflow.

A more recent study involving the baseflow and recession behavior of tiled watersheds at scales ranging from 5.3 to 2574 km^2 in Iowa indicated that tiling most likely creates exponential recessions, while more complex power function recession

responses were typical in non-tiled watersheds [*K E Schilling and Helmers*, 2008]. Most studies discussed above investigate the change in hydrologic conditions due to tiling by comparing data before and after installation. Consequently, the number of studies at larger scales is relatively sparse due to lack of adequate records on drainage installation and streamflow response. Further, the studies discussed above focused primarily on peak flow or baseflow, while recent research highlights the importance of the entire distribution of flows on stream ecosystem responses [*Carlisle et al.*, 2010]. To address these gaps, this research focuses on understanding the role of artificial drainage by comparing the entire streamflow distribution in catchments with different percentages of artificial drainage. Basins within the state of Iowa were selected for the analysis.

Iowa is a major contributor to agriculture production and is a prime example of land-use and land cover (LULC) change; approximately 2/3 (9.3 million ha) of the state has been put to the purpose of producing annual row crops [*Baker et al.*, 2004]. Historically, 3.1 million ha of Iowa's 14 million ha consisted of poorly drained prairie marsh-pothole landscape, but 99% of this landscape type has been artificially drained [*Bishop et al.*, 1998]. Iowa now has an estimated 3.6 million ha of artificially drained landscape [*Baker et al.*, 2004]. This state-wide anthropogenic manipulation of hydrologic conditions would be expected to have a distinct signature on the hydrologic cycle within these heavily managed catchments, but few studies have addressed this topic at a scale other than that necessary for maximizing agricultural productivity [*Robinson*, 1990; *Robinson and Rycroft*, 1999; *Skaggs et al.*, 1994] .

The overall objective in this chapter is to quantify the effect of spatial observation scale and presence of artificial drainage on the streamflow distribution. We are interested in the absolute magnitude of the effect of artificial drainage on hydrologic response, as well as the spatial variability in responses within tiled and non-tiled systems. A range of metrics were used for this purpose: mean annual runoff ratio, mean annual baseflow ratio,

the flow duration curve, Lorenz Curve, Gini coefficient, Tq_{mean}, and the recession behavior.

2.2 Methodology

2.2.1 Study Area and Data Sources

Daily average streamflow records from twenty-four gaging stations across the state of Iowa were used for the analysis, courtesy of the U.S. Geological Survey[4]. The spatial distribution of sites selected within the various landform regions is shown in Figure 2.1 while the relevant attributes are listed in Table 2.1. The landform region dataset was generated by [*Jean C. Prior and Kohrt*, 2006]; for more information regarding the various regions see [*J.C. Prior*, 1991]. The selection process was guided by the need to include a variety of spatial scales and significantly different landform types within the state. Criteria imposed on the selection involved insuring that there were no major impoundments in the catchments of interest and that catchments were not nested within other catchments used in the analysis. Watersheds selected were predominantly agricultural (20 out of the 24 watersheds had greater than 40% land under row crop agriculture). A ten year period of data, starting from 1996 through 2005 was used for the analysis.

ArcGIS was used to estimate various watershed parameters, including watershed area, elevation, slope and land-use characteristics using a 30m resolution National Elevation Dataset (NED)[*USGS*, 1999]. The prevalence of tiling was evaluated by the Iowa Geological Survey (IGS), who created a grid covering the state and determined whether or not each cell in the raster set would need tiling to attain full agricultural

---

[4] http://waterdata.usgs.gov/ia/nwis/rt

productivity by using certain criteria[5] [*IDNR*, 2008]. These criteria were slopes less than

5%, drainage class 45-70, subsoils with clay $< 40\%$, and a land class of 2 or greater[6].
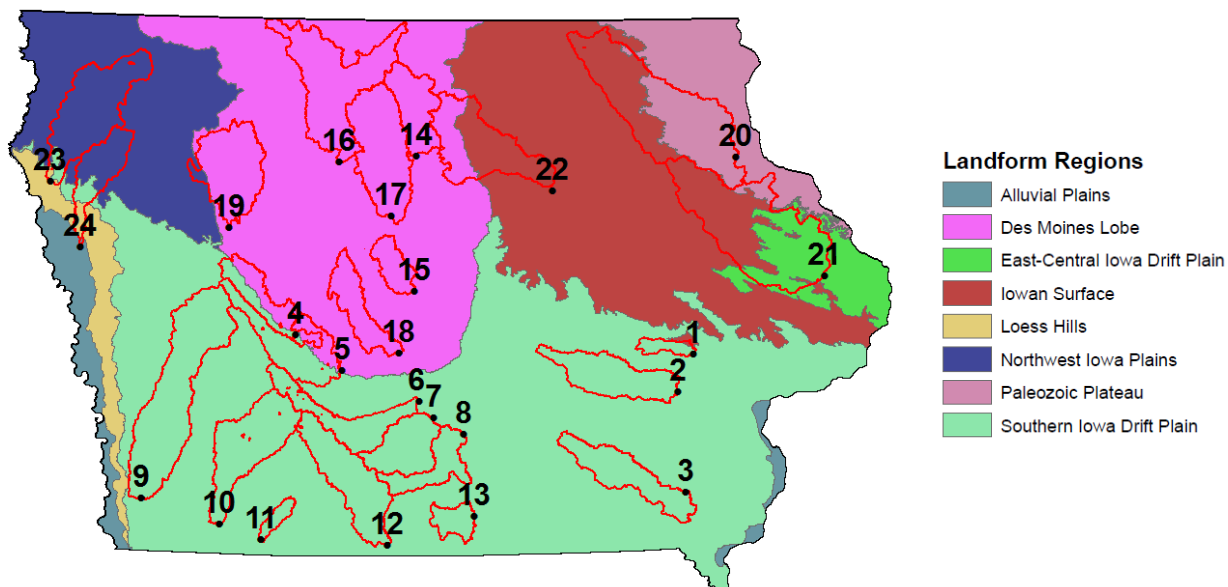
Figure 2.1. USGS stream gaging sites and respective delineated drainage areas selected for analysis, presented in the context Iowa's major landform regions. Delineated sites generated using ArcGIS and a 30m digital elevation model produced by [*USGS*, 1999]. Landform regions data generated by [*Jean C. Prior and Kohrt*, 2006] and gaging sites dataset courtesy of the Iowa DNR [*IDNR*, 2005].

---

[5] http://extension.agron.iastate.edu/soils/SSDS_maps.html

[6] http://soils.usda.gov/technical/handbook/contents/part622.html

Table 2.1. Eight Digit HUC code for each station and relevant catchment characteristics.

ID	USGS Site ID	Site Name	km²	% Tiled	% Row-cropped
		Southern Iowa Drift Plain			
1	5454300	Clear Creek near Coralville, IA	254	14.3	53.4
2	5455500	English River at Kalona, IA	1482	17.5	52.8
3	5473400	Cedar Creek near Oakland Mills, IA	1370	26.7	56.7
4	5483450	Middle Raccoon River near Bayard, IA	867	34.6	72.3
5	5484000	South Raccoon River at Redfield, IA	1438	17.4	52.2
6	5486490	Middle River near Indianola, IA	1261	8.3	33.1
7	5487470	South River near Ackworth, IA	1185	10.4	17.4
8	5487980	White Breast Creek near Dallas, IA	879	8.3	15.9
9	6808500	West Nishnabotna River at Randolph, IA	3436	8.5	72.9
10	6817000	Nodaway River at Clarinda, IA	1966	7.1	47.0
11	6819185	East Fork 102 River at Bedford, IA	222	11.8	40.3
12	6898000	Thompson River at Davis City, IA	1798	5.3	22.3
13	6903700	South Fork Chariton River near Promise City, IA	438	6.7	24.5
		Des Moines Lobe			
14	5449500	Iowa River near Rowan, IA	1113	65.3	81.6
15	5470500	Squaw Creek at Ames, IA	543	58.9	76.3
16	5479000	East Fork Des Moines River at Dakota City, IA	2757	72.9	84.8
17	5481000	Boone River near Webster City, IA	2178	80.6	85.4
18	5481950	Beaver Creek near Grimes, IA	963	59.2	78.4
19	5482300	North Raccoon River near Sac City, IA	1818	67.3	85.4
		Paleozoic Plateau			
20	5412500	Turkey River at Garber, IA	4020	22.9	51.0
		East-Central Iowa Drift Plain			
21	5418500	Maquoketa River near Maquoketa, IA	4015	19.7	53.7
		Iowa Surface			
22	5463000	Beaver Creek at New Hartford, IA	2159	54.3	77.5
		Northwest Iowa Plains			
23	6600500	Floyd River at James, IA	2287	24.8	84.1
24	6602020	West Fork Ditch at Hornick, IA	1042	12.7	79.7

2.2.2 Flow Metrics

2.2.2.1 Intra and Inter-annual Variability in Streamflow

Response

The following metrics were used to characterize the inter- and intra-annual variability in streamflow response: mean annual runoff ratio, mean annual baseflow ratio, the flow duration curve (FDC), the fraction of time the daily mean discharge exceeds the mean annual discharge (Tq_{mean}), the Lorenz curve , and the Gini coefficient. Details of these parameters are described below.

The mean annual runoff ratio is the ratio of the runoff depth (area-normalized discharge) Q (L) to precipitation P (L). To find Q/P for each catchment, annual sums of area normalized discharge from the catchment outlet were divided by annual cumulative precipitation based on NEXRAD data taken from the National Weather Service (NWS). The baseflow ratio was calculated using the digital recursive filter outlined by [*Arnold et al.*, 1995]. The metric Tq_{mean}, an indicator of flashiness, is estimated as the fraction of time that discharge exceeds the mean annual discharge[*Konrad and Booth*, 2002; *Yang et al.*, 2010]. A low Tq_{mean} is indicative of a flashy hydrograph while a high Tq_{mean} is indicative of flow attenuation.

The FDC describes the relationship between flow magnitude and frequency by plotting discharge against the proportion of the observation period in which that discharge has been equaled or exceeded. Area-normalized FDCs were plotted to compare responses between tiled and non-tiled catchments. While FDCs represent exceedance probabilities for a specific discharge, the concept of Lorenz Curves (LC), which was originally developed in the field of economics to illustrate income inequality, can be used to show cumulative exceedance probabilities (x-axis) for cumulative discharge (y-axis). If flow were to be perfectly distributed over time, all points will fall

along the diagonal of the Lorenz Curve. This line of perfect equality is the upper limit of the Lorenz Curve.

The lower limit of the Lorenz curve is the line of perfect inequality where all of the flow is allocated to a single observation. The Gini coefficient is a metric that describes the deviation of the Lorenz Curve from the line of perfect equality. A perfectly unequal distribution, where the total discharge would be observed in a single day, would result in a Gini coefficient of 1. Mathematically, the FDC, Lorenz Curve and Gini coefficient can be expressed as:

Flow Duration Curve:

$$P(X \geq x) = 1 - \int_{-\infty}^{x} p(x)dx \qquad (2.1)$$

Lorenz Curve (LC):

$$Y(X(x)) = \frac{\int_0^x xp(x)dx}{\int_0^\infty xp(x)dx} \qquad (2.2)$$

Gini Coefficient (G):

$$G = 1 - 2\int_0^1 Y(X)dX \qquad (2.3)$$

where the probability P that a random variable X is greater than x is related to the variable's probability distribution $p(x)$ to produce the FDC. The FDC, LC and Gini Coefficient are useful metrics that provide information on the distribution of flow values over the year, and are expected to provide greater insight on the effect of tiling on the flow regime, rather than merely on the peak flow or baseflow fractions.

2.2.2.2 Hydrograph Recession Analysis

Hydrograph recessions provide valuable insight into a catchment's storage characteristics and mean catchment residence time [*Tallaksen*, 1995; *Wittenberg*, 1999; *Wittenberg and Sivapalan*, 1999]. Both linear and non-linear models have been used to describe catchment recession response [*Tallaksen*, 1995; *Wittenberg*, 1999]. Boussinesq's nonlinear solution of free surface groundwater flow was used to develop a kinematic equation to describe hydrograph recession [*Brutsaert and Nieber*, 1977], which if assuming a linear model, results in an equation describing a linearized Dupuit-Boussinesq aquifer:

$$Q(t) = Q_0 e^{-kt} \qquad\qquad (2.4)$$

Where Q_t is the discharge at time *t*, and Q_0 is the initial discharge value. The coefficient *k* in Equation 2.4 is referred to as the recession constant and in traditional analyses is considered to be constant through time for a particular basin. The dilemma in enumerating a consistent description of recession behavior is that many times there is a large amount of variability between recession segments occurring within the same catchment [*Tallaksen*, 1989; 1995]. There are many explanations for this variability, including the history of recharge events, slope variability, agricultural practices, and the subjectivity of the methodology [*Harman et al.*, 2009].

While it has been shown that nonlinear models can outperform simple exponential decays in describing recession behavior, often the linear model is chosen for its simplicity and adequate accuracy [*Dijk*, 2010; *Tallaksen*, 1995]. The applicability of both linear and non-linear models in describing the recession behavior of tiled and non-tiled catchments was explored in our analysis, with the power law being used to describe non-linear behavior:

$$Q(t) = at^b \qquad\qquad\qquad (2.5)$$

Where *a* is a scaling parameter and *b* is a shape parameter.

Two methods were used to estimate catchment recession behavior: (1) Master Recession Curve (MRC) method and (2) Ensemble Method. The MRC method is based on fitting a single exponential model through the entire dataset of recession segments [*Arnold et al.*, 1995; *Nathan and Mcmahon*, 1990; *Posavec et al.*, 2006; *Toebes and Strang*, 1964]. There are traditionally three methods for developing MRCs; the correlation method, the tabulating method, and the matching strip method [*Toebes and Strang*, 1964]. For this study the matching strip method was used to aggregate the recession segments, primarily because it does not presuppose an exponential decay to describe recession behavior. The method involved rank sorting all recession segments during a period of interest based on their initial discharge value (Q_0), and then plotting them to create a continuous curve. The investigator can then fit a model of their choosing, be it linear or nonlinear to the continuous curve. The automated version of the matching strip method created by [*Posavec et al.*, 2006] was used in this study, with Equations used 2.4 and 2.5 fit to the data.

The Ensemble method is based on fitting each recession segment in the period of interest using a regression model of the investigator's choice to evaluate its respective recession constant. Thus, instead of a single aggregation of segments for a site, a distribution of recession descriptions is generated. If applying the exponential model this implies a distribution of recession constants (*k*) is generated. This method provides certain advantages over the more typical methods in that it can allow for a probabilistic interpretation of recession behavior [*Biswal and Marani*, 2010; *Botter*, 2010; *Wang and Cai*, 2010]. As with the MRC method, both Equations 2.4 and 2.5 were fit to the data to evaluate linear and non-linear behavior. Criteria imposed on the method were that each recession segment had to be at least 4 days long and each catchment must have at least 50

recession segments during the period of interest. Additionally, to avoid the influence of surface runoff, the first three days of each segment were eliminated from the analysis.

<div align="center">2.3 Results and Discussion</div>

<div align="center">2.3.1 Flow Variability and Inequality</div>

2.3.1.1 Mean Annual Runoff Ratio

The mean annual runoff ratio (Q/P) did not vary significantly between basins, or with tiling (Figure 2.2). A mean Q/P ratio of 0.28 ± 0.033 was consistent with typical values noted for the Midwest [*Jayawickreme and Hyndman*, 2007]. The lack of variation of Q/P with tiling is consistent with the overall understanding that tile drainage alters the flow path (surface vs. subsurface) and the distribution of flows, but not the total streamflow. The latter is controlled by the land-use that defines the mean evapo-transpiration (ET) [*Jayawickreme and Hyndman*, 2007]. To minimize the effect of differences in land use on our analysis, we attempted to select basins with significant row-crop cover ($> 40\%$), with a resulting mean cover of $56.3 \pm 23.6\%$. Although ideally we would want to select basins with $\sim 100\%$ row crop cover, practically this is not feasible when synthesizing data at large scales. However, the relative constancy of Q/P over the 24 basins studied indicate that differences in water balance change driven by land use and ET is minimal in these basins. The metrics in the remaining portion of the analysis will focus on the intra-annual distribution of the flow, which is expected to be the primary effect of artificial drainage in the landscape.
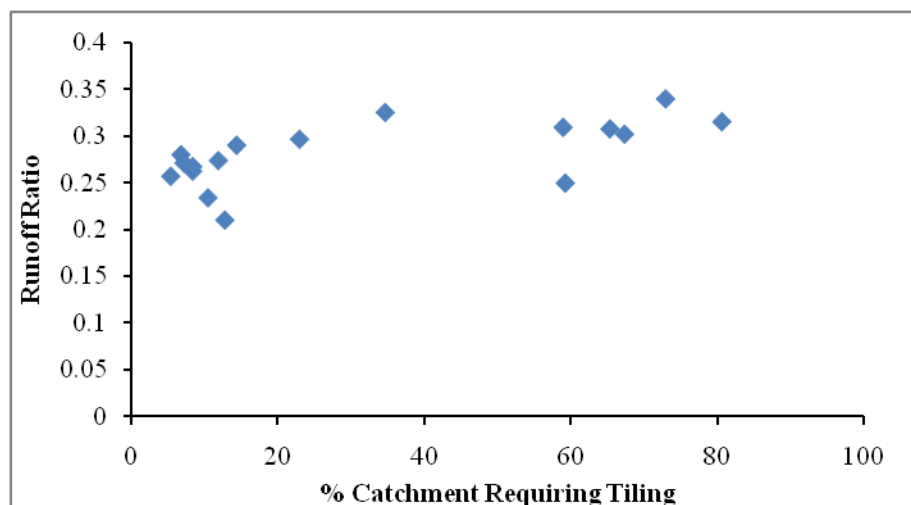
Figure 2.2. Runoff Ratio (Q/P) of the twenty-four study basins as a function of the percent tiling requirement. Limited variability is consistent with understanding that tiling alters flow path but not the total streamflow.

2.3.1.2 Mean Annual Baseflow Ratio

The mean annual baseflow ratio, calculated using the recursive filter outlined in Section 2.2.2, is presented in Figure 2.3. The twenty-four basins interrogated in our study spanned a range of tiling percentages (5% − 80%). In order to explore the question of tiling more closely we isolated six basins with <10% tiling (basins 6, 8, 9, 10, 12, and 13) and six basins with > 50% tiling (basins 14, 15, 16, 17, 18, and 19). This was done so that an equal number of basins could be compared while still providing a perspective on the spectrum of behavior across Iowa. Hereafter, we have referred to watersheds with < 10% tiling as non-tiled systems, while the watersheds with > 50% tiling are referred to as tiled systems. For watersheds with low % tiling (< 10%), the mean annual baseflow ratio increases with scale, from 0.33 at 438 km^2 to 0.77 at 3436 km^2. This is consistent with the understanding of increasing baseflow ratios with scales due to a greater fraction of the aquifer being intercepted at larger scales. For basins with high percent tiling (>

50%), however, this expected response is absent and the baseflow ratio is approximately constant across scales. The relatively constant baseflow ratio of ~ 0.67 ± 0.032 across catchment sizes ranging from 543 – 2,760 km^2 is quite remarkable, and points towards the role of tiles in homogenizing landscape hydrologic responses. For basins with intermediate levels of tiling, the results are mixed as expected.
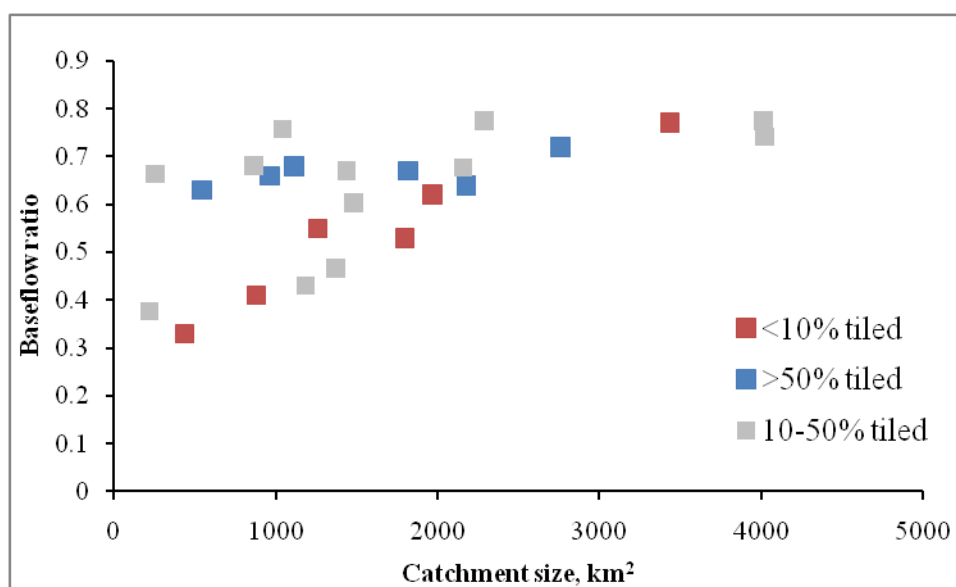
Figure 2.3. Baseflow ratios of the various catchments are presented in the context of catchment scale and partitioned by prevalence of tiling. Scale invariant behavior is observed in the tiled (> 50% tiling) regions, while an increasing trend in baseflow ratio with increasing drainage area is observed in non-tiled (< 10% tiling) regions.

At smaller spatial scales (~ 500 km^2), baseflow ratios of basins with >50% tiling was approximately twice that of basins with <10% tiling (Figure 2.3). This is consistent with the understanding that tiling leads to greater fraction of the flow being transported through the subsurface pathway and thus an increased baseflow ratio. [*K E Schilling and*

Helmers, 2008] found a 3-fold increase in the baseflow ratio in DRAINMOD simulations using tiled and non-tiled cases to simulate flow in a 51.3 km^2 watershed. This difference between baseflow ratios in tiled and non-tiled basins disappeared at larger scales, and the basins converged to a constant baseflow ratio of ~ 0.67 (Figure 2.3). These results indicate that tiling impacts hydrologic responses at smaller spatial scales, but the effect disappears at larger scales, which was also consistent with findings from [*K E Schilling and Helmers*, 2008].

The caveat in this analysis is that the twenty-four basins studied were also different with respect to other attributes like percent row crop coverage or slope. The confounding effect from multiple factors is almost always true in data synthesis studies at larger spatial scales. To explore the effect of row crop coverage further, we examined 5 basins within the dataset that have row crop coverage of 51 to 53%, but increasing tiling percentages (14 to 23%). A Pearson's linear correlation coefficient of 0.64 was observed between increasing baseflow ratio and increasing percentages of tiling, which corroborates the hypothesis that tiling increases baseflow ratio. We further compared catchments #14 and #24, which were of similar size (~1100 km^2) and had similar row crop coverage (~ 80%), but different tiling percentages (#14 had a 65% tiling and #24 had 12% tiling). Consistent with our previous observations of tiling increasing baseflow ratio, #14 had a baseflow ratio of 0.76 while #24 had a baseflow ratio of 0.68.

2.3.1.3 Peak Flow Response

There lies considerable interest in evaluating if tiling affects flood response. To explore this question, we examined peak flow, 100 year and 500 year flood frequencies as a function of catchment size. At smaller spatial scales, the area normalized peak discharge Q_P (L^3/L^2) for the tiled basins was lower than the non-tiled basins, while the differences between the two decreased with increase in scale (Figure 2.4). Consistent

with the previous observations, Q_P for tiled basins was scale invariant, while peak flows decreased with increase in spatial scale in the non-tiled basins (Figure 2.4). Similar results were also observed for the 100 year and 500 year flood frequencies. A noteworthy result is that the difference in area normalized discharge between a 100 year storm and a 500 year storm is relatively low in the tiled regions (Figure 2.5). These two results are indicative of the efficiency with which the improved drainage of the tiled regions removes water from the landscape with limited dependence event size.
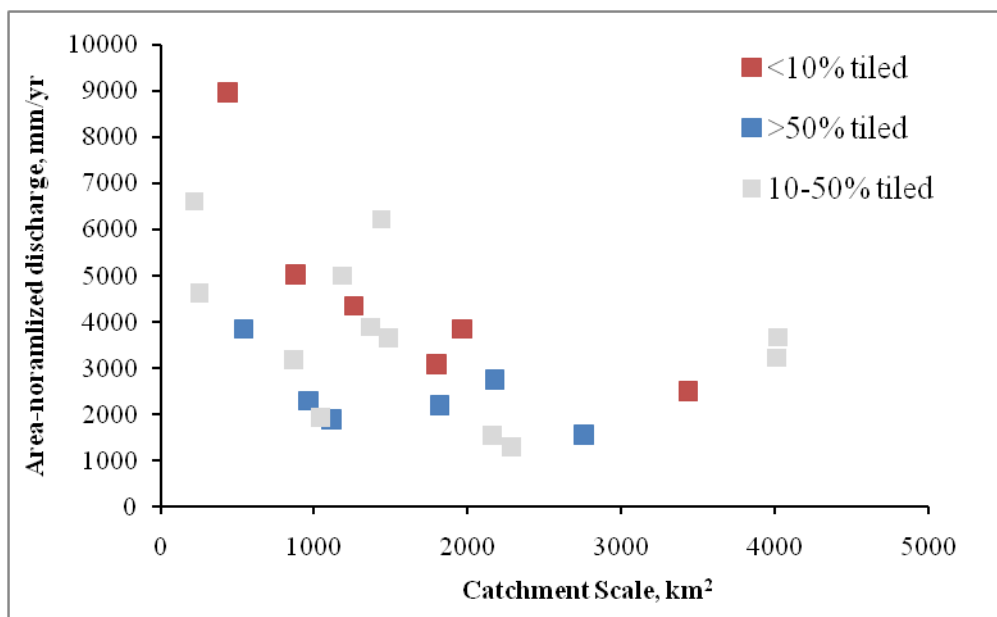
Figure 2.4. Mean annual peak of area-normalized discharge is plotted in the context of spatial scale and prevalence of tiling. In comparing catchments of similar drainage areas, values are lower in tiled regions than non-tiled. Scale invariance is also observed in the tiled regions.
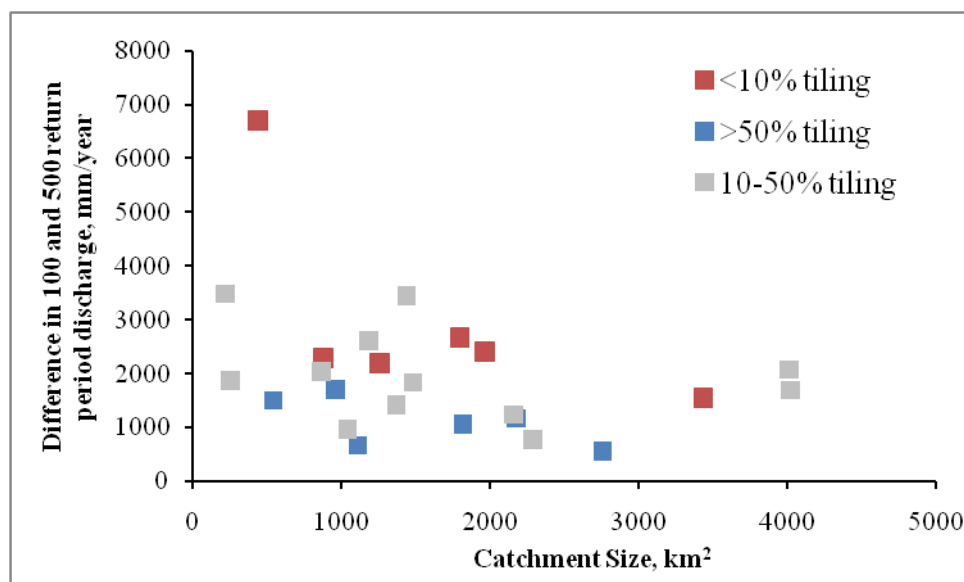
Figure 2.5. Differences between discharges associated with 100 year and 500 year storm events are presented as area-normalized values. Results show relatively low differences between storm discharges in tiled regions, suggesting that responses to extreme events artificially drained basins are less sensitive to event size

2.3.1.4 Fraction of time that daily mean flow exceeds

annual mean flow

The results of the Tq_{mean} calculations presented in Figure 2.6 substantiate what is becoming a prevalent difference between tiled and non-tiled systems. The Tq_{mean} of tiled landscapes is scale invariant, while it increases with increase in scale for non-tiled landscapes. A higher Tq_{mean} is indicative of a flashier system; at smaller spatial scales the Tq_{mean} of tiled landscapes is greater than non-tiled systems, while the differences between the two decrease with increase in scale. The average Tq_{mean} for the non-tiled set of basins is 21.5 ± 0.31 and is 28.3 ± 0.019 for the set of tiled basins. The lower mean value for the non-tiled basins is indicative of the higher slopes prevalent in these catchments, which leads to more "flashy" responses [*Konrad and Booth*, 2002].
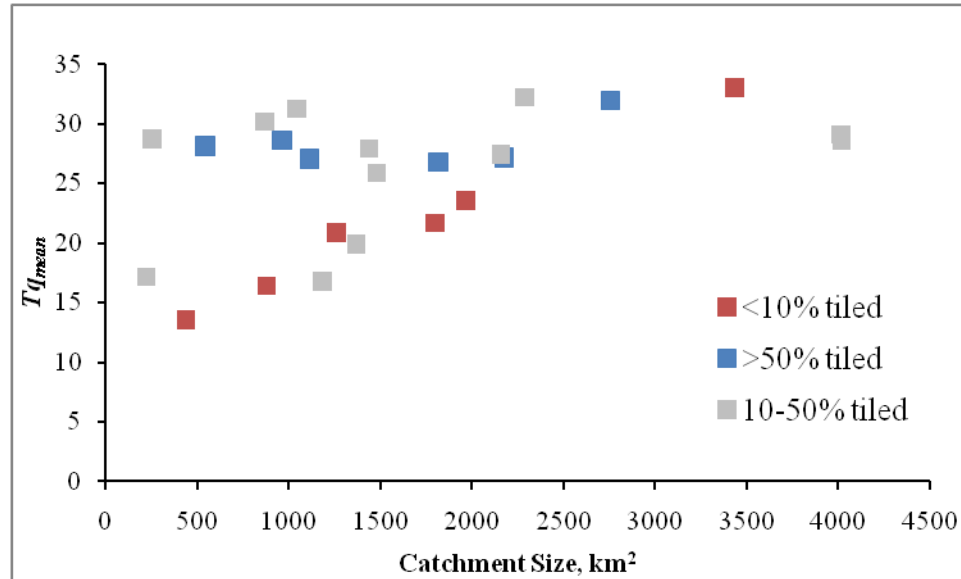
Figure 2.6. Tq_{mean} is plotted versus catchment size. Values represent the average number of days per year that the mean annual discharge value is exceeded. Results indicate that non-tiled systems are flashier than tiled systems. Additionally, scale invariance in tiled systems that has been observed in other metrics is paralleled here.

2.3.1.4 Flow Duration Curves

The flow duration curves (FDCs) for the six basins with < 10% tiling and six basins with greater than 50% tiling are presented in Figure 2.7 (A) and (B), respectively. An impression consistent with the results of the previous analysis is provided by the large scatter in the FDCs of the non-tiled regions as compared to the tiled regions. Thus, tiling not only homogenizes the peak flow and the partitioning of streamflow into stormflow and baseflow, it homogenizes the entire temporal distribution of flows at all spatial scales.
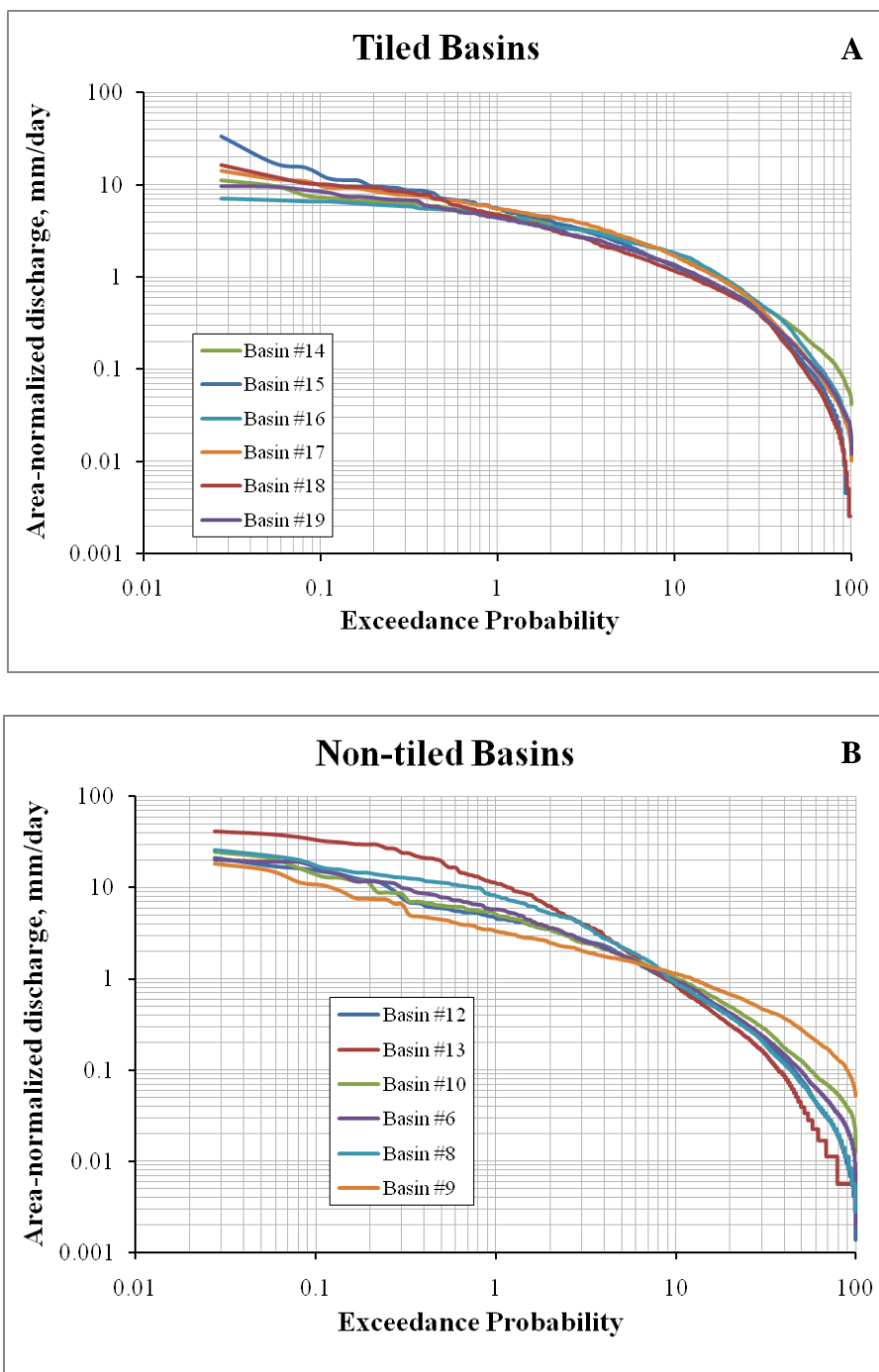
Figure 2.7. Log-log plots of flow duration curves for (A) the 6 catchments with >50% tiling and (B) the catchments with <10% tiling. Across the range of flows observed in tiled regions there is limited variability; a single flow duration curve could be used to describe all flow in all 6 basins. This is in contrast to the non-tiled basins, which display a more typical variability in hydrologic response

2.3.1.4 Lorenz Curve and Gini Coefficient

The Lorenz curves for the six basins with < 10% tiling and the six basins with > 50% tiling are presented in Figure 2.8. As evident in the other metrics interrogated so far, the range of variability in the Lorenz curves for the tiled basins is much lower than the non-tiled basins. Lorenz curves are a measure of temporal inequality in flow. In tiled basins, 25 - 35% of the time accounts for 80% of the flow, an observation that is consistent for basins ranging from 543 km^2 to 2760 km^2. In contrast, in non-tiled basins 8% of the time accounts for 80% of the flow at smaller spatial scales, while at larger scales 42% of the total time period is responsible for the same flow percentage. The Gini coefficient describes the deviation of the Lorenz Curve from the line of equality. Consistent with our previous observations, the Gini coefficient is homogeneous across scale in tiled basins, while the effect of scale and landscape heterogeneity becomes much more evident in non-tiled systems. The lower absolute magnitude of the Gini coefficient for the tiled basins, especially at smaller scales is consistent with the observations before that the tiled basins have a more damped response to precipitation inputs.
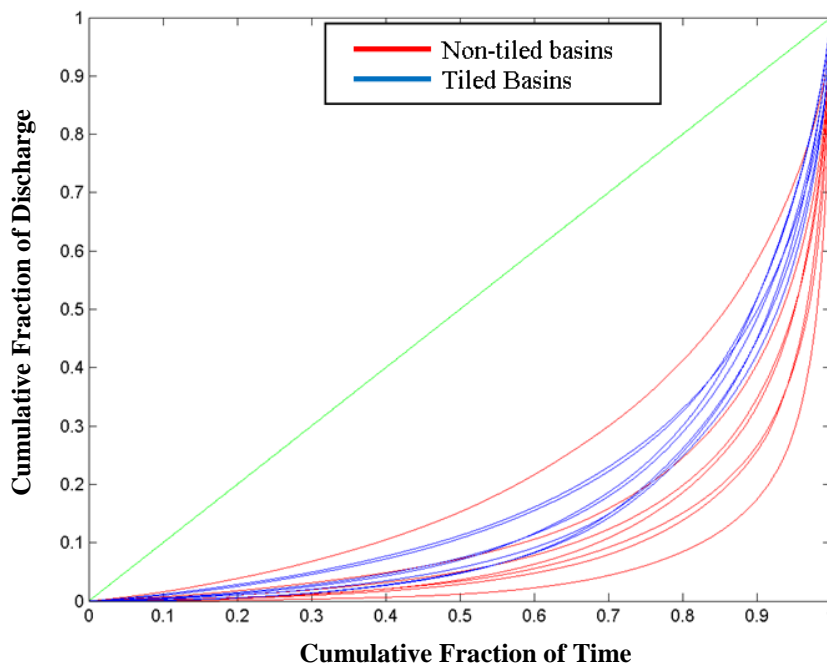
Figure 2.8. Lorenz Curves, which are a measure of the inequality in temporal distribution of total discharge, for the six tiled and six non-tiled catchments. Results indicate greater variability non-tiled basins compared to tiled basins.

2.3.2 Streamflow Recession

Before delving into the recession behavior of the various watersheds included in this study, the validity of the linear and non-linear models for describing hydrograph recession was evaluated. Using both MRC and ensemble methods, the quality of fits of exponential and power law models were quantified using the coefficient of determination (R^2). The overall result of this comparison is shown in Figure 2.9. For the MRC method, the mean R^2 value produced by the non-linear model is slightly greater than the linear model, though statistically there is no difference in the distribution of values produced by both models. For the ensemble method, on the other hand, the linear model outperforms the non-linear model when considering only mean values. Further, the variability in quality of fit is much smaller in the ensemble method than in MRC method. This is

likely due to the fact that each R^2 value is based on a much smaller number of points in the ensemble method than in the MRC method.
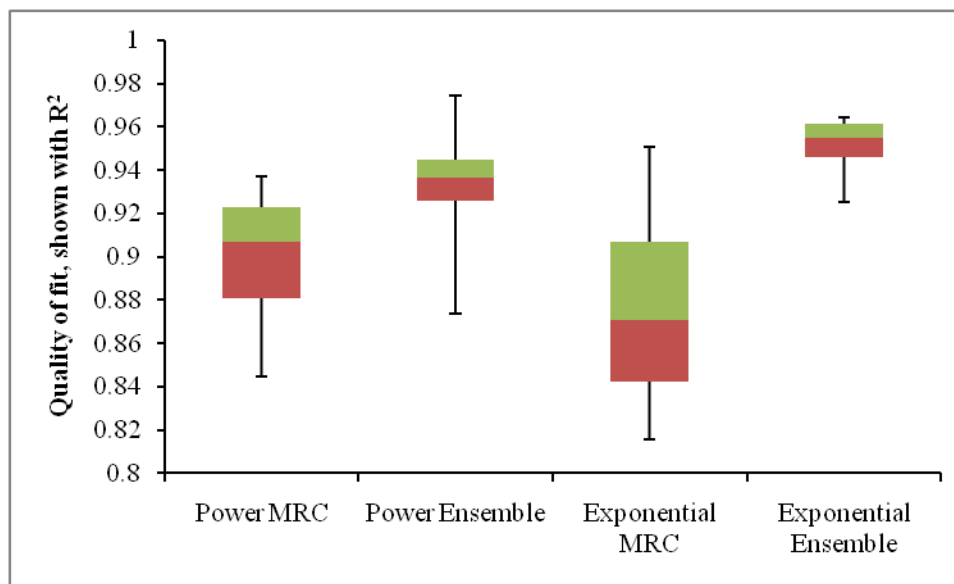
Figure 2.9. Comparison of the performance of power and exponential models in describing recession behavior, as measured by the coefficient of determination (R^2). Results are presented in the context of the two different methods used to apply the models. Results indicate that the exponential model performs comparably to the power model thus the exponential fit is adequate for describing recession behavior.

The absence of first order catchments in the analysis may aid in explaining the competitiveness of the exponential model. An increase in the coefficient of determination for the MRC method as likelihood of tiling increases occurred. The coefficient of determination derived from the MRC method is plotted in the context of tiling and catchment size in Figure 2.10. In relation to the two sets of basins highlighted in the previous section, the average R^2 value for the non-tiled basins is 0.86 ± 0.03 while

for tiled basins it is 0.92 ± 0.03. While both values are high enough to verify the validity of applying the linear reservoir model, the increased R^2 suggests that the presence of tiling may linearize the storage-discharge relationship, as proposed by [*K E Schilling and Helmers*, 2008]. Additionally, the exponential model had an R^2 value that was higher in the tiled regions versus the non-tiled regions, based on the results from the ensemble method. The significance was quantified using the Kruskal-Wallis test, which provides a p-value for the null hypothesis that all samples are drawn from the same population, thus the closer to zero the p-value is the more significant between the two sets of data compared. The p-value was 6.6737e-7. The test has a null hypothesis that all samples are drawn from the same population, thus if the p-value is close to zero the two samples are drawn from different groups. [*Harman et al.*, 2009] found that nonlinear recession behavior arose from landscape heterogeneities; perhaps the opposite can be said for homogeneous landscapes.
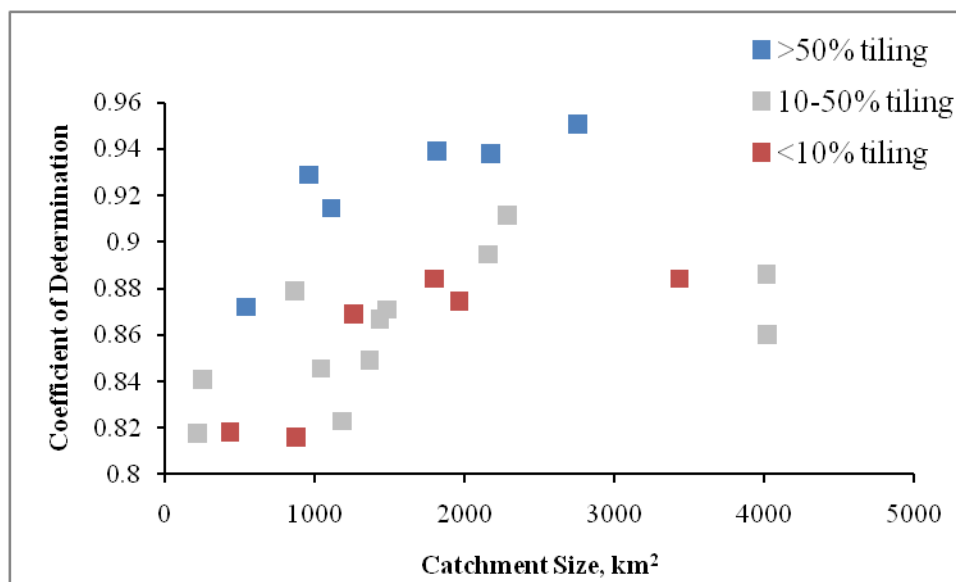
Figure 2.10. Coefficients of determinations (R^2) resulting from fitting Master Recession Curves with an exponential model. Higher values were observed for tiled catchments, suggesting a linearization of the storage-discharge relationship with increasing tiling.

Since there was not a significant difference between the quality of fits obtained by the linear and non-linear models, the effect of artificial drainage on recession behavior was evaluated using the linear model, which is attractive because of its parsimony. The calculated recession constants based on the Ensemble and the MRC methods are presented in Figure 2.11 (A) and (B), respectively. Both the mean and the variance in the recession constant decreased with an increase in tiling. The decrease in the absolute magnitude of the recession constant indicates that hydrographs in tiled regions are less flashy than those in non-tiled regions. The decrease in the variability in the recession constant is consistent with our observation of tiling homogenizing hydrograph responses. A final interesting point is that the presence of tiling reduces the correlation between the discharge level and the rate of recession.
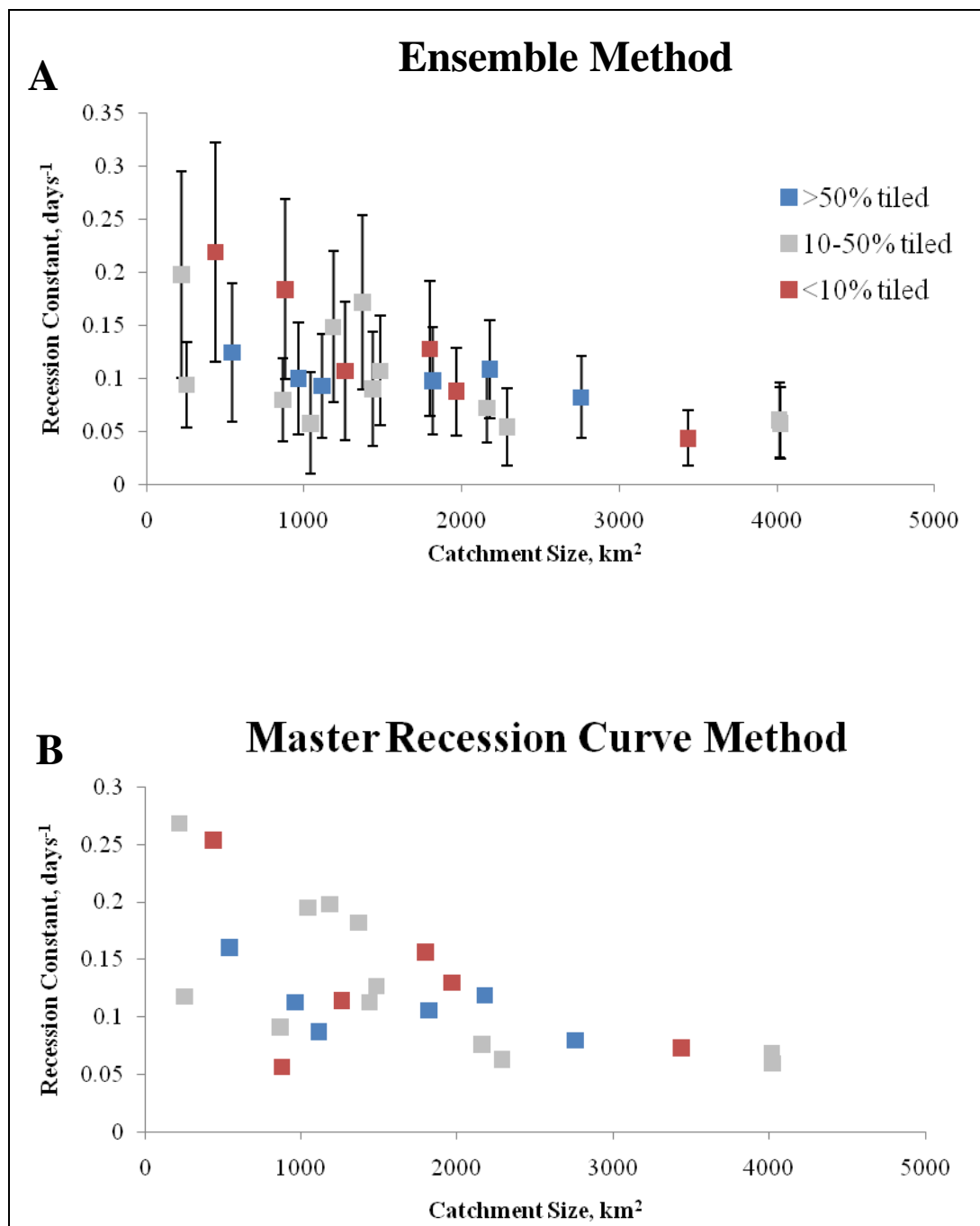
Figure 2.11. Recession constants calculated using (A) the Ensemble method and (B) the Master Recession Curve (MRC) method. Points in (A) are based on mean values, while the error bars indicate the standard deviation of the recession constant for each basin.

2.4 Summary

2.4.1 Artificial drainage homogenizes hydrologic response

The effect of artificial drainage on the streamflow distribution was analyzed by comparing watersheds within the state of Iowa with different percentages of artificial drainage. The most noteworthy finding of this study is that the presence of artificial subsurface drainage leads to homogenization of landscape responses; that is the spatial and scale dependence of the streamflow distribution that is present in natural landscapes is absent in tiled regions. For tiled basins, the within year distribution of flow characteristics (peak flow, baseflow, recession constant) is independent of soil characteristics and spatial scale of observation. In contrast, non-tiled watersheds exhibited peak flow decreases (due to flow attenuation) and baseflow increases (due to greater fraction of the aquifer being intercepted) with increase in the spatial scale. What is the physical mechanism responsible for such homogenization of landscape responses by tiling?

One possible explanation is that since tiles are consistently placed at approximately 1 m below the land surface, their installation may have taken what was originally a spatially variable phreatic surface and homogenized it [*Smakhtin*, 2001]. Further, it has been documented that following installation of tiles, a vertical macropore network oriented towards the tiles develops since plant roots preferentially grow in the directions of water in the landscape. The landscape thus co-evolves post installation of tiled to create an effective bypass flow network (through vertical macropore, tiles and surface ditches) that bypasses the complexity of catchment travel pathways characteristic of natural landscapes. We hypothesize that these factors contribute to the homogenization of hydrologic responses in tiled watersheds that is observed in our data synthesis. Future work is required, however, to prove this hypothesis by developing simple models for tiled landscapes.

The other finding of this study is that at smaller spatial scales, tiled landscapes have less flashy hydrographs with smaller recession constants and peak flows compared to non-tiled landscapes. Does this indicate that at smaller scales tiling decreases flashiness of hydrographs, and thus flooding? In order to answer this question one must first acknowledge that areas of the landscape considered in this study that are tiled are low lying areas with lower slopes (<1.2%) that might have corresponded to slow draining wetland areas in the 1900s. In contrast, the non-tiled areas are the ones that have greater slope (> 3.3%) and must have always been relatively well drained. Thus, the natural landscape had a distribution of recession constants, from prairie pothole wetlands with drainage times in the order of months [*Halford and Mayer*, 2000], to areas with larger slopes and faster recessions [*Zecharias and Brutsaert*, 1988]. Human intervention, aimed at maximizing benefit from the landscape (by row crop agriculture), drained the slow draining areas by tiling and increased recession constants to be greater than in the original low lying wetlands, and closer in magnitude to areas with greater landscape relief. Thus, despite the fact that tiled watersheds have lower peak flows than non-tiled watersheds, it is possible that the peak flows have actually increased post tiling. This is a hypothesis that needs to be proven by developing a model for tiled landscapes, since the availability of such long term data is sparse.

Finally, the differences between tiled and non-tiled landscapes disappear at scales approximately >2,200 km^2 and responses converge to consistent baseflow and peak flow ratios. The effect of channelization and in-stream attenuation dominating at larger scales is attributed to such convergence of responses. This also indicates that 2,200 km^2 is probably a threshold scale and thus studies on the effect of tile drainage should focus on scales that are smaller.

2.4.2 Implications for agricultural landscapes

The findings of this study have significant implications for modeling hydrologic responses in agricultural catchments. Scale independence implies that it might be possible to develop more parsimonious hydrologic models for this regions, such as the approach presented by [*N Basu et al.*, 2010]. Most importantly, the results indicate a distinctly different hydrologic signature in tiled landscapes compared to non-tiled, so they must be modeled differently. Current efforts based around hillslope scale models must address the role the significant role groundwater plays in contributing to total flow, as shown by the increased baseflow ratios [*J C Rozemeijer et al.*, 2010; *van der Velde et al.*, 2010].

The short-circuiting of typically heterogeneous flow patterns found in this study provides a lens to focus understanding of the filtering action of the landscape. This would aid in developing simplified models for streamflow prediction based on a small number of parameters that are quantifiable and consistent. The uniform nature of the tile drains that are providing the short-circuit route may also allow for a more consistent quantification of recession behavior, or at least produce a more uniform recession response. With some catchments having more than 80% of land use devoted to row crops, and these row crops associated with massive environmental concerns, it is important that any simplification that aids in modeling efforts be identified and analyzed. If basin-wide issues such as gulf hypoxia are to be adequately understood, the propagation of anthropogenic signatures such as artificial drainage must be more readily understood in order to enhance modeling and management efforts.

CHAPTER 3: NUTRIENT REGIMES IN AGRICULTURAL

CATCHMENTS

3.1 Introduction

Anthropogenic signatures manifest in intensively managed catchments through the homogenization of the hydrologic response, as illustrated in Chapter 2. These patterns in hydrology are expected to be paralleled by emergent behaviors in the biogeochemical responses of watersheds, particularly due to the fact that hydrology plays an integral role in driving these cycles. Riverine export of nutrients is a major component of nutrient cycles, particularly with respect to nitrogen; 25 percent of terrestrially applied nitrogen is removed via riverine export [*Galloway et al.*, 2004]. This is significant due to the direct links between nutrient loads and hypoxic zones in coastal regions [*Rabalais et al.*, 2010]. The impact of this export on receiving water bodies is quantified and regulated using the concept of Total Maximum Daily Loads (TMDLs), a regulatory term put forth by the U.S. Clean Water Act (CWA) of 1977[7]. The method of calculating the load (*L;* M/T) delivered by riverine transport is to find the product of the discharge (*Q*; L^3/T) of the stream and the respective concentration (*C*; M/T) of solute associated with that discharge. Thus, variations and covariations in *C* and *Q* are important to the calculation of *L* [*Borsuk et al.*, 2004].

While the variations of both *C* and *Q* play an important role in calculating *L*, it has recently been brought to light that variations in *C* are often several orders of magnitude lower than variations in *Q* [*N B Basu et al.*, 2010; *Godsey et al.*, 2009; *Guan et al.*, 2011]. This behavior was initially demonstrated by [*Godsey et al.*, 2009] using geogenic solute export in pristine catchments. Fifty-nine catchments from the U.S. Geologic Survey's Hydrologic Benchmark Network (HBN) with drainage areas ranging

---

[7] http://water.epa.gov/lawsregs/lawsguidance/cwa/tmdl/index.cfm

from 6 to 5196 km^2 that have been sampled between 5 and 7 times per year for 30 years were used for the analysis [*Godsey et al.*, 2009]. They found that concentrations of solutes such as Ca, Mg, Na, and Si produced by mineral weathering varied by factors of 3 to 20, while discharge varied by several orders of magnitude. This relatively limited variability in *C* compared to *Q*, termed "chemostatic" behavior, was interpreted as implying that solute production (due to weathering) and mobilization was directly proportional to water fluxes, and thus solute loads are determined by water fluxes. The authors evaluated chemostatic behavior by fitting a power law ($C = aQ^b$) to the *C-Q* data and assessing how close to zero *b* was, with $b = 0$ representing perfectly chemostatic behavior. Such chemostatic behavior leads to a linear relationship between *L* and *Q*, with perfectly chemostatic behavior corresponding to a linear relationship ($R^2 = 1$) between *L* and *Q*. This finding is an example of how an emergent pattern in watershed response allows for a simplified understanding of biogeochemical behavior. *Godsey et al.* (2009) then use these patterns to infer the impact of alterations in riverine flow, caused by climate change or anthropogenic withdrawals, on ocean alkalinity. While these observations of chemostatic response have significant potential applications, they were limited to geogenic solutes. Recent work however, has observed similar chemostatic responses in the export of nutrients from agricultural catchments.

Basu et al. (2010) observed chemostatic behavior of nutrient solutes exported from intensively managed agricultural catchments across the world. Two major nutrients, Total-N (TN) and Total-P (TP), were evaluated across 21 catchments (10^4 to 10^6 km^2) within the Mississippi-Atchafalaya River Basin and 14 catchments (10^2 to 10^5 km^2) in the Baltic Sea Drainage Basin. The authors observed what they termed biogeochemical stationarity, which is synonymous with chemostatic behavior; that the relationship between *L* and *Q* was linear. This indicates that the annual flow-averaged concentration $C_{f,a}$ of TN is insensitive to water yield. A high R^2 value of the *L-Q* fit was used to indicate the existence of chemostatic behavior.

The authors hypothesized that intensive agricultural activity over the past several decades have led to the development of a ubiquitous legacy of nutrient stores in the landscape. This legacy build-up can be considered analogous to the availability of weathering products observed by [*Godsey et al.*, 2009] for geogenic solutes. While the ubiquity of geogenic solutes leading to chemostatic response is intuitively obvious, such response for anthropogenic solutes like nitrates is hypothesized to arise from human activities over decades that has created legacy sources of N. This ubiquitous legacy store of nutrient in the landscapes leads to anthropogenic solutes such as N acting like geogenic solutes. The hypothesis was confirmed by exploring nutrient exports from pristine catchments [*Thompson et al.*, 2011] where legacy build up was absent and non-chemostatic behavior was apparent. The lack of linearity between L and Q observed in the pristine catchment provides evidence that the patterns observed elsewhere were not merely a facet of spurious correlation [*Kenney*, 1982]. The linkage between biogeochemical stationarity and legacy build-up allowed *Basu et al.,* (2010) to characterize the fluxes of nutrients from agricultural catchments as transport limited, analogous to the availability of weathering products. This is in contrast to a supply limited scenario that was observed in nitrate export from the pristine catchment.

The datasets that have been used to test the chemostatic hypothesis for nutrients in managed catchments have been primarily at coarse temporal resolution (weekly to a few times a year). It is difficult to establish relationships between concentration and discharge using such low resolution data. Further, the estimation of annual loads is subject to interpolation errors, which leads one to question whether the observed linearity between L and Q is an artifact of such errors. To answer this question in this chapter we will explore C-Q and L-Q relationships using high resolution nitrate concentration data. The other question that is relevant to this thesis is the temporal persistence of the slope C_f of the L-Q relationship. As discussed in Chapter 1 and Chapter 4, we have developed a new passive flux meter that measures the flow-averaged concentration over the duration

of a storm event (3 to 5 days), $C_{f,e}$. Thus, we are interested in exploring the following question: What is the relationship between the flow-averaged concentration over a storm event, $C_{f,e}$, the flow-averaged concentration over a month, $C_{f,m}$, and the flow-averaged concentration over a year, $C_{f,a}$? If the event-averaged $C_{f,e}$ is a good approximation of the annual $C_{f,a}$, the measured $C_{f,e}$ can be used to estimate the annual load L without significant loss in accuracy.

Modern technologies now allow near continuous collection of nitrate data, and one such dataset exists for three nested watersheds within the Raccoon River Basin in Iowa. This dataset will be used to explore two broad questions: (1) Does chemostatic behavior that is apparent with coarser temporal resolution time series data persist with finer resolution datasets? (2) How does the flow-averaged concentration change with temporal averaging? The questions will be explored using data collected by the USGS at three nested gaging stations along the Raccoon River System in Iowa.

3.2 Materials and Methods

3.2.1 Site and Data Characteristics

Nitrate plus nitrite concentration data was collected over a four year period by the USGS using a Nitratax sonde fixed in the streamflow that measured solute spectrophotometrically at three nested USGS gaging stations along the Raccoon River system that drains north-central Iowa (Figure 3.1). The parameter being measured and presented here is unfiltered nitrate plus nitrite concentration in milligrams per liter as nitrogen. Due to the high ratio of nitrate to nitrite in natural environments, the concentration data will be referred to as nitrate data for ease of reference. The relevant attributes of the data used in the analysis are provided in Table 3.1. Basins I and II are nested and of increasing stream order within III. All data was collected on a 15 minute interval except for the period of 10/26/2006 through 06/04/2008 at the Raccoon River at

Van Meter site, which was collected on a 30 minute interval. The nitrate concentration data acquired from the USGS was paired with 15 minute resolution discharge data (collected at the same locations) to create a dataset of 15 minute resolution concentration-discharge points. Data collection for the most part did not occur during the months of December, January, or February.

Table 3.1. Relevant information pertaining to the high temporal resolution nitrate data used in the analysis; a site ID was assigned to each location for ease of reference.

Site ID	HUC Code	Station Name	Drainage Area, km^2	Period of NO_3^- Data
I	05482300	North Raccoon River near Sac City, IA	1813	03/26/2008 to 09/30/2010
II	05482500	North Raccoon River near Jefferson, IA	4193	04/02/2008 to 09/30/2010
III	05484500	Raccoon River at Van Meter, IA	8912	10/25/2006 to 9/30/2010
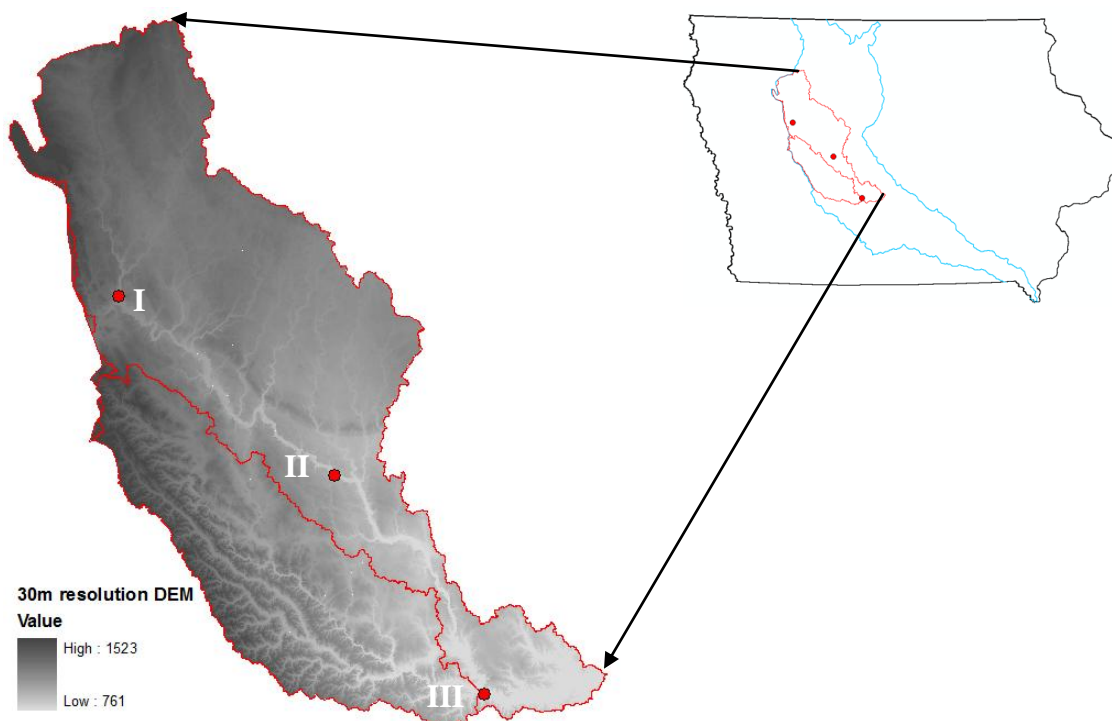
Figure 3.1. Location of USGS gage stations where continuous nitrate data was collected. A 30m digital elevation model of the 8 digit HUCs that the sites are located in is also provided. 8 digit HUC borders are outlined in red while 6 digit HUC is outlined in blue; data courtesy of the Iowa DNR [*Conrad*, 2004; *IDNR*, 2005; *NRCS-Iowa*, 2008; *USGS*, 1999].

3.2.2 Evaluation of Chemostatic Response

The existence of a chemostatic response in the three catchments outlined above shall be evaluated through the use of two metrics taken from the studies mentioned earlier. *Basu et al.* (2010) investigated the extent of biogeochemical stationarity by the coefficient of determination (R^2) of a zero-intercept linear fit of the annual *L-Q* relationship. This method will be applied to the available data, but due to a lack of multiple years of data, monthly *L-Q* relationships will be used instead of annual *L-Q*. To address concerns of spurious correlation, due to the definition of *L* as the product of *C*

and Q [*Kenney*, 1982], the other metric that will be used is the ratio of the coefficients of variation (*CV*) of concentration *C* and discharge *Q*, adopted from [*Thompson et al.*, 2011]. The coefficient of variation is defined as the standard deviation of a dataset normalized by its mean. A chemostatic response is one in which the solute concentration varies little over a wide range of variations in discharge. Thus, a perfectly chemostatic system would have a $CV_C/CV_Q = 0$ [*Thompson et al.*, 2011], with increasing values of the CV_C/CV_Q ratio indicating divergence from chemostatic behavior. This metric will be calculated for each site and compared to values for geogenic and nutrient solutes taken from [*Thompson et al.*, 2011]. We will also explore the relationship between concentration and discharge which is expected to provide further insight into the the emergent chemostatic response.

3.2.3 Temporal Persistence of C_f

In addition to evaluating the chemostatic nature of nitrate export from the three catchments, the persistence of said chemostatic behavior across different time scales will be evaluated. The studies mentioned thus far have focused on annual, or in the case of [*Guan et al.*, 2011], seasonally averaged values of load and discharge. The term temporal persistence will be used to refer to the impact on C_f of different temporal scales of aggregation. Load and discharge averages based on the event and monthly temporal scales will be compared to annual *L-Q* relationships to determine whether or not there are significant differences. *L* and *Q* will be averaged at a monthly timescale and plotted to generate a monthly flow-averaged concentration $C_{f,m}$. Event averaged concentration, $C_{f,e}$ will be calculated in the same manner; beginning and ends of hydrograph peaks were identified manually. The resulting mean event duration was 9.5 ± 4.6 days with site specific means increasing with scale as expected due to attenuation of hydrograph peaks.

3.3. Results

3.3.1 Evaluation of Chemostatic Response

The calculated values of CV_C/CV_Q for each of the three basins are presented below in Table 3.2. The CV ratio associated with geogenic export, and thus chemostatic behavior was specified as 0.3 by [*Thompson et al.*, 2011]. The CV_C/CV_Q ratio of the three basins range between 0.227 and 0.380 with higher ratios associated with larger spatial scales of observation. The coefficient of determination R^2 of the monthly *L-Q* relationship is also high, corroborating the chemostatic hypothesis (Table 3.2).

Table 3.2. Metrics of chemostatic behavior applied to the three catchments.

Site	R^2	CV_C/CV_Q
I	0.7584	0.227
II	0.8632	0.389
III	0.8826	0.380

3.3.2 Temporal Persistence of C_f

The load-discharge relationship at annual, monthly and event-scale averaging are presented in Figure 3.2 for the three basins. The basins are presented in increasing spatial scale in the vertical direction and decreasing temporal aggregation along the horizontal direction. Note that at the annual averaging time-scale there are only two data-points for basins I and II, so the interpretation of this data should be made with caution. There is a close correspondence (maximum difference = 35%) between the flow-averaged concentrations, especially at the monthly and event time scales. On closer examination, a

decrease in C_f is apparent with decrease in the averaging time window; thus $C_{f,a} > C_{f,m} > C_{f,e}$. This difference, however, decreases with increase in the spatial scale, and is practically non-existent for the largest basin (III). R^2 values at all averaging timescales remained sufficiently high to justify the claim of a linear L-Q relationship. One clear trend in C_f values is that within the nested basins I, II, III, there is a dilution of flow-averaged concentration with increasing scale. This suggests that trends and behavior associated with C_f may be damped as the scales of observation increase.

A closer examination of the L-Q relationship reveals a saturation response at the monthly and event time scales. At higher Q values the load L is lower than would be predicted by a linear L-Q relationship (Figure 3.2). This indicates that concentrations are actually lower at larger flow. To examine this effect further, we censored the data such that L values corresponding to Q values with an exceedance probability of less than 5% were removed from the dataset (Figure 3.3). Exclusion of these high Q (red squares in Figure 3.3) values shifts the L-Q relationship such that C_f remains approximately constant with temporal averaging. An additional point to note is that several of the points excluded correspond to historic flood levels that occurred in Iowa during 2008 and 2010. These impacts are noted at the monthly scale, with green circles around points denoting the flooding periods of 2010 and yellow circles denoting the flooding periods of 2008.
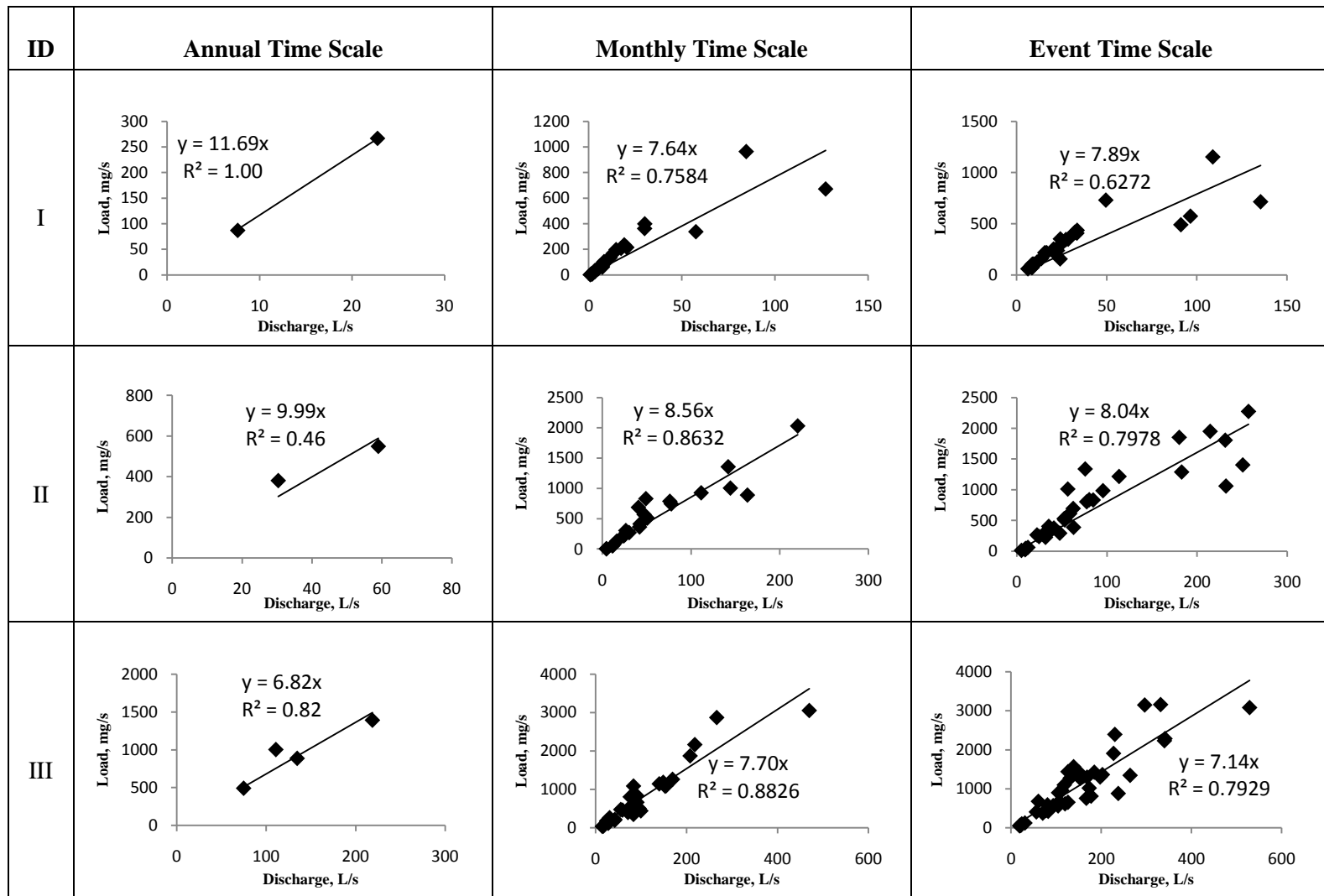
Figure 3.2. Plots of nitrate load versus stream discharge at different spatial and temporal scales of averaging. Temporal aggregation decreases from left to right, while spatial scale increases from top to bottom. The slope of the linear fits is the flux-averaged concentration C_f in mg/L as N.
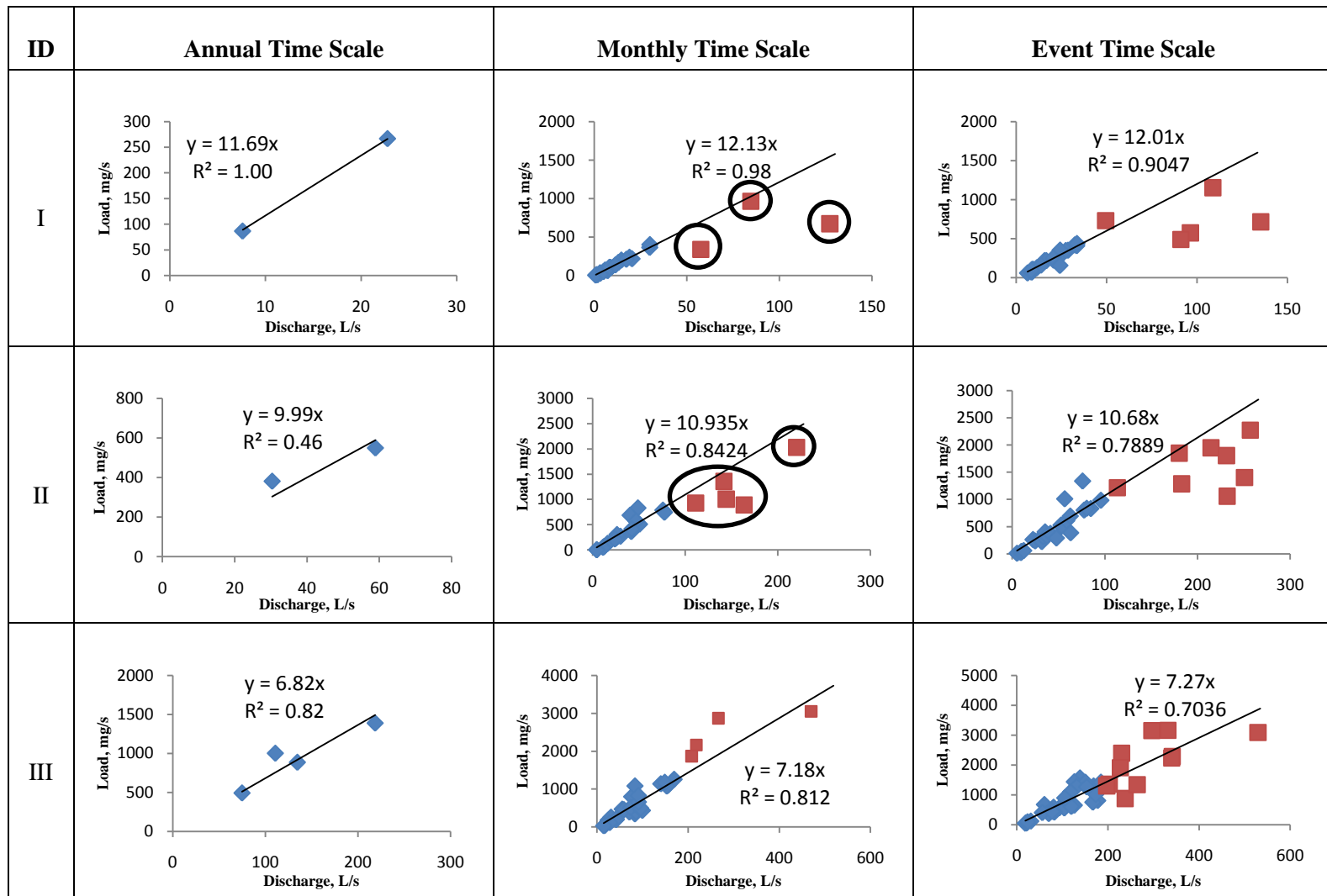
Figure 3.3. Plots of nitrate load versus stream discharge at different spatial and temporal scales of averaging. Temporal aggregation decreases from left to right, while spatial scale increases from top to bottom. The linear fits have been done after removing the discharge values with greater than 5% exceedance probability. The points contributing to the regression are shown in blue, while the excluded points are in red. The slope of the linear fits is the flux-averaged concentration C_f in mg/L. Data points circles in black illustrate dilution caused by historic flooding in Iowa during 2008 and 2010.

The ability of the event-scale C_f to estimate the annual load was evaluated by multiplying C_f with the annual discharge, and comparing the annual load thus estimated with the true measured load. Results from both before and after the exclusion are presented, with multiple results given when more than one year of data is available (Table 3.3). A general trend of under-prediction is observed based on the full range of flows, while over-prediction occurs when high flows are excluded, with an average error of -13% before exclusion reducing to +4% after exclusion.

Table 3.3. Comparison of the percent error of the ability of the event-averaged Cf value to predict mean annual load.

Site ID	Difference between predicted and actual annual load, all Q values considered	Difference between predicted and actual annual load, highest 5% of flows excluded
I (2008)	-32.63%	2.41%
(2009)	-30.64%	5.44%
II (2008)	-13.64%	14.82%
(2009)	-35.90%	-14.78%
III (2006)	-21.18%	-16.98%
(2007)	8.32%	14.08%
(2008)	8.24%	14.00%
(2009)	12.31%	18.29%
Mean	-13.14%	4.66%

An analogous illustration of the impact of removing large events from the analysis is to present the increase in the standard error of the C_f caused by not including data points in the linear regression of L-Q. Table 3.4 compares the loss in accuracy of the two regressions providing the normalized root mean square error (NRMSE) at the event

temporal scale. NRMSE is calculated based on a comparison of the actual data points to the values predicted by the fit, in our case the value of C_f, and is demonstrated by Equation 3.1.

$$NRMSE = \frac{\sqrt{E[(\hat{X}-X)^2]}}{X_{max}-X_{min}}$$ (3.1)

where the square root of the expected value E, or mean, of the squared differences between the estimated value $\hat{X}$ and the actual value X is normalized by dividing by the difference of the minimum and maximum observed value. Site III had relatively little difference in performance, while the performance for sites II and III decreased by 64% and 48% respectively. This loss is due to the previously noted more pronounced attenuation in the linear L-Q response at these sites. While the accuracy in of the linear fit in describing the full data set of L-Q values at each site is lowered, the large increases in the linearity of the L-Q relationship at moderate and low flows is significant, with $R^2 > 0.9$.

Table 3.4. Normalized RMSE of the linear regression between L and Q.

Site	All Q values considered	Highest 5% of flows excluded
I	0.139	0.227
II	0.120	0.178
III	0.121	0.121

3.3.3 Concentration-Discharge Relationships

In order to further evaluate the dilution effects observed in the *L-Q* relationship, we explored the *C-Q* relationship of the raw data and at daily averaging timescales. Three regimes were apparent in the *C-Q* relationship: (a) linear regime where concentration increased linearly with discharge, (b) saturation regime where concentration was invariant with discharge, and (c) dilution regime where concentration decreased with increase in discharge. It is hypothesized that linear regimes (increasing *C* with *Q*) arise at low flows since the entire watershed is not active and contributing. Such increase in concentration with *Q* due to larger and larger portions of the watersheds contributing was also observed in other studies [*Barco et al.*, 2008]. This is followed by the saturation regime in which *C* does not change with increase in *Q*. This could correspond to a scenario in which the entire watershed is contributing and the N mobilization rates from the legacy stores are fast enough to maintain a constant concentration.

The linear regime and the saturation regime fall in the domain of transport limited scenarios described before; there is an effectively "infinite" supply of solute in the landscape and mobilization of solute into the streams is limited solely by the availability of water for transport. Finally, we have the dilution regime where *C* decreases with increase in *Q*. This corresponds to the supply limited scenario. This most likely occurs due to increase in the contribution from the overland flow pathway that is low in nitrate concentrations, and hence results in dilution at high flows. Plots illustrating the three regimes are presented below, with *C-Q* data points based on both the raw 15-minute data and points created from daily averages. To illustrate the three regimes, the 5% exceedance probability used previously as a threshold is denoted by a vertical red line while the observed shift from the linear regime to the saturation regime is denoted by a green line.
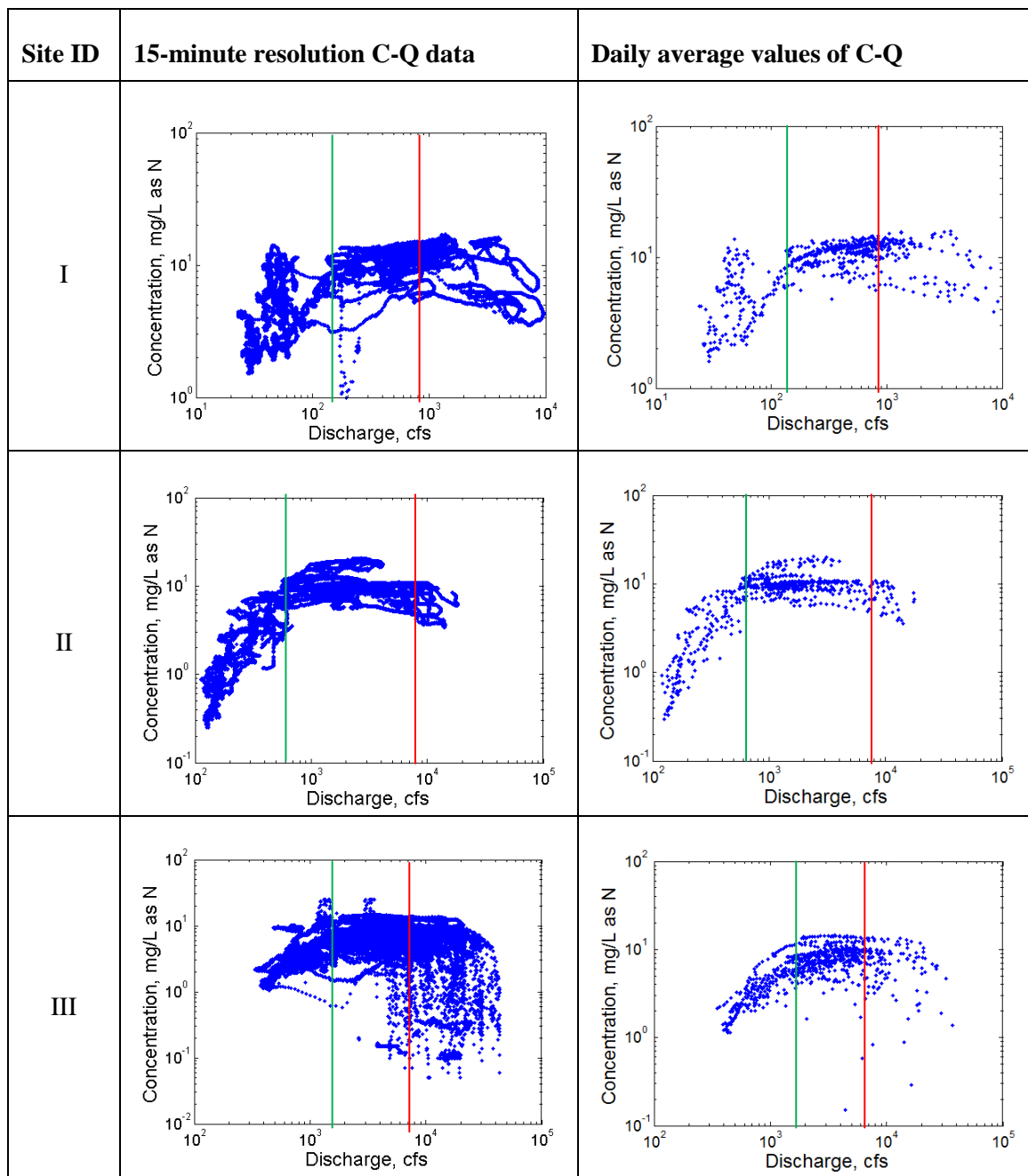
Figure 3.4. Plots of C-Q at 15 minute and daily average temporal resolutions. A red vertical line is used to illustrate the flow corresponding to the 5% exceedance probability and corresponds to shift in regime of constant *C* to increasingly diluted *C*. Green line corresponds to shift in regime of linearly increasing *C* with *Q* to regime in which *C* is constant with increase in *Q*.

3.4 Implications

High frequency (15 minute) discharge and nitrate concentration data in the Raccoon River Catchment was used to evaluate the relationship between concentration (C), discharge (Q), and load (L). Three distinct regimes of nitrate transport were apparent from the C-Q behavior: (1) a linear regime in which C increases with increasing Q, (2) a saturation regime in which C remains constant against increasing Q, and (3) a dilution regime in which concentration decreases as Q increases. The dominance of the saturation regime leads to the observed linearity in the L-Q response. Thus, the lower variability in C compared to Q in managed catchments that was observed by *Basu et al* (2010) and *Thompson et al* (2011) using temporally coarser data is verified using high resolution nitrate data.

This low variability in C relative to Q which leads to linearity in the L-Q response was used to develop the chemostatic hypothesis by *Basu et al.* (2010). The essence of this hypothesis is that in managed agricultural catchments, which have been fertilized for decades, there exists a legacy of nutrient stores in the landscapes that provides a relatively constant concentration. The constancy of the concentration despite year to year variations in temperature, precipitation, microbial kinetics etc. is a unique feature of intensively managed catchments where such stores have accumulated over time [*Thompson et al.*, 2011]. This accumulation is linked with long soil and groundwater residence times that, in conjunction with an organic N half life on the order of decades, result in slow removal of N from the subsurface system [*Haag and Kaupenjohann*, 2001; *Thompson et al.*, 2011]. This hypothesis is supported by previous observations of large stores (1410 kg/ha) of organic N in agricultural landscapes [*Addiscott*, 1996].

The other finding of this study is that the flow-averaged concentration C_f is temporally persistent over event, monthly and annual time scales; that is the flow-averaged concentration over a storm event, $C_{f,e}$, is equal to the flow-averaged concentration over a month, $C_{f,m}$, and the flow-averaged concentration over a year, $C_{f,a}$.

This data synthesis study thus leads to the next chapter in which the initial stages of the design of a passive sampler are documented. The passive sampler is expected to measure the flow-averaged concentration over a storm event that can be used to estimate the annual load without significant loss in accuracy due to the temporally persistent behavior discussed above.

CHAPTER 4: PASSIVE SAMPLER DEVELOPMENT

4.1 Introduction

The emergent patterns in catchment response identified in the previous chapter provide a glimpse into anthropogenic impacts on nutrient cycles while illustrating the opportunity for a new sampling strategy to resolve spatially sparse nutrient data. As discussed in Chapter 1, a passive sampling approach will provide improved estimates of flow averaged concentrations while overcoming the limitations of both discrete and continuous sampling methods. The analysis in Chapter 3 demonstrates the temporal persistence of C_f, thus C_f determined over the scale of a single hydrologic event (3 to 5 days) can be used to estimate the mean annual or seasonal load without significant loss in accuracy. This chapter discusses the initial steps taken towards the design of a passive surface water flux meter. Specifically, laboratory experiments towards sampler design and initial testing are discussed.

4.1.1 Conceptual Framework

The passive sampler will be deployed in the stream water along the flow path, and it is expected to simultaneously measure the flux of water and solute. The flow-averaged concentration is then estimated as the ratio of solute flux and water flow. The device is deployed in the field over a certain period of time (3 to 5 days), and the measured flow-averaged concentration over the deployment period can then be used in conjunction with the measured flow to estimate the total solute load crossing that section. The much lower cost of the device would enable its deployment at multiple spatial locations in the watershed, and provide a more exhaustive dataset that can be used for model development and management decisions. Further details of the device and relevant equations are presented in Chapter 1 (Section 1.3.2 and 1.3.3)

4.1.2 Design Criteria

As discussed in Chapter 1, there are a few alternate designs of PSFM that have been tested in the field. The two primary limitations of the existing PSFM design are as follows: (a) small deployment times (< 0.5 days); (b) steady flow requirement. The requirement of small deployment times is based on the flow rate through the sampler that depletes the alcohol tracers. Previous studies in the groundwater domain indicate that a minimum m_{tr} of 20% is required for reproducible results [*Hatfield et al.*, 2004]. Flow velocities in surface water are orders of magnitude greater than typical groundwater flow velocities necessitating smaller deployment period for similar depletion percentages. The flow velocity through the sampler is a function of the (a) flow velocity in the stream and sampler orientation with respect to this flow that defines the pressure drop across the sampler, and (b) the sampler hydraulic conductivity (*K*; L/T). One of the modifications proposed in the new design is the addition of a sand resistor that reduces the effective hydraulic conductivity, and thus the flow velocity. Reduction of hydraulic conductivity also addresses some of the issues that arise in the field from clogging of the sampler during deployment. Clogging leads to a time-varying *K* during the deployment period, making equations 4.1, 4.3, and 1.9 difficult to implement. Conductivity reduction from 192 to 88 m/day over a 3 day deployment period was observed during some preliminary field testing. The sand restrictor reduces *K* from 160 to ~0.4 m/day, effectively pre-clogging the device and preventing further *K* reduction during deployment.

4.1.3 Chapter Organization

Details on the sampler components (sorbents and physical structure) are provided in Materials and Methods (Section 4.2.1). We have also provided details on sampler preparation before deployment and sorbent analysis after deployment in Section 4.2.2 of Materials and Methods. Finally, details of the methodology for the flume experiments

conducted, for laboratory verification of sampler performance, are provided in Section 4.2.3. Results of the flume experiment are presented in Section 4.3.

4.2 Materials and Methods

4.2.1 Sampler Components and Sorbent Characterization

Two different sampler designs were evaluated; an initial design V1 that was modified to create V2. Both were constructed from PVC piping that has an inside diameter of 11.4 cm^2, but differ in that sampler V1 has a single compartment while sampler V2 is comprised of three compartments. Stainless steel woven wire mesh is used to partition the compartments and to contain the materials within the sampler. For sampler V1, 70x70 mesh is used at the inlet and outlet. For sampler V2, 70x70 mesh was used at the inlet and between the first and second compartments while a 400x400 mesh was used between the second and third compartments and at the outlet. PVC funnels were used at the inlet and outlet of the sampler column to create a streamline design. The sorbent compartment in sampler V1 has a length of 11.5 cm, while sampler V2 compartment lengths are 11.6 cm, 7.8 cm, and 4.2 cm for the first, second, and third compartments. Images of sampler V2 can be found in Figures 4.1 and 4.2.
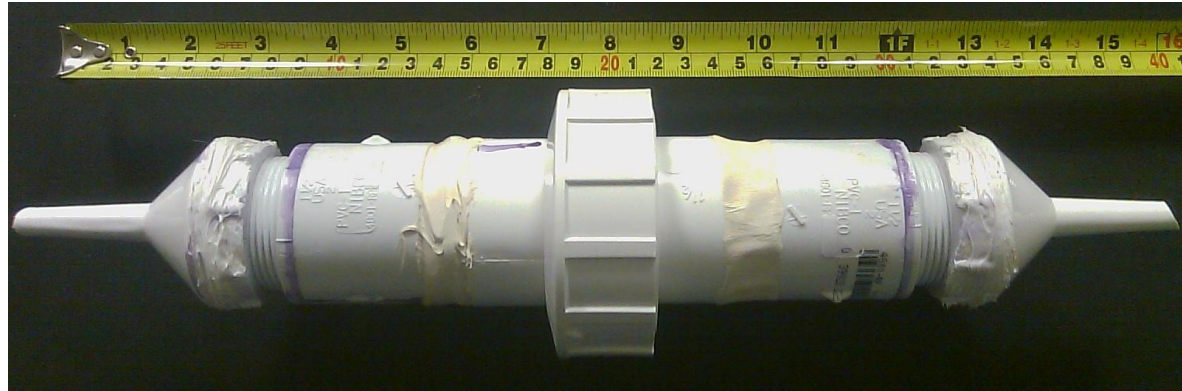
Figure 4.1. Image of fully-assembled sampler V2 that has three distinct compartments; the first to hold the anion exchange resin that retain nitrates, the second to contain granular activated carbon, and the third to hold a fine silica that will act as a flow constrictor. Flow direction is from left to right.

Figure 4.2. Image of sampler V2, dismantled to illustrate different components. Inlet is on the left side. Woven wire mesh is placed in center section before fastening left and right sections together.

The sampler is composed of granular activated carbon (GAC), on which alcohol tracers are pre-sorbed for estimation of water flux, and an anion exchange resin (Lewatit S6368A produced by LANXESS) for capturing the contaminant of interest. Sampler V1 was for initial testing and contained only the resin. The first upstream compartment in V2 contained resin, the second one had GAC while the third compartment was packed with fine silica. The choice in constructing a third compartment in sampler V2 was based on the previously discussed need to reduce the flow velocities through the device. The silica used was a mixture of two U.S. silica products, F-75 and SIL-CO-CIL 250, which were mixed together at a ratio of 2:1 to attain the desired final hydraulic conductivity. The procedure for selection and evaluation of this silica is presented in Appendix A. Sampler V2 also provides logistical advantages over sampler V1; the PVC union used to join the first and second compartments allows for easy dismantlement and well-defined separation between sorbent materials. Thus the three materials could be conveniently placed in series.

Lewatit S6368A anion exchange resin has a macroporous structure with a cross-linked polystyrene matrix. It belongs to the quaternary amine type I functional group and is in the chloride ionic form. The relevant properties of the resin are provided in Table 4.1 and are taken from information provided by Lewatit. The high capacity (1 eq/L) of the resin is of note and will not be exceeded during field deployment. The nitrate uptake and release behavior of the resin was evaluated to determine an extraction efficiency to be used when determining total mass of sorbed nitrate. For resin samples of one to two grams, the extraction efficiency was found to range between 88 and 93 percent. For further information pertaining to the methods and results of this evaluation, refer to Appendix A.

The GAC was a 12x50 mesh silver-impregnated granular activated carbon manufactured by Calgon Carbon. The physical properties of the GAC, as measured in the laboratory, are also presented in Table 4.1.

Table 4.1. Relevant Physical Chemical Properties of Lewatit S6368A Anion Exchange
Resin and the granular activated carbon

Property	Resin Value	GAC Value
Mean Bead Size (mm)	0.62 ± 0.05	12x50 mesh size
Bulk Density (g/L)	640	440 ± 6
Porosity	0.4	0.65 ± 0.037
Total Capacity (eq./L)	1.0	N/A

4.2.2 Pre-Deployment Sampler Preparation and Post-

Deployment Analysis

4.2.2.1 Pre-Deployment Sampler Preparation

Prior to deployment of the sampler, the GAC was prepared by sorbing alcohol tracers through equilibration. To maintain continuity with prior PFM and PSFM investigations, four alcohols were selected to serve as tracers; methanol (MeOH), ethanol (EtOH), isopropanol (IPA) and tert-butyl alcohol (TBA) [*Hatfield et al.*, 2004]. Additionally, a fifth alcohol (2,4 dimethyl-3-pentanol) was used as an internal standard. The *R* values for each respective tracer are given below in Table 4.2 and were provided by Steve Sassman of Purdue University. It should be noted that these R values are lower than previous studies due to the smaller particle size of GAC used. To load the tracers onto the GAC, the tracers were first added to a fixed volume of water and allowed to equilibrate. GAC was then slowly added to the container and the container sealed using Teflon tape. This container was then gently mixed periodically over the course of several days.

Table 4.2. Retardation factors determined from column experiments conducted by Steve Sassman of Purdue University.

Tracer	R (based on column experiment)	R (based on K_d)
Methanol	1.5	1.6
Ethanol	4.2	5.5
Isopropanol	17	23
t-Butanol	59	82

Once the GAC was ready for use, a sampler was prepared by first adding a fixed weight of silica to the third compartment and sealed into place by screwing on the outlet funnel. The sand was kept at the liquid limit while packing, thus leaving a thin layer of water above the sand to prevent air from becoming trapped. The GAC was then added, with samples taken before and after packing to determine the initial mass of tracers sorbed onto the GAC. Upon completely filling the second compartment with GAC, steel mesh was placed on top of the exposed GAC and the PVC union screwed into place to fix the mesh separating the first and second compartments. Resin was then added and secured by screwing on the inlet funnel. Similar to the silica, a thin layer of purified water was maintained above both the GAC and the resin during packing to ensure that no air was trapped inside the device. The device was also gently knocked using a rubber mallet during packing to release confined air. The sampler thus prepared was deployed in the flume (Section 4.2.3 Flume Experimental Procedure) for different periods of time. Upon retrieval of the sampler, the contents (GAC and resin) were removed and placed in beakers, homogenized and sub-sampled for analysis.

4.2.2.2 Post-Deployment Nitrate Analysis

A fixed amount of the resin (approximately 1 to 2g) was sampled into a 40ml VOA (volatile organic analysis) vial containing 35 ml of 2M potassium chloride brine solution for extraction of nitrate. This extractant was chosen based on previous studies, specifications for regeneration of Lewatit resin, and conversations with a representative from LANXESS [*Cho et al.*, 2007]. The high ionic strength of the brine solution causes preferential sorption of the chloride ions and subsequent desorption of the nitrates. The resin is rotated in the brine solution for 24 hours after which a sample of the brine solution is taken for analysis. A minimum of three replicates were performed for each batch of resin.

Due to the high ionic strength of the supernatant, ion chromatography or standard colorimetric measurement of nitrate concentration was not possible. To accommodate this problem, ultraviolet spectrophotometry was used to measure aqueous nitrate concentration. Nitrate is known to absorb wavelengths <250 nm, thus a relationship between absorbance (Abs.) and nitrate concentration was developed using a Cari 50 Bio UV - Visible Spectrophotometer manufactured by Varian. Several wavelengths of light were tested, with a wavelength of 212 nm being selected. 3 replicates, each consisting of 0.1 sec duration exposures were used to measure absorbance in each sample. A calibration curve consisting of 5 independent points and concentrations ranging from 0 to 20 mg/L of NO_3^- was developed. Concentrations higher than 20 mg/L resulted in nonlinear absorption, thus samples with higher concentrations were diluted using 2M KCl solution. Separate calibration curves were developed to measure nitrates in water and in brine solution to account for the attenuation caused by chloride ions. These methods are consistent with previous studies that quantified nitrate using spectrophotometric methods [*F A J Armstrong*, 1963; *Kaneko et al.*, 2010; *Norman and Stucki*, 1981].

4.2.2.3 Post-Deployment Alcohol Tracer Analysis

Tracer elution was evaluated in a fashion similar to that of resin. Prior to sampler preparation and after sampler deployment homogenized samples of GAC were placed in 40 ml VOA vials. Isobutyl alcohol (IBA) was used to extract the alcohols from the GAC. After addition of 35 ml of IBA to the VOA vials and Teflon tape to the cap threading to ensure air-tight seal, the samples were rotated for 24 hours. A ~2.0ml aliquot of the supernatant was then transferred to a 2.0 ml vial for subsequent analysis using gas chromatography (GC). An Agilent 6890N with flame ionization detection (FID) equipped with a DB-624 column (30 m length, inside diameter of 0.320 mm, film thickness of 1.8 μm) was used to conduct the GC analysis. GC method development was conducted using manual injection while the GAC samples from the flume experiments were injected using an autosampler. Alcohol standard solutions were prepared using a gas-tight 10 μL Hamilton syringe and based on measured densities.

The GC method developed is as follows; the oven temperature was held at 80 ^{o}C for 2.90 minutes, then ramped to 200 ^{o}C at 20 ^{o}C/min and held for 1 minute. The inlet conditions were a temperature of 250 ^{o}C, a pressure of 11.9 psi, an injection volume of 1 μL, and a split ratio of 30:1 which resulted in a total flow of 61.0 ml/min. The detector temperature was 280 ^{o}C with an air flow of 450 ml/min, an H_2 flow of 40.0 ml/min, with a nitrogen carrier gas used to provide a make-up flow of 20 ml/min. A linear standard calibration curve comprised of 6 independent points was used, with the R^2 values for each alcohol >0.995. A PC based data acquisition/analysis software package, Chemstation, was used to process the results. A blank spike, a matrix spike, and a calibration point were run before each set of samples, with an additional calibration point being run every 20 samples. Triplicates of each GAC supernatant were run.

4.2.3 Flume Experimental Procedure

4.2.3.1 Flume Description

A re-circulating flume driven by a 7.5 hp Hupp Electric Motors pump controlled by a Magnetek GPD 505 variable frequency drive (VFD) was used (Figure 4.3). The flume has a test section that is 9.12 m long, with a total length including head and tail tanks of 11.42 m. The width is 0.61 m and the standard flow depth is 0.3 m. Flow velocities were measured in the flume using a Nixon propeller meter that had been calibrated against an acoustic Doppler velocimeter. The calibration was based on 5 different settings of the pump with at least 1 minute averages of velocity taken at each setting.

Due to the re-circulating operation of the flume, a consistent nitrate concentration could be maintained after dosing with KNO_3. To ensure a uniform concentration of aqueous NO_3^-, solid KNO_3 was first dissolved into a volume of roughly 1 L. This highly concentrated solution was then added at a steady rate to the flume operating at minimum flow velocity such that the dosing lasted approximately the time required for a volume of water to re-circulate. The VFD was then turned to the highest setting and the flume water mixed for a minimum of 24 hours prior to beginning experiments. To verify a homogenous concentration, 5 samples were taken before and after each experiment at uniform time intervals such that samples spanned approximately one retention time.

4.2.3.2 Flume Experiments: Set One

To develop a relationship between internal velocities through the sampler versus the free stream velocity, several flume experiments were conducted using sampler V1 packed with resin. The set contained 9 deployments of the sampler in the flume; 7 unique free stream velocities and two duplicates. To record average free stream velocity in the flume, readings taken during experiments were 10 second averages of velocity, 6 of

which were taken at each point to provide 1 minute averages. To determine flow through the sampler, the mass of nitrate captured during the experiment was used in conjunction with the ambient nitrate concentration in the flume and the duration of the experiment to determine a water flux through the device.

During each experiment, the sampler was placed at a depth of 0.15 m in the mid section of the flume 4 m from the flume inlet, with the sampler inlet normal to the direction of flow. One minute averages of flow velocity were measured at 3 points upstream and 3 points downstream of the sampler at the depth of the inlet. Additionally, a flow-profile was taken at 0.06 m intervals along the centerline of the flume at a location 0.3 m upstream from the inlet of the sampler. To attain a wider range of flow velocities in the set of experiments, two experiments were conducted at a flow depth of 0.25 m. An image of the flume, along with an image of the propeller meter and the clamp used to hold the sampler are shown in Figure 4.3.

4.2.3.3 Flume Experiments: Set Two

The purpose of the second experimentation set was to compare concentrations of nitrate predicted by sampler V2 with the actual concentrations of the flume. The sampler was packed with all three materials; anion exchange resin, tracer-laden GAC, and silica. Five different flow velocities were tested; each conducted in a manner similar to Set 1, except that the flow depth was maintained at 0.25 m for all experiments.

4.2.3.4 Flume Experiments: Set Three

Upon completion of the five experiments, a subsequent verification of accurate prediction flow-averaged concentration was conducted. This involved 3 different flume velocities, with two samplers deployed simultaneously. Samplers were placed 8 ft apart to avoid interference between flow fields, with velocities measured in a manner similar to

Set 1 to verify approximately uniform flow and a fixed run time of 25 hours. The samplers will be referred to as A and B.
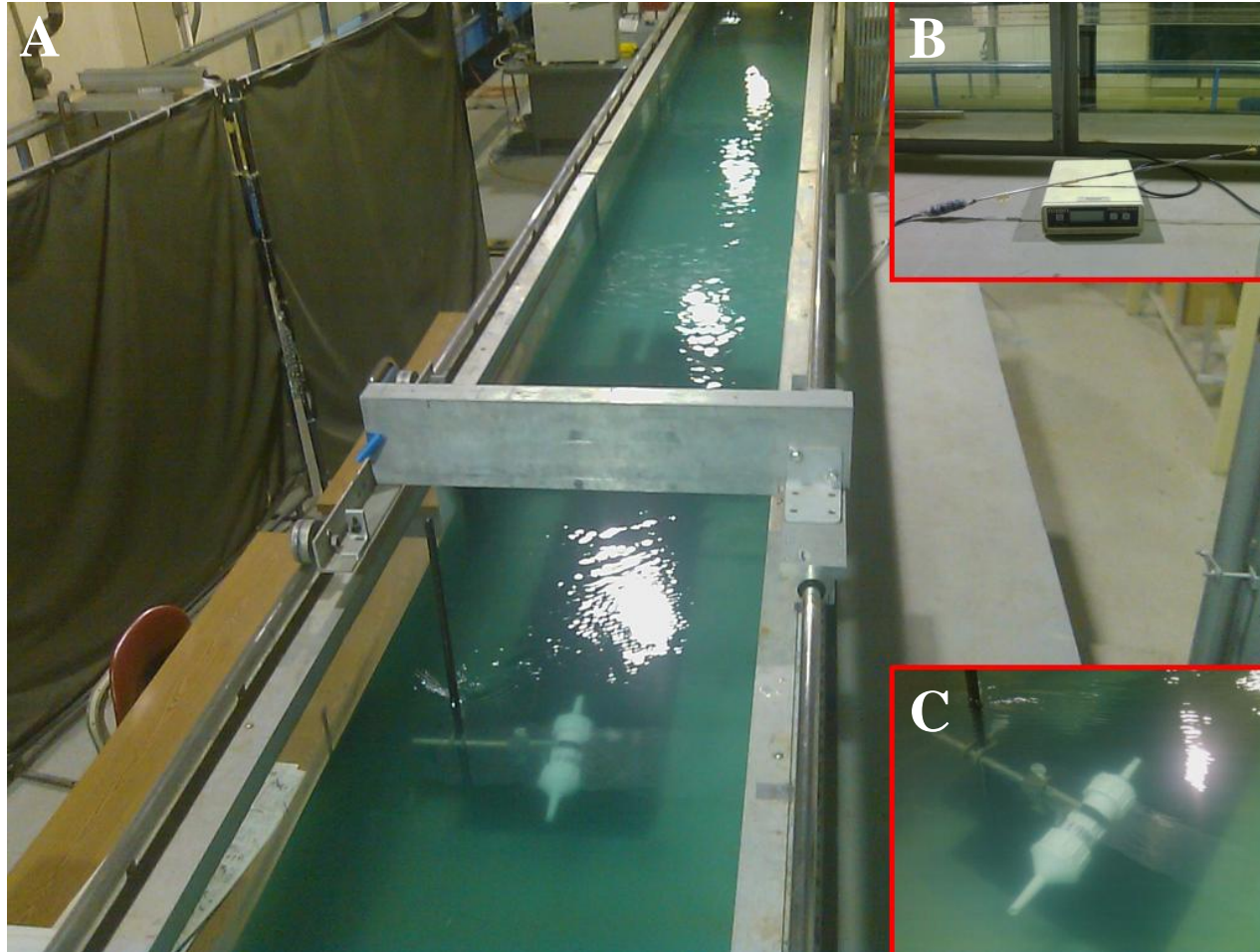
Figure 4.3. Images of the experimental set-up used for procedures outlined in Section 4.2.3 Flume Experimental Procedure. (A) Displays the flume used for all experiments, along with positioning of sampler during experiment. (B) Nixon propeller meter used to measure flume velocities. (C) A beaker clamp was used to hold the sampler in the flow

4.3 Results

4.3.1 Characterization of Flow through Sampler

A relationship between internal and external velocities of sampler V1 in an open channel flow scenario is presented in Figure 4.4. A linear positive relationship is observed between velocities. The ordinate velocity is provided in units of cm/day, as this is a more typical metric for flows in porous media. It should be noted that the velocities are two to three orders of magnitude higher than those observed in groundwater flow domains. These high velocities were a factor in deciding to devote a portion of the sampler to a porous material with a significantly lower hydraulic conductivity (sampler V2). Additionally, the experimental process involved with preparing the sampler and unpacking the sampler contents after deployment provided insights into logistical improvements that could be made. These included creating distinct compartments and addition of a silica material that reduced the effective hydraulic conductivity by three orders of magnitude.

The impact of these changes on internal velocities is illustrated by Figure 4.5, which provides the internal velocities of sampler V2 that resulted from Set 3. The addition of the silica resulted in a significant decrease in internal flow velocities, from an observed range of 127 -1364 cm/day associated with sampler V1 (Figure 4.4) to a range of 4.3 to 18.9 cm/day associated with sampler V2 (Figure 4.5). An increasing trend is observed between internal velocities and increasing external velocities. There was a shift in internal velocities between sampler A and sampler B, due to the slightly differing hydraulic conductivities of the two samplers. To correct for this shift, the velocities through the sampler can be normalized by the effective hydraulic conductivity of each sampler by calculating the head drop through the sampler. The results of this calculation are presented in Figure 4.6. The result from Sampler B at the flume velocity of ~0.2 m/s was not included due to a malfunction. The relationship between internal and external

velocities is best described using a power law ($R^2 = 0.99$ for sampler A), however a zero-intercept linear fit provides a sufficient approximation ($R^2 = 0.86$ for sampler A). A similar result occurred for sampler V1, where a power law fit resulted in an R^2 value of 0.83 while a zero-intercept linear fit resulted in an R^2 value of 0.79.
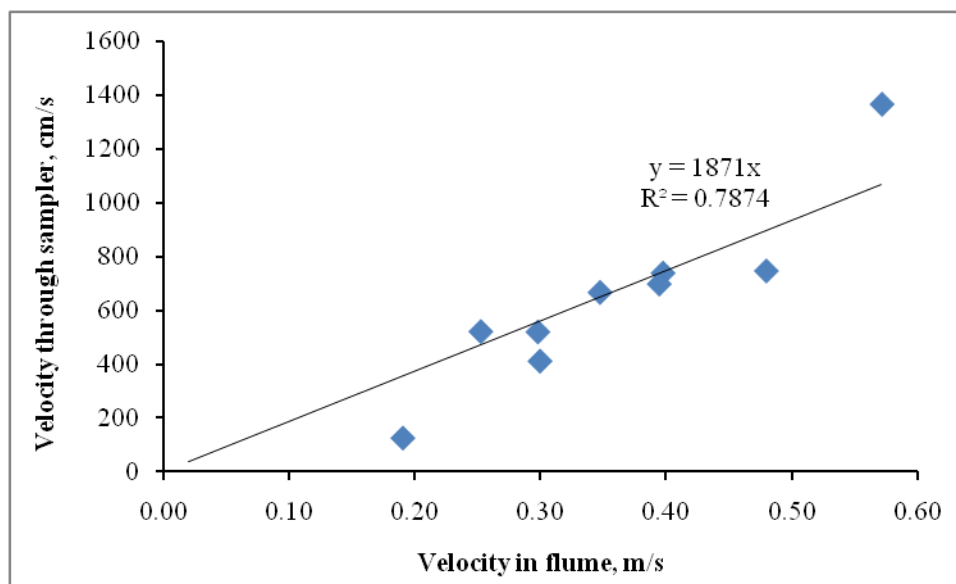
Figure 4.4. Results of the nine flume experiments involving sampler V1 that was packed only with resin. A linear relationship was observed between the flow within the sampler and the ambient flow in the flume.
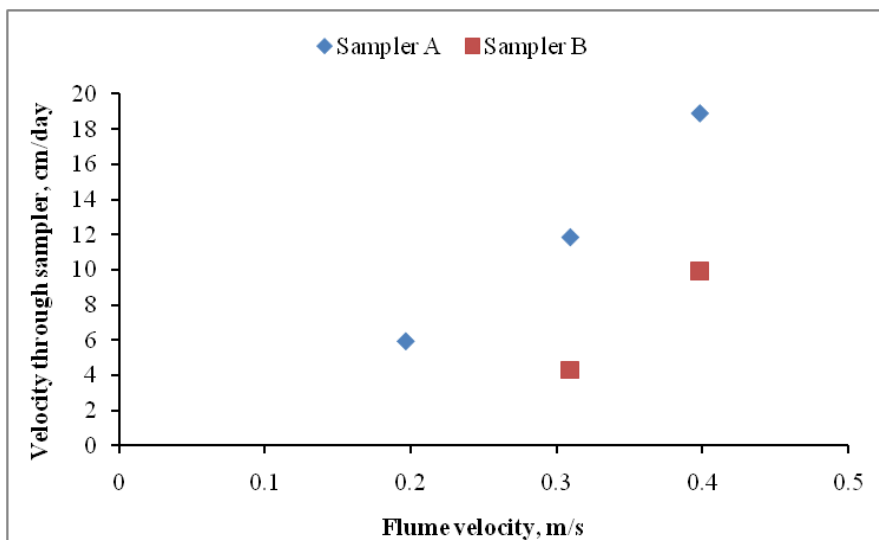
Figure 4.5. Flow velocities through the two different samplers (design V2: GAC, resin and sand restrictor). Difference in the two samplers is attributed to difference in the hydraulic conductivities that vary between packings.
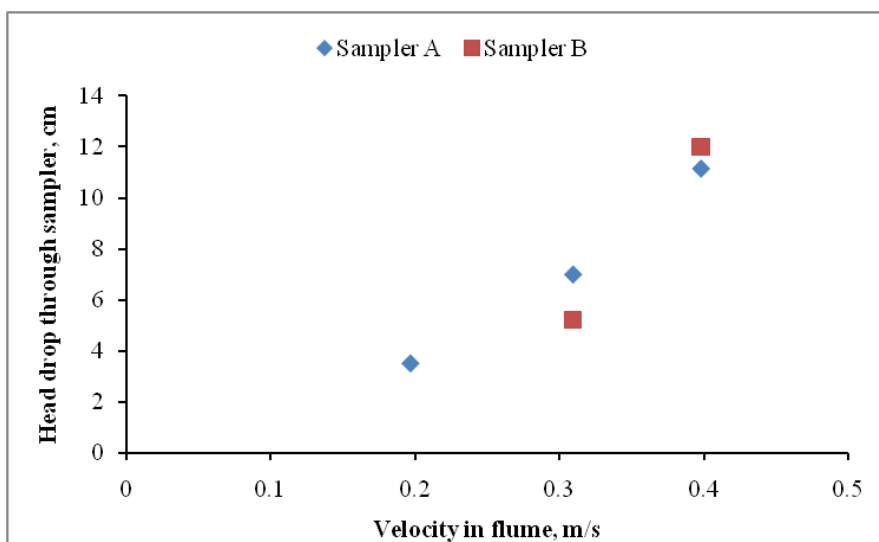
Figure 4.6. Calculated head drops for each flume run. Results indicate that incorporating measured differences in hydraulic conductivity between samplers provides consistency in measured head drop through device versus flume velocity.

4.3.2 Measurement of Flow-Averaged Concentration

Set 2 of flume experiments to evaluate sampler V2 were the first experiments to utilize all three components of the sampler; anion exchange resin, GAC, and silica. This allowed for an evaluation of how well flow averaged concentrations predicted by the sampler aligned with actual concentrations in the flow. The comparison of predicted and actual values is presented in Figure 4.7 which presents the values in the context of flume velocity. The proximity of the predicted values to the actual concentrations presents evidence of the ability of the sampler to capture flow averaged concentration over the duration of an event. Run times for each experiment spanned between 14 and 21 hours, which is shorter than an event. However, concentrations in the flume are approximately three times higher than those expected in natural waters. This implies that the total mass of NO_3^- captured during the experiment is comparable to the mass that would be captured under field conditions. The flow velocities used in the set of experiments presented represents the full range possible in the flume used. This range represents the expected variations in velocities that would be experienced during a moderate storm event, based on velocities in the Clear Creek watershed.

Set 3 verifies the performance of the sampler for measuring flow-averaged concentration by providing 5 additional experimental results that illustrate a reasonable prediction of actual concentrations in the flume (Figure 4.8). Additionally, due to the longer run time of Set 3, it can be inferred that the sampler has sufficient capacity to capture a three to five day event. 25 hours at a rate of 0.39 m/s resulted in $m_{t,r}$ values of 0.664 and 0.827 for IPA and TBA respectively in sampler A and values of 0.905 and 0.962 in sampler B. Thus the sampler would have at sufficient IPA and TBA remaining after a deployment 3 to 5 times longer than the flume run at similar average velocities.
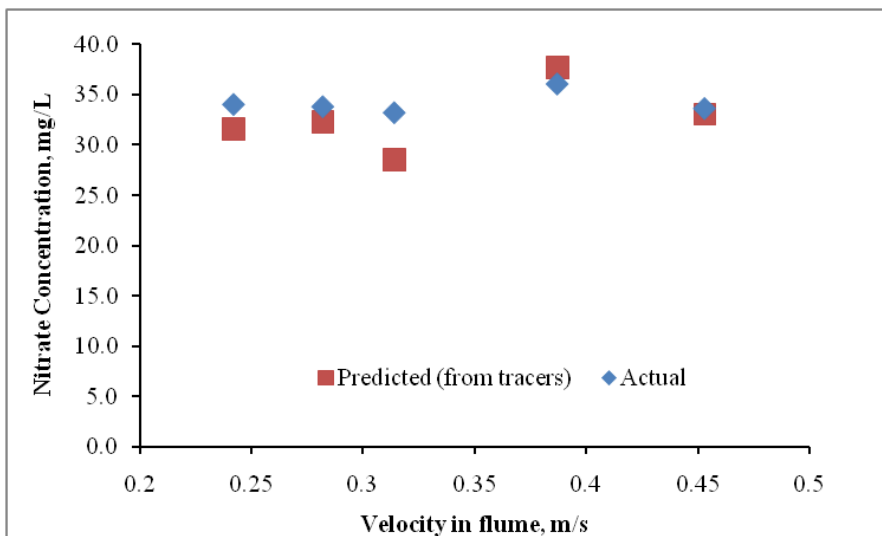
Figure 4.7. Results from 5 flume experiments utilizing resin, tracer-laden GAC, and silica are displayed. Predicted flow averaged concentration based on mass of nitrate captured and water flux estimated from mass fraction of tracer eluted.
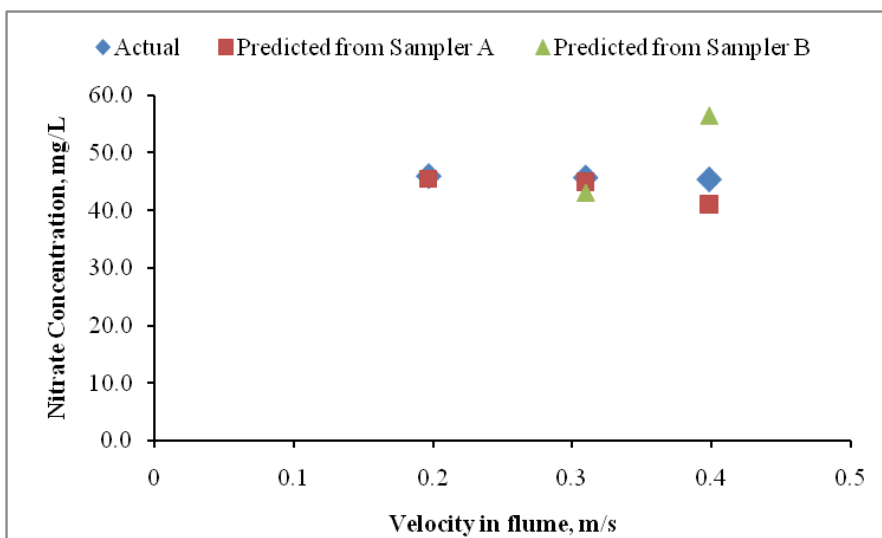
Figure 4.8. Additional flume experiments utilizing all three components of sampler are presented. Sampler A and Sampler B were placed in the flume simultaneously for the three experiments. Results provide a duplication of the sampler's ability to measure average concentration

4.4 Summary and Future Work

A new design of the passive surface water flux meter concept has been tested and validated through laboratory flume experiments. This concept is centered on capturing a flow-weighted average concentration, C_f, over the duration of a hydrologic event by quantifying both a mass flux of contaminant and a cumulative water flux passing through the device. The ratio of the total captured mass to the total volume of water to have passed through the device is then used to give a direct measurement of concentration. To improve over prior designs, a new physical housing was designed and constructed that can control internal velocities through adjustment of the effective hydraulic conductivity of the device. Illustrated by the differences in internal velocities observed between samplers V1 and V2, the desired decrease in conductivity was successful in controlling flow through the device. The consistently increasing trend between internal and external flow velocities illustrated through the variety of flume experiments demonstrates that the sampler can be responsive to the changing flow conditions of a hydrologic event.

Uptake and subsequent consistent extraction of nitrates by means of an anion exchange resin was demonstrated (Appendix A) to provide a method for capturing mass fluxes through the device. Sorption and partitioning behavior of the tracers was shown to be consistent by Steve Sassman of Purdue University, thus enabling the measurement of water fluxes through the device. The ability of the device to provide accurate measurements of C_f confirms the performance of both the resin and GAC. Due to the accuracy in measurement of C_f, it can also be inferred that flows through the device are sufficiently low to avoid non-equilibrium desorption of the tracers.

While the ability of the sampler to estimate C_f has been illustrated in a laboratory setting, these results need to be verified under field conditions. Adjustment of the conductivity addresses the primary concern of changes in flow due to sediment clogging, but simultaneous deployment alongside a device reliably measuring real-time nitrate

concentration (such as the nitratax sonde mentioned in Chapter 3) is necessary to confirm that the device is field capable.

While the focus of this study was on capturing nitrate C_f, the design of the device is easily generalized and can be applied to other surface water constituents. The filtering action of the tightly-packed resin, i.e. the cause of sediment clogging in the device, presents promise for quantifying sediment fluxes, an application that no currently available passive samplers are capable of. Finally, a distributed deployment of multiple samplers must be performed. This would serve to illustrate the full capability of the device in providing spatially distributed data on the behavior of C_f.

CHAPTER 5: CONCLUSION

Anthropogenic modifications to the landscape have led to ubiquitous adverse impacts on the hydrologic and biogeochemical cycles. Agricultural activities are a primary driver of these modifications [*Foley et al.*, 2004; *Matson*, 1997; *Rabalais et al.*, 2010; *Tilman*, 1999; *Vitousek*, 1997]. Significant research has been focused on measuring and modeling these impacts with the overall goal of sustainable management of water resources and maintenance of ecosystem functioning. Despite the enormous progress in understanding the first principles associated with the physicochemical, biological, and geological processes that dictate hydrological and biogeochemical cycles, there remains difficulty in applying this knowledge to describing catchment scale functioning [*Beven*, 1989; 2001]. Confounding effects associated with the difficulty of parameterizing inherent heterogeneity at the catchment scale has resulted in the surfacing of a new approach to catchment research [*McDonnell et al.*, 2007; *Sivapalan*, 2003].

This approach is characterized by a "top-down" approach that relies on emergent patterns in data and catchment classification in an attempt to circumvent the heterogeneous nature of the processes of interest. Should this approach be further developed, it could result in a synergistic relationship between more typical modeling efforts ("bottom-up approaches") and top-down approaches. Simplifications identified in emergent patterns could aid in efficiencies and reduced dependence on calibration in distributed modeling, while process-based modeling could be used to test hypotheses or identify emergent patterns that would be otherwise hidden by the confounding effects of catchment scale heterogeneity.

It has been found that the homogenous and all-pervading nature of agricultural activities may provide opportunities to successfully apply top-down approaches [*N Basu et al.*, 2010]. To further these successes in parsimonious modeling, a conjunctive data synthesis and development of an innovative data collection approach was under-taken to

aid in the evaluation of anthropogenic modifications to the landscape. The specific objectives of this research were to (1) identify emergent patterns in the hydrologic (Chapter 2) and biogeochemical (Chapter 3) responses of intensively managed catchments using available data; (2) develop a flux-integrated passive sampling device for water quality measurements that will further future data collection efforts (Chapter 4). The symbiotic relationship between these two objectives will aid in furthering catchment scale understanding of the impacts of anthropogenic modifications to the natural environment related to agricultural activities. The key conclusions relevant to the three chapters and the future work are discussed below.

5.1 Hydrologic Regimes in Artificially Drained
Agricultural Catchments

Anthropogenic signatures in the hydrologic response of agricultural watersheds were evaluated through an investigation into the effect of artificial drainage on the streamflow response. This was accomplished through a comparison of watersheds within the state of Iowa that have different intensities of artificial drainage. A range of metrics were used to characterize the streamflow response: mean annual runoff ratio, mean annual baseflow ratio, the flow duration curve, Lorenz Curve, Gini coefficient, Tq_{mean}, and the recession behavior. It was found that the scale dependence of the streamflow distribution that is present in natural landscapes is absent in tiled regions.

For tiled basins, the within year distribution of flow characteristics (peak flow, baseflow, recession constant) is independent of the spatial scale of observation. In contrast, in non-tiled watersheds the peak flow decreases (due to flow attenuation) and baseflow increases (due to greater fraction of the aquifer being intercepted) with increase in the spatial scale. All metrics characterizing the streamflow distribution indicate that the spatial variability in hydrologic responses in catchments with high percent of artificial

drainage is much lower than that in non-tiled catchments. This behavior is suggestive of tiling homogenizing the hydrologic response. Finally, the differences between tiled and non-tiled landscapes disappear at scales approximately $>2,200$ km^2 and responses converge to consistent baseflow and peak flow ratios. The effect of channelization and in-stream attenuation dominating at larger scales is attributed to such convergence of responses. This also indicates that 2,200 km^2 is probably a threshold scale in the context of this study and thus studies on the effect of tile drainage should focus at scales below this value.

The homogenization of landscape responses is hypothesized to arise from landscape evolution following installation of tiles. Artificial drainage creates an effective bypass flow network (through vertical macropore, tiles and surface ditches) which bypasses the complexity of catchment travel pathways characteristic of natural landscapes, and leads to more spatially homogeneous responses. The findings of this study have significant implications for modeling hydrologic responses in agricultural catchments. Scale independence implies that it might be possible to develop more parsimonious hydrologic models for these regions, such as the approach presented by [*N Basu et al.*, 2010].

Most importantly, the results indicate a distinctly different hydrologic signature in tiled landscapes compared to non-tiled, so they must be modeled differently. Current efforts based around hill-slope scale models must be modified to address the role the significant role groundwater plays in contributing to total flow in these tiled landscapes, particularly due to the dominant (up to 80%) contribution that baseflow makes to nitrate exports [*K Schilling and Zhang*, 2004]. Future work should involve a modeling approach to verify our hypothesis on the effect of tile drainage in homogenizing hydrologic response. This could be accomplished through the use of a groundwater-surface water interaction models to explicitly identify the mechanisms (e.g. homogenization of the phreatic surface) through which homogenization occurs.

5.2 Emergent Patterns in Nutrient Loading

The relationship between hydrology and biogeochemistry was evaluated by using high resolution (15 minute) discharge and nitrate concentration measurements, in nested basins within the agriculturally dominated Raccoon River watershed in Iowa. The relationship between concentration (C) and discharge (Q) revealed three distinct regimes of nitrate transport: (1) a linear regime in which C increases with increasing Q, (2) a saturation regime in which C remains constant against increasing Q, and (3) a dilution regime in which concentration decreases as Q increases. Linear regimes may arise at low flows as C increases with Q due to larger and larger portions of the watersheds contributing to the nitrate load. Saturation regime corresponds to the scenario when the entire watershed is contributing and the N mobilization rates from the legacy stores are fast enough to maintain a constant concentration. The linear regime and the saturation regime fall in the domain of transport limited scenarios – that is there is an "infinite" supply of solute in the landscape and mobilization of solute into the streams is limited solely by the availability of water for transport. In contrast, the dilution regime corresponds to the supply limited scenario. This most likely occurs due to increase in the contribution from the overland flow pathway that is low in nitrate concentrations, and hence results in dilution at high flows.

Despite these regimes apparent in the C-Q relationship, the L-Q relationship is distinctly linear at both the event, monthly and annual aggregation of loads. Further, the ratio of the coefficient of variation of concentration (CV_C) versus the coefficient of variation of discharge (CV_Q) was low in these systems pointing to the existence of chemostatic behavior [*N B Basu et al.*, 2010; *Godsey et al.*, 2009; *Thompson et al.*, 2011]. It should be noted that "chemostatic" in this case does not mean that concentration does not vary with discharge, rather that the variability in C is much lower than that of Q. For nitrate it has been shown that the CV_C/CV_Q ratio can range from as high as 2 in pristine catchments where chemostatic response is absent to ~ 0.3 in managed catchments. The

development of chemostatic behavior in managed catchments is attributed to arise from the build-up of legacy nitrogen stores (in the form of organic N) in these landscapes that buffer the episodicity in concentration fluxes. Previous studies have identified chemostatic response in managed catchments using temporally sparse (monthly at best) data, leading one to question the role of interpolation errors in the observation [*N B Basu et al.*, 2010]. The continuous nature of the nitrate data used in the analysis verifies the chemostatic behavior of managed catchments that has been observed using temporally coarser data.

The concept of a legacy store of nitrate that has accumulated over time and is providing a ubiquitous source for transport was further verified by the observation of transport and supply limited regimes within the basins. The supply-limited threshold observed in the *C-Q* data, set arbitrarily as flows with greater than a 5% exceedance probability, corresponded with the existence of the point beyond which the L-Q relationship becomes slightly non-linear. Thus, in addition to verifying the existence of chemostatic behavior in agriculturally dominated catchments, through application of the previously used metrics of *Basu et al.* (2010) ($R^2 > 0.8$) and *Thompson et al.* (2010) ($CV_C/CV_Q < 0.3$), the high temporal resolution of the data implied the existence of thresholds associated with this chemostatic behavior.

In addition to the existence of chemostatic response and regimes, the temporal persistence between event averaged, monthly averaged, and annual averaged flow-averaged concentration, C_f was evaluated. The exclusion of extreme discharges (>5% exceedance probability) resulted in a C_f value that was temporally invariant within each of the catchments studied. This indicates that the application of a passive sampler designed to capture flow-averaged concentration over the duration of an event would provide direct insight into mean annual nitrate loads. To further the observations of chemostatic response, additional datasets of fine temporal resolution must be analyzed.

This analysis could also be expanded to the frequency domain as performed by [*Guan et al.*, 2011].

5.3 Passive Sampler Development

A new design of the passive surface water flux meter that extends the current PSFM design from short-term (40 to 495 minutes) measurement of under steady flow conditions to event-scale transient conditions was tested and validated in a laboratory setting. The concept is centered on quantifying both a mass flux of contaminant and a cumulative water flux passing through the PSFM over a specified deployment period (e.g, storm duration). The flow-averaged concentration, estimated as the ratio of the solute flux and the water flux, can then be used in conjunction with flow measurements to estimate the solute load that the watershed upstream of the monitoring point contributes over the deployment period. To improve over prior designs, a new physical housing was designed and constructed and tested using laboratory flume studies. Anion exchange resin was chosen as the sorbent material to capture nitrate fluxes, while alcohol tracers that de-sorb from granular activated carbon were used to quantify water fluxes. Reliable extraction of nitrates from the resin was demonstrated by laboratory experiments. The sorption and partitioning behavior of the tracers was studied by Steve Sassman of Purdue University, and the results verified through our flume experiments.

Flows through the device were successfully controlled through adjustment of the effective hydraulic conductivity by means of a fine silica compartment at the rear end of the sampler. Subsequently a relationship between flow velocities through the sampler and external flow velocities was developed through a series of flume experiments. By seeding the water in the re-circulating flume with known nitrate concentrations, the flume experiments were also used to demonstrate that the sampler can successfully estimate average nitrate concentration under laboratory settings.

While the ability of the sampler to estimate the flow-averaged concentration C_f has been illustrated, these results need to be verified under field conditions. Adjustment of the conductivity addresses the primary concern of changes in flow due to sediment clogging, but simultaneous deployment alongside a device reliably measuring real-time nitrate concentration (such as the nitratax sonde mentioned in Chapter 3) is necessary to confirm that the device is field capable. Although the focus of this study was on capturing nitrate concentrations, the design of the device is easily generalizable and can be applied to other surface water constituents. The filtering action of the tightly-packed resin, i.e. the cause of sediment clogging in the device, presents promise for quantifying sediment fluxes, an application that no currently available passive samplers are capable of. Finally, a distributed deployment of multiple samplers must be performed. This would serve to illustrate the full capability of the device in providing spatially distributed data on the sources of nutrient stores that contribute to the chemostatic behavior of C_f. Such spatially explicit data could strengthen both top-down and bottom-up modeling approaches.

APPENDIX

A.1 Experimental Methods Pertaining to Characterization

of Sampler Contents

A.1.1 Nitrate Extraction Efficiency

To evaluate the performance of the anion exchange resin in capturing nitrate, an adsorption/desorption batch experiment was conducted and mass balance verified. A single concentration of NO_3^- of 20 mg/L was used, made through dilution of 1000 NO_3^- mg/L standard using de-ionized (DI) water. 35 ml of nitrate solution was added to 21 VOA vials and seven different weights of resin, each in triplicate were added to the VOA vials. The approximate weights of resin were 0.1, 0.2, 0.5, 1, 2, 4 and 8 grams. 3 vials containing 35 ml of DI water and resin were used as controls. Upon completion of the initial experiment, a second experiment was conducted at a solid to liquid ratio (S/L) that was used for the remainder of nitrate extractions.

A.1.2 Hydraulic Conductivity Adjustment

To evaluate the effective hydraulic conductivity of the device, a falling head permeability test was developed. The concept behind the falling head test is to relate the change in height of water in a reservoir (that is hydraulically connected to the inlet of the sampler) over time to hydraulic conductivity using Darcy's Law. The discharge (Q; L^3/T) through the sampler can be measured as the change in height of the reservoir over time (dh/dt) multiplied by the cross-sectional area of the reservoir (a_R; L^2), as shown by

$$Q = -a_R \left(\frac{dh}{dt}\right) \qquad\qquad \text{(A-1)}$$

Setting Equation A-1 equal to Darcy's Law and integrating results in:

$$\frac{\ln(H_t)}{\ln(H_0)} = \frac{KAt}{a_R L}$$ (A-2)

Where (H_t; L) is the height above datum of the reservoir water after time t and (H_0; L) is the initial height above datum. (A; L^2) is the cross-sectional area of the sampler and L is the length of the porous medium inside the sampler. At least three points of $\ln(H_t)/\ln(H_0)$ are plotted versus the time required to for the water level to change from H_0 to H_t and the resulting slope of the points is equivalent to (KA)/(aL). The experimental set-up to conduct the test included a reservoir with a cross sectional area of 15.9 cm^2 and a constant initial height H_0 of 2.1 m. The length of the porous portion of the sampler V1 was 11.5 cm and sampler V2 was 23.6 cm. The inside diameter of the sampler was 11.4 cm^2.

Several different materials were evaluated in an effort to find an optimal method for controlling flow through the device. These include heterogeneous play sand, sand passing a 100 mesh size, and two different size distributions of U.S. Silica brand pure silica. The two U.S. silica products are F-75 and SIL-CO-CIL 250 (SCS 250) and their respective particle size distributions are given in Figure A.1 (A) and (B). It was ultimately decided that mixing the two silica products in differing ratios was the most feasible way of adjusting hydraulic conductivity; 2 different ratios were evaluated. The impact of the silica on conductivity was determined using sampler V2 by packing the three compartments with their respective materials, while the conductivities of the GAC, resin, and sands were evaluated individually using sampler V1.

In addition to laboratory tests, an initial field deployment of sampler V1 was conducted to evaluate the impact of sediment collection inside the sampler on the sampler's effective hydraulic conductivity.
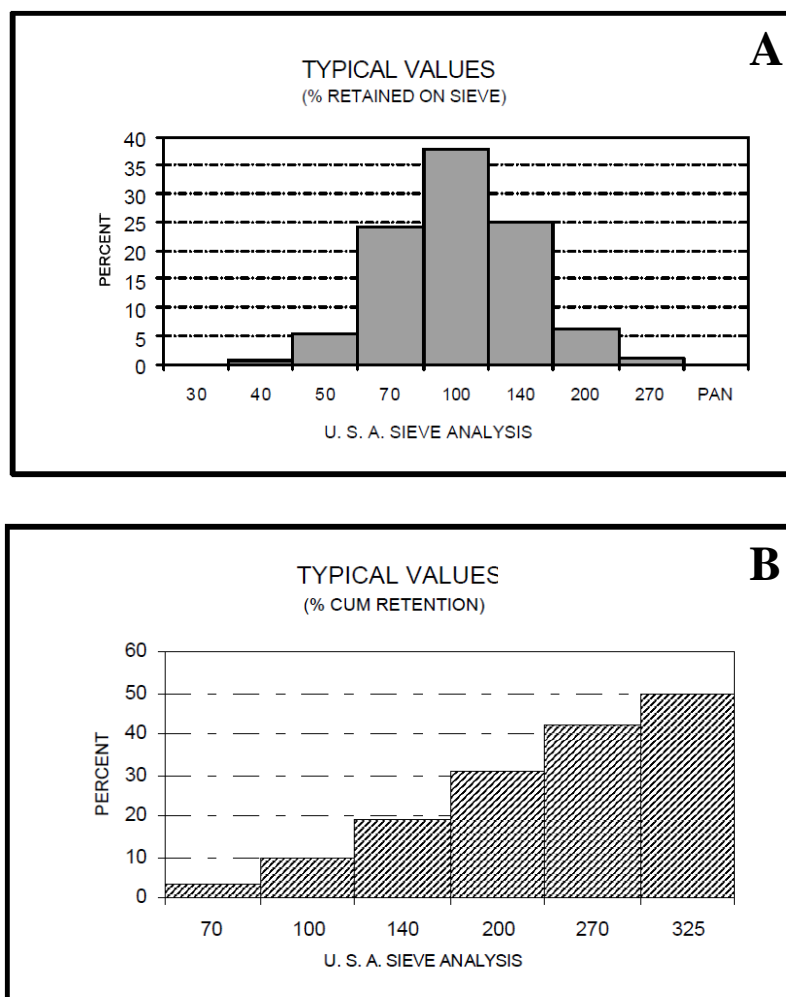
Figure A.1. Particle size distributions of U.S. Silica products used to control hydraulic conductivity. (A) F-75 silica and (B) SIL-CO-SIL 250 silica

A.2 Results of Sampler Characterization

A.2.1 Anion Exchange Resin Sorption Test

Upon the initial completion of the procedure outlined in Section A.1.1 Nitrate Extraction Efficiency, it was observed that a solute was being released from the resin that interfered with the absorbance of nitrate. This resulted in extracted masses being greater

than inputs. This phenomenon was evaluated by rotating differing weights of resin in pure 2M KCl and testing for nitrate. The results are illustrated in Figure A.2, which demonstrates that there is a direct relationship between absorbance and resin weight. The adsorption/desorption experiment was repeated and the linear relationship observed in Figure A.2 was used to correct for the unknown solute. The removal of nitrate from solution is demonstrated in Figure A.3, which shows the resulting nitrate concentration in solution after 24 hours of mixing with resin. As can be seen, even the lowest weights of resin adsorbed the majority of the nitrates in solution. The results of the subsequent extraction of the adsorbed nitrates are shown in Figure A.4, which presents the results in terms of mass balance ratios. The mass balance ratio is the mass of nitrate extracted (M_{out}; M) divided by the mass adsorbed to the resin (M_{in}; M) and can be interpreted as the extraction efficiency.
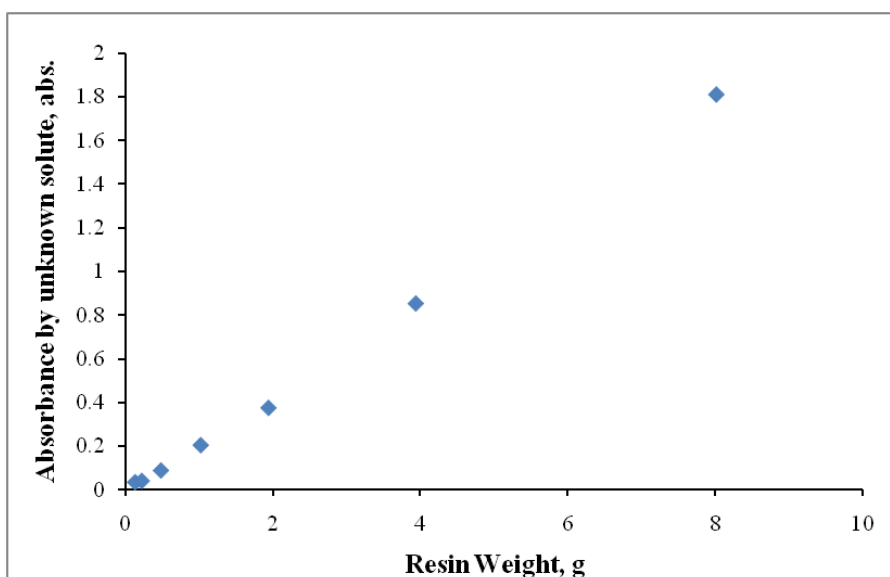
Figure A.2. Absorbance of unknown solute at a wavelength of 212 nm is plotted against resin weight. A direct relationship is evident and is used to adjust concentrations of nitrate extracted from resin.
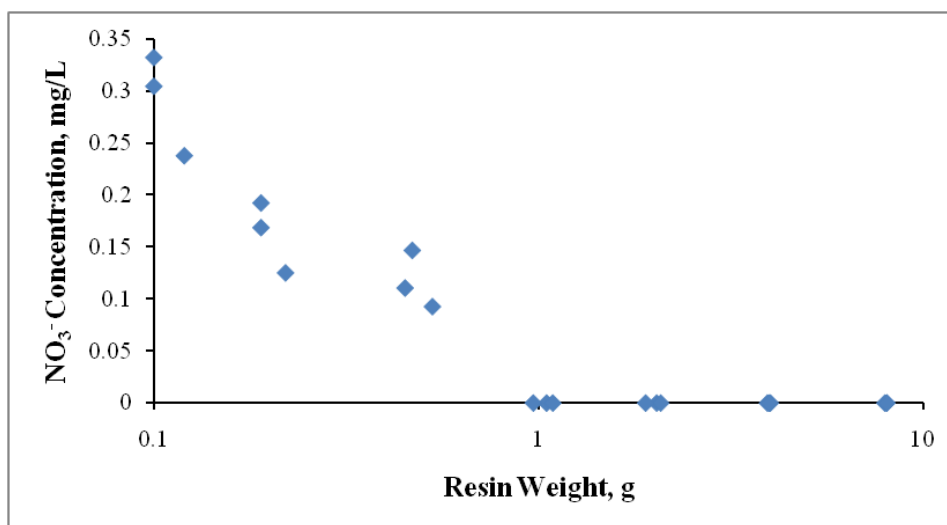
Figure A.3. Removal of nitrate is plotted versus resin weight. The fixed concentration of 20 mg/L results in 0.7 mg being available for sorption, which all but the lowest weights of resin adsorb completely
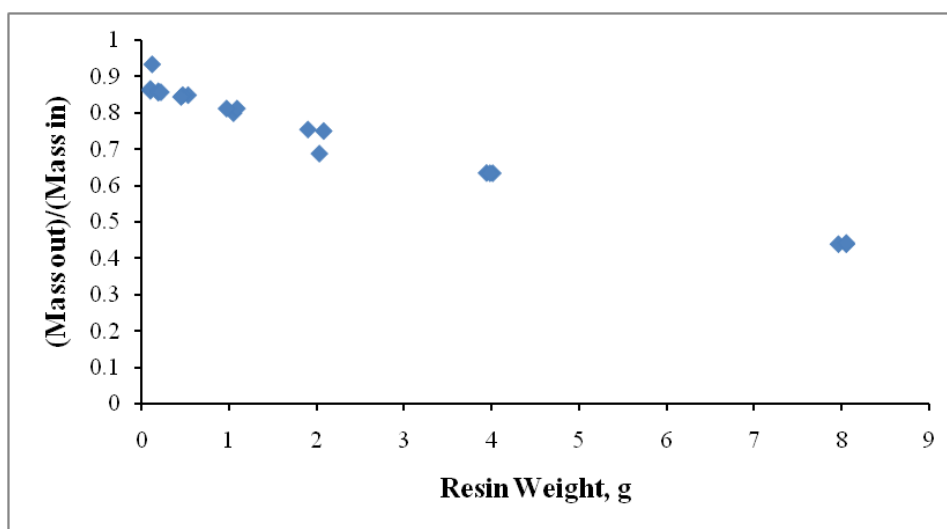
Figure A.4. Extraction efficiency of nitrates plotted against respective resin weight. Since the solution volume was fixed, this illustrates the decreasing effectiveness of the extractant with increasing solid (resin) to liquid (brine solution) ratio.

A decreasing trend in extraction efficiency is observed with increasing S/L ratios. This is due to the increase in sorption sites that the chloride ions interact with, reducing the preferential sorbtion of the ions. Recommended regeneration levels are 200 g/L, which in this case implies a ratio of 7 g of resin per 0.035 L of brine solution should be sufficient for regeneration of resin. As stated in Section 4.2.2.2 Post-Deployment Nitrate Analysis, an additional experiment was conducted to verify the extraction efficiency at a S/L ratio that will be used for the remainder of research. This ratio was chosen as 1 to 2 grams of resin per 0.035L of solution. This verification of extraction efficiency is presented in Table A.1. For a 1 gram sample of resin the extraction efficiency had a mean value of 93.1 ± 2.9%, while a 2 gram sampler had a mean value of 88.3 ± 4.4%.

Table A.1. Verification of extraction efficiency at the solid to liquid ratio to be used for the remainder of extraction procedures; future extractions will involve only 1-2 grams of resin.

Mass of Resin, g	[NO3] in supernatant, mg/L	$Mass_{out}/Mass_{in}$
0.93	0.07	0.885
1.03	0.08	0.938
1.05	0.14	0.936
1.12	0.11	0.938
0.93	0.13	0.972
1.98	0.20	0.836
2.09	0.26	0.962
1.95	0.17	0.894
2.33	0.20	0.871
2.35	0.24	0.852
0.97	0.08	0.917
2.11	0.17	0.881

A.2.2 Hydraulic Conductivity Adjustment

Before evaluating different materials to slow the effective hydraulic conductivity of the device, the conductivity of the GAC and the resin were tested. The conductivity of the resin was found to be very high; 192 ± 11 m/day. The conductivity of the GAC was slightly lower, with a mean value of 147.6 ± 0.8 m/day. The first two materials tested for potential use as flow constrictors were standard heterogeneous play sand and sand that passed through a 100 size standard U.S. mesh. Their respective conductivities were 27.2 ± 3.1 m/day and 117 ± 11.1 m/day. Based on calculated effective hydraulic conductivity of materials in series, this was found to an insufficient difference in conductivities.

Three V1 samplers containing only resin were deployed in Clear Creek to provide an estimate of how suspended sediment collection would impact conductivity. A three day deployment resulted in an average drop of 104 ± 21 m/day, due mostly to sediment that had collected on the mesh at the inlet to the sampler. This result led two U.S. silica products being evaluated as potential materials; the company had significantly finer particle size distributions available as standard products. The silica were tested using sampler V2 and placed in series with resin and GAC. A 1:4 mixture of SCS 250 to F-75 resulted in a mean effective conductivity of 1.69 ± 0.71 m/day while a 1:2 mixture resulted in an effective conductivity of 0.31 ± 0.18 m/day. The 1:2 mixture was chosen as the material to use as a flow constrictor, and as such the value above is based on 12 different falling head permeameter tests. Tests for other materials were conducted 5 times. A fixed weight of silica was used for each subsequent sampler preparation in order to keep conductivity values consistent.

BIBLIOGRAPHY

Abbott, M. B., J. C. Bathurst, J. A. Cunge, P. E. Oconnell, and J. Rasmussen (1986), An introduction to the European Hydrological System - Systeme Hydrologique Europeen, SHE .2. Structure of a physically-based distributed modeling system, *Journal of Hydrology*, *87*, 61-77.

Addiscott, T. M. (1996), Fertilizers and nitrate leaching, in *Agricultural Chemicals and the Environment*, edited by R. E. Hester and R. M. Harrison, pp. 1-26, The Royal Society of Chemistry.

Alewell, C., G. Lischeid, U. Hell, and B. Manderscheid (2004), High temporal resolution of ion fluxes in semi-natural ecosystems - gain of information or waste of resources?, *Biogeochemistry*, *69*(1), 19-35.

Alexander, R. B., R. A. Smith, G. E. Schwarz, E. W. Boyer, J. V. Nolan, and J. W. Brakebill (2008), Differences in phosphorus and nitrogen delivery to the gulf of Mexico from the Mississippi river basin, *Environmental Science & Technology*, *42*(3), 822-830.

Annable, M. D., K. Hatfield, J. Cho, H. Klammler, B. L. Parker, J. A. Cherry, and P. S. C. Rao (2005), Field-scale evaluation of the passive flux meter for simultaneous measurement of groundwater and contaminant fluxes, *Environmental Science & Technology*, *39*(18), 7194-7201.

Arabi, M., R. S. Govindaraju, and M. M. Hantush (2006), Cost-effective allocation of watershed management practices using a genetic algorithm, *Water Resources Research*, *42*(10).

Armstrong, A. C. (1983), The hydrology and water quality of a drained clay catchment - Cockle Park, Northumberland*Rep.*, MAFF, London.

Armstrong, F. A. J. (1963), Determination of Nitrate in Water by Ultraviolet Spectrophotometry, *Anal Chem*, *35*(9), 1292-1294.

Arnold, J. G., P. M. Allen, R. Muttiah, and G. Bernhardt (1995), Automated Base-Flow Separation and Recession Analysis Techniques, *Ground Water*, *33*(6), 1010-1018.

Atkinson, S. E., M. Sivapalan, R. A. Woods, and N. R. Viney (2003), Dominant physical controls on hourly flow predictions and the role of spatial variability: Mahurangi catchment, New Zealand, *Advances in Water Resources*, *26*(3), 219-235.

Baker, J. L., S. W. Melvin, D. W. Lemke, P. A. Lawlor, W. G. Crumpton, and M. J. Helmers (2004), Subsurface Drainage in Iowa and the Water Quality Benefits and Problems in *Drainage VIII Proceedings of the Eighth International Symposium*, edited by R. Cooke, pp. 39-50, ASAE, Sacramento, California USA.

Barco, J., T. Hogue, V. Curto, and L. Rademacher (2008), Linking hydrology and stream geochemistry in urban fringe watersheds, *Journal of Hydrology*, *360*(1-4), 31-47.

Basu, N., P. S. C. Rao, H. E. Winzeler, S. Kumar, P. Owens, and V. Merwade (2010), Parsimonious modeling of hydrologic responses in engineered watersheds: Structural heterogeneity versus functional homogeneity, *Water Resources Research*, *46*(4).

Basu, N. B., P. S. C. Rao, I. C. Poyer, M. D. Annable, and K. Hatfield (2006), Flux-based assessment at a manufacturing site contaminated with trichloroethylene, *Journal of Contaminant Hydrology*, *86*(1-2), 105-127.

Basu, N. B., et al. (2010), Nutrient loads exported from managed catchments reveal emergent biogeochemical stationarity, *Geophysical Research Letters*, *37*(23).

Beven, K. (1989), Changing Ideas in Hydrology - the Case of Physically-Based Models, *Journal of Hydrology*, *105*(1-2), 157-172.

Beven, K. (2001), How far can we go in distributed hydrological modelling?, *Hydrology and Earth System Sciences*, *5*(1), 1-12.

Bishop, R. A., J. Joens, and J. Zohrer (1998), Iowa's Wetlands, Present and Future with a Focus on Prairie Potholes, *Journal of Iowa Academy of Sciences*, *105*(3), 89-93.

Biswal, B., and M. Marani (2010), Geomorphological origin of recession curves, *Geophysical Research Letters*, *37*(24).

Bloschl, G. (2001), Scaling in hydrology, *Hydrological Processes*, *15*(4), 709-711.

Borsuk, M. E., C. A. Stow, and K. H. Reckhow (2004), Confounding effect of flow on estuarine response to nitrogen loading, *J. Environ. Eng.-ASCE*, *130*(6), 605-614.

Botter, G. (2010), Stochastic recession rates and the probabilistic structure of stream flows, *Water Resources Research*, *46*(12).

Brutsaert, W., and J. L. Nieber (1977), Regionalized Drought Flow Hydrographs from a Mature Glaciated Plateau, *Water Resources Research*, *13*(3), 637-644.

Campbell, T. J., K. Hatfield, H. Klammler, M. D. Annable, and P. S. C. Rao (2006), Magnitude and directional measures of water and Cr(VI) fluxes by passive flux meter, *Environmental Science & Technology*, *40*(20), 6392-6397.

Carlisle, D. M., D. M. Wolock, and M. R. Meador (2010), Alteration of streamflow magnitudes and potential ecological consequences: a multiregional assessment, *Frontiers in Ecology and the Environment*, *In Press*.

Cho, J., M. D. Annable, J. W. Jawitz, and K. Hatfield (2007), Passive Flux Meter Measurement of Water and Nutrient Flux in Saturated Porous Media: Bench-Scale Laboratory Tests, *Journal of Environment Quality*, *36*(5), 1266.

Conrad, C. (2004), US 6-Digit HUCs edited by U. a. I. DNR, Iowa DNR, Geological Survey, Iowa City, Iowa.

Cooter, W. S. (2004), Clean Water Act assessment processes in relation to changing US Environmental Protection Agency management strategies, *Environmental Science & Technology*, *38*(20), 5265-5273.

Crutzen, P. J. (2002), Geology of mankind, *Nature*, *415*(6867), 23-23.

de Jonge, H., and G. Rothenberg (2005), New Device and Method for Flux-Proportional Sampling of Mobile Solutes in Soil and Groundwater, *Environmental Science & Technology*, *39*(1), 274-282.

Dehotin, J., and I. Braud (2008), Which spatial discretization for distributed hydrological models? Proposition of a methodology and illustration for medium to large-scale catchments, *Hydrology and Earth System Sciences*, *12*, 769-796.

Diaz, R. J., and R. Rosenberg (2008), Spreading dead zones and consequences for marine ecosystems, *Science*, *321*, 926-929.

Dijk, A. I. J. M. v. (2010), Climate and terrain factors explaining streamflow response and recession in Australian catchments, *Hydrology and Earth System Sciences*, *14*, 159-169.

Donner, S. D., and C. J. Kucharik (2008), Corn-based ethanol production compromises goal of reducing nitrogen export by the Mississippi River, *P Natl Acad Sci USA*, *105*(11), 4513-4518.

Durhan, E. J., C. S. Lambright, E. A. Makynen, J. Lazorchak, P. C. Hartig, V. S. Wilson, L. E. Gray, and G. T. Ankley (2006), Identification of metabolites of trenbolone acetate in androgenic runoff from a beef feedlot, *Environmental Health Perspectives*, *114*, 65-68.

Ellis, E. C. (2011), Anthropogenic transformation of the terrestrial biosphere, *Philosophical Transactions of the Royal Society A: Mathematical, Physical and Engineering Sciences*, *369*(1938), 1010-1035.

Foley, J., C. Kucharik, T. Twine, M. Coe, and S. Donner (2004), Land Use, Land Cover, and Climate Change Across the Mississippi Basin: Impacts on Selected Land and Water Resources, in *Land Use in the Mississippi*, edited by R. S. DeFries, G. P. Asner and R. A. Houghton, pp. 249-261.

Friedrichs, G., H. Halliwell, B. Johnson, K. Keegan, T. McClure, L. Moy, D. Owens, and J. Pagano (2000), Water Quality: Key EPA and State Decisions Limited by Inconsistent and Incomplete Data*Rep.*, U.S. General Accounting Office, Washington, DC.

Fuortes, L., M. K. Clark, H. L. Kirchner, and E. M. Smith (1997), Association between female infertility and agricultural work history, *American Journal of Industrial Medicine*, *31*(4), 445-451.

Galloway, J. N., J. D. Aber, J. W. Erisman, S. P. Seitzinger, R. W. Howarth, E. B. Cowling, and B. J. Cosby (2003), The nitrogen cascade, *Bioscience*, *53*(4), 341-356.

Galloway, J. N., et al. (2004), Nitrogen cycles: past, present, and future, *Biogeochemistry*, *70*(2), 153-226.

Godsey, S. E., J. W. Kirchner, and D. W. Clow (2009), Concentration-discharge relationships reflect chemostatic characteristics of US catchments, *Hydrological Processes*, *23*(13), 1844-1864.

Greenwood, R., G. Mills, and B. Vrana (2007), *Passive Sampling Techniques in Environmental Monitoring*, Elsevier.

Guan, K., S. E. Thompson, C. J. Harman, N. B. Basu, P. S. C. Rao, M. Sivapalan, A. I. Packman, and P. K. Kalita (2011), Spatiotemporal scaling of hydrological and agrochemical export dynamics in a tile-drained Midwestern watershed, *Water Resources Research*, *47*.

Gupta, H. V., S. Sorooshian, and P. O. Yapo (1999), Status of Automatic Calibration for Hydrologic Models: Comparison with Multilevel Expert Calibration, *J Hydrol Eng*, *4*(2), 135-143.

Haag, D., and M. Kaupenjohann (2001), Landscape fate of nitrate fluxes and emissions in Central Europe: A critical review of concepts, data, and models for transport and retention, *Agriculture, Ecosystems & Environment*, *86*(1), 1-21.

Halford, K. J., and G. C. Mayer (2000), Problems associated with estimating ground water discharge and recharge from stream-discharge records, *Ground Water*, *38*(3), 331-342.

Harman, C. J., M. Sivapalan, and P. Kumar (2009), Power law catchment-scale recessions arising from heterogeneous linear small-scale dynamics, *Water Resources Research*, *45*.

Hatfield, K., M. Annable, J. Cho, P. Rao, and H. Klammler (2004), A direct passive method for measuring water and contaminant fluxes in porous media, *Journal of Contaminant Hydrology*, *75*(3-4), 155-181.

IDNR (2005), USGS Stream Gage Stations in Iowa edited by I. G. S. o. t. I. D. o. N. Resources, Iowa DNR, Iowa City, Iowa.

IDNR (2008), Soils Requiring Tile Drainage for Full Productivity edited by D. Iowa Geological and Water Survey, Iowa Department of Natural Resources, Iowa City, Iowa

Jayawickreme, D. H., and D. W. Hyndman (2007), Evaluating the influence of land cover on seasonal water budgets using Next Generation Radar (NEXRAD) rainfall and streamflow data, *Water Resources Research*, *43*(2).

Kaneko, S., M. Inagaki, and T. Morishita (2010), A simple method for the determination of nitrate in potassium chloride extracts from forest soils, in *19th World Congress of Soil Science, Soil Solutions for a Changing World*, edited, Brisbane, Australia.

Kemp, W. M., J. M. Testa, D. J. Conley, D. Gilbert, and J. D. Hagy (2009), Temporal response of coastal hypoxia to nutrient loading and physical controls, *Biogeosciences*, *6*, 2985-3008.

Kenney, B. C. (1982), Beware of Spurious Self-Correlations! , *Water Resources Research*, *18*(4), 1041-1048.

Kirchner, J. W., X. H. Feng, C. Neal, and A. J. Robson (2004), The fine structure of water-quality dynamics: the (high-frequency) wave of the future, *Hydrological Processes*, *18*(7), 1353-1359.

Klammler, H., M. A. Newman, E. Szilagyi, J. C. Padowski, K. Hatfield, J. W. Jawitz, and M. D. Annable (2007), Initial test results for a passive surface water fluxmeter to measure cumulative water and solute mass fluxes, *Environmental Science & Technology*, *41*(7), 2485-2490.

Konrad, C. P., and D. B. Booth (2002), Hydrologic Trends Associated with Urban Development for Selected Streams in the Puget Sound Basin, Western Washington*Rep.*, USGS, Tacoma, Washington.

Madsen, H. (2003), Parameter estimation in distributed hydrological catchment modelling using automatic calibration with multiple objectives, *Advances in Water Resources*, *26*(2), 205-216.

Matson, P. A. (1997), Agricultural Intensification and Ecosystem Properties, *Science*, *277*(5325), 504-509.

Mayer, P., J. Tolls, J. L. M. Hermens, and D. Mackay (2003), Equilibrium sampling devices (vol 37, pg 186, 2003), *Environmental Science & Technology*, *37*(15), 270A-270A.

McDonnell, J. J., et al. (2007), Moving beyond heterogeneity and process complexity: A new vision for watershed hydrology, *Water Resources Research*, *43*(7).

McLean, J. J. J., and G. O. Schwab (1982), Flood peak flows and subsurface drainage, *ASAE Papers*, *82*.

Merz, R., and G. Blöschl (2009), A regional analysis of event runoff coefficients with respect to climate and catchment characteristics in Austria, *Water Resour. Res.*, *45*(1), W01405.

Milly, P. C. D., J. Betancourt, M. Falkenmark, R. M. Hirsch, Z. W. Kundzewicz, D. P. Lettenmaier, and R. J. Stouffer (2008), Climate change - Stationarity is dead: Whither water management?, *Science*, *319*(5863), 573-574.

Mutel, C. F. (2010), *A watershed year: Anatomy of the Iowa Floods.*, Iowa University Press, Iowa City.

Namieśnik, J., B. Zabiegała, A. Kot-Wasik, M. Partyka, and A. Wasik (2004), Passive sampling and/or extraction techniques in environmental analysis: a review, *Analytical and Bioanalytical Chemistry*, *381*(2), 279-301.

Nathan, R. J., and T. A. Mcmahon (1990), Evaluation of Automated Techniques for Base-Flow and Recession Analyses, *Water Resources Research*, *26*(7), 1465-1473.

Norman, R. J., and J. W. Stucki (1981), The determination of nitrate and nitrite in soil extracts by ultraviolet spectrophotometry, *Soil Sci Soc Am J*, *45*(2), 347-353.

NRCS-Iowa (2008), Watershed Boundary Dataset, Eight-Digit Hydrologic Units (Sub-Basins) with Hydrologic Relevance in Iowa edited by N. R. C. S. U. S. Department of Agriculture, Iowa DNR, Fort Worth Texas.

Osterman, L. E., R. Z. Poore, P. W. Swazenski, D. B. Senn, and S. F. DiMarco (2009), The 20th Century development and expansion of Louisiana hypoxia, Gulf of Mexico, *Geo-Mar Letters*, *29*, 405-414.

Padowski, J. C., E. A. Rothfus, J. W. Jawitz, H. Klammler, K. Hatfield, and M. D. Annable (2009), Effect of Passive Surface Water Flux Meter Design on Water and Solute Mass Flux Estimates, *J Hydrol Eng*, *14*(12), 1334-1342.

Pavelis, G. (1987), Farm Drainage in the United States. History, Status, and Prospects*Rep.*, Economic Research Service (DOA), Washington, D.C.

Perrin, C., C. Michel, and V. Andreassian (2001), Does a large number of parameters enhance model performance? Comparative assessment of common catchment model structures on 429 catchments, *Journal of Hydrology*, *242*(3-4), 275-301.

Posavec, K., A. Bacani, and Z. Nakic (2006), A Visual Basic Spreadsheet Macro for Recession Curve Analysis, *Ground Water*, *0*(0), 060526082055001-???

Prestegaard, K. L., A. M. Matherne, B. Shane, K. Houghton, M. Oconnell, and N. Katyl (1994), Spatial variations in the magnitude of the 1993 floods, Raccoon River Basin, Iowa, *Geomorphology*, *10*(1-4), 169-182.

Prior, J. C. (1991), Landforms of Iowa*Rep.*, Department of Natural Resources, Iowa City, Iowa.

Prior, J. C., and C. J. Kohrt (2006), The Landform Regions of Iowa, edited by D. Iowa Geological Survey, Iowa Geological Survey, DNR Iowa City, Iowa.

Rabalais, N. N., R. E. Turner, and W. J. Wiseman (2002), Gulf of Mexico hypoxia, aka "The dead zone", *Annual Review of Ecology and Systematics*, *33*, 235-263.

Rabalais, N. N., W. J. Wiseman, R. E. Turner, B. K. SenGupta, and Q. Dortch (1996), Nutrient changes in the Mississippi River and system responses on the adjacent continental shelf, *Estuaries*, *19*(2B), 386-407.

Rabalais, N. N., R. J. Diaz, L. A. Levin, R. E. Turner, D. Gilbert, and J. Zhang (2010), Dynamics and distribution of natural and human-caused hypoxia, *Biogeosciences*, *7*(2), 585-619.

Ramankutty, N., and J. A. Foley (1999), Estimating historical changes in global land cover: Croplands from 1700 to 1992, *Global Biogeochemical Cycles*, *13*(4), 997-1027.

Raymond, P. A., N.-H. Oh, R. E. Turner, and W. Broussard (2008), Anthropogenically enhanced fluxes of water and carbon from the Mississippi River, *Nature*, *451*(7177), 449-452.

Refsgaard, J. C., and B. Storm (1995), MIKE SHE, in *Computer Models of Watershed Hydrology*, edited by V. P. Singh, pp. 809–846, Water Resources Publications, Highland Ranch, Colorado, USA.

Robinson, M. (1989), Small catchment studies of Man's impact on flood flows: agricultural drainage and plantation forestry, *International Association of Hydrological Sciences Publication*, *187*, 299-308.

Robinson, M. (1990), Impact of improved land drainage on river flows. Institute of Hydrology Report no. 113.*Rep.*, Center for Ecology and Hydrology, Edinburgh, U.K.

Robinson, M., and K. J. Beven (1983), The effect of mole drainage on the hydrologic response of a swelling clay soil, *Journal of Hydrology*, *63*, 205-223.

Robinson, M., and D. W. Rycroft (1999), The impact of drainage on stream flows, *Agronomy Monograph*, *38*, 767-800.

Robinson, M., E. L. Ryder, and R. C. Ward (1985), Influence on streamflow of field drainage in a small agricultural catchment, *Agricultural Water Management*, *10*(2), 145-158.

Royer, T. V., M. B. David, and L. E. Gentry (2006), Timing of Riverine Export of Nitrate and Phosphorus from Agricultural Watersheds in Illinois: Implications for Reducing Nutrient Loading to the Mississippi River, *Environmental Science & Technology*, *40*(13), 4126-4131.

Rozemeijer, J., Y. van der Velde, H. de Jonge, F. van Geer, H. P. Broers, and M. Bierkens (2010), Application and Evaluation of a New Passive Sampler for Measuring Average Solute Concentrations in a Catchment Scale Water Quality Monitoring Study, *Environmental Science & Technology*, *44*(4), 1353-1359.

Rozemeijer, J. C., Y. van der Velde, F. C. van Geer, M. F. P. Bierkens, and H. P. Broers (2010), Direct measurements of the tile drain and groundwater flow route contributions to surface water contamination: From field-scale concentration patterns in groundwater to catchment-scale surface water quality, *Environ Pollut*, *158*(12), 3571-3579.

Savenije, H. H. G. (2009), "The art of hydrology", *Hydrology and Earth System Sciences*, *13*, 157-161.

Schaefli, B., C. J. Harman, M. Sivapalan, and S. J. Schymanski (2011), Hydrologic predictions in a changing environment: behavioral modeling, *Hydrology and Earth System Sciences*, *15*(2), 635-646.

Schilling, K., and Y. K. Zhang (2004), Baseflow contribution to nitrate-nitrogen export from a large, agricultural watershed, USA, *Journal of Hydrology*, *295*(1-4), 305-316.

Schilling, K. E., and M. Helmers (2008), Effects of subsurface drainage tiles on streamflow in Iowa agricultural watersheds: Exploratory hydrograph analysis, *Hydrological Processes*, *22*(23), 4497-4506.

Schilling, K. E., M. K. Jha, Y. K. Zhang, P. W. Gassman, and C. F. Wolter (2008), Impact of land use and land cover change on the water balance of a large agricultural watershed: Historical effects and future directions, *Water Resources Research*, *44*.

Schuch, M. (1978), Regulation of water regime of heavy soils by drainage, subsoiling and liming and water movement in this soil, in *International Drainage Workshop*, edited by J. Wesseling, IILRI, Wageningen.

Seuna, P., and L. Kauppi (1981), Influence of subsurface drainage on water quantity and quality in a cultivated area in Finland*Rep.*, Water Resources Institute Publication no. 43, Helsinki, Finland.

Sivapalan, M. (2003), Process complexity at hillslope scale, process simplicity at the watershed scale: is there a connection?, *Hydrological Processes*, *17*(5), 1037-1041.

Skaggs, R. W., M. A. Breve, and J. W. Gilliam (1994), Hydrologic and Water-Quality Impacts of Agricultural Drainage, *Critical Reviews in Environmental Science and Technology*, *24*(1), 1-32.

Smakhtin, V. U. (2001), Low flow hydrology: a review, *Journal of Hydrology*, *240*(3-4), 147-186.

Smith, V. H., G. D. Tilman, and J. C. Nekola (1999), Eutrophication: impacts of excess nutrient inputs on freshwater, marine, and terrestrial ecosystems, *Environmental Pollution*, *100*(1-3), 179-196.

Soto, A. M., et al. (2004), Androgenic and estrogenic activity in water bodies receiving cattle feedlot effluent in eastern Nebraska, USA, *Environmental Health Perspectives*, *112*(3), 346-352.

Steffen, W., P. J. Crutzen, and J. R. McNeill (2007), The Anthropocene: Are humans now overwhelming the great forces of nature, *Ambio*, *36*(8), 614-621.

Stone, M., and B. G. Krishnappan (1997), Transport characteristics of tile-drain sediments from an agricultural watershed, *Water Air Soil Pollut.*, *99*(1-4), 89-103.

Tallaksen, L. M. (1989), Analysis of time variability in recessions*Rep.*, 85-96 pp, IAHS Publication No. 187.

Tallaksen, L. M. (1995), A Review of Baseflow Recession Analysis, *Journal of Hydrology*, *165*(1-4), 349-370.

Thompson, S. E., N. B. Basu, J. Lascurain, A. Aubeneau, and P. S. C. Rao (2011), Relative Dominance of Hydrologic vs. Biogeochemical Factors on Solute Export Across Impact Gradients, *Water Resources Research*, *XX*, XX-XX.

Tilman, D. (1999), Global environmental impacts of agricultural expansion: The need for sustainable and efficient practices, *P Natl Acad Sci USA*, *96*(11), 5995-6000.

Tilman, D. (2001), Forecasting Agriculturally Driven Global Environmental Change, *Science*, *292*(5515), 281-284.

Toebes, C., and D. D. Strang (1964), On recession curves. 1. Recession equations, *Journal of Hydrology NZ*, *3*(2), 2-15.

USGS (1999), National Elevation Dataset of Iowa as a 30 meter Floating Point GRID, Vertically Attributed in Feet edited by E. D. C. U.S. Geological Survey (USGS), Iowa DNR, Sioux Falls, South Dakota.

Vache, K. B., and J. J. McDonnell (2006), A process-based rejectionist framework for evaluating catchment runoff model structure, *Water Resources Research*, *42*(2).

van der Velde, Y., G. H. de Rooij, J. C. Rozemeijer, F. C. van Geer, and H. P. Broers (2010), Nitrate response of a lowland catchment: On the relation between stream concentration and travel time distribution dynamics, *Water Resources Research*, *46*, -.

Vitousek, P. M. (1997), Human Domination of Earth's Ecosystems, *Science*, *277*(5325), 494-499.

Vrana, B., I. J. Allan, R. Greenwood, G. A. Mills, E. Dominiak, K. Svensson, J. Knutsson, and G. Morrison (2005), Passive sampling techniques for monitoring pollutants in water, *TrAC Trends in Analytical Chemistry*, *24*(10), 845-868.

Wagener, T., M. Sivapalan, P. Troch, and R. Woods (2007), Catchment Classification and Hydrologic Similarity, *Geography Compass*, *1*(4), 901-931.

Wagener, T., N. McIntyre, M. J. Lees, H. S. Wheater, and H. V. Gupta (2003), Towards reduced uncertainty in conceptual rainfall-runoff modelling: dynamic identifiability analysis, *Hydrological Processes*, *17*(2), 455-476.

Wagener, T., M. Sivapalan, P. A. Troch, B. L. McGlynn, C. J. Harman, H. V. Gupta, P. Kumar, P. S. C. Rao, N. B. Basu, and J. S. Wilson (2010), The future of hydrology: An evolving science for a changing world, *Water Resources Research*, *46*(5).

Wahl, K. L., J. Wilbert O. Thomas, and R. M. Hirsch (1995), Stream-Gaging Program of the U.S. Geological Survey*Rep.*, US Geological Survey, Reston, VA.

Wang, D., and X. Cai (2010), Comparative study of climate and human impacts on seasonal baseflow in urban and agricultural watersheds, *Geophysical Research Letters*, *37*(6).

Winchester, P. D., J. Huskins, and J. Ying (2009), Agrichemicals in surface water and birth defects in the United States, *Acta Paediatrica*, *98*(4), 664-669.

Wittenberg, H. (1999), Baseflow recession and recharge as nonlinear storage processes, *Hydrological Processes*, *13*(5), 715-726.

Wittenberg, H., and M. Sivapalan (1999), Watershed groundwater balance estimation using streamflow recession analysis and baseflow separation, *Journal of Hydrology*, *219*(1-2), 20-33.

Yang, G., L. C. Bowling, K. A. Cherkauer, B. C. Pijanowski, and D. Niyogi (2010), Hydroclimatic Response of Watersheds to Urban Intensity: An Observational and Modeling-Based Analysis for the White River Basin, Indiana, *J Hydrometeorol*, *11*(1), 122-138.

Zalasiewicz, J., M. Williams, A. Haywood, and M. Ellis (2011), The Anthropocene: a new epoch of geological time? INTRODUCTION, *Philos T R Soc A*, *369*(1938), 835-841.

Zecharias, Y. B., and W. Brutsaert (1988), Recession Characteristics of Groundwater Outflow and Base-Flow from Mountainous Watersheds, *Water Resources Research*, *24*(10), 1651-1658.

Zhang, L., N. Potter, K. Hickel, Y. Zhang, and Q. Shao (2008), Water balance modeling over variable time scales based on the Budyko framework - Model development and testing, *Journal of Hydrology*, *360*(1-4), 117-131.